Satellite Gradiometry Using a Satellite Pair

by

Mohammad Ali Sharifi

Submitted in conformity with the fulfilment
of conditions to commence the PhD studies
Department of Geodesy and GeoInformatics
University of Stuttgart

Abstract

Providing global and high-resolution estimates of the Earth's gravity field and its temporal variations with unprecedented accuracy is the primary science objective of the *GRACE* mission. These twin satellites are the second spacecraft of the type gravity field dedicated missions which have realized satellite to satellite tracking in the low-low mode (**SST-LL**). The preceding spacecraft is the low orbiting *CHAMP* satellite which has substantiated the high-low mode satellite to satellite tracking concept(**SST-HL**). Observing inter-satellite range and range rate by the ***K-band Ranging System (KBR)*** with the highest possible accuracy is the superiority of *GRACE* over *CHAMP*. Nevertheless, **LL**-configuration can be combined with the **HL**-concept implemented in *CHAMP* to provide a much higher sensitivity. The line of sight *(LOS)* acceleration differences between the twin satellites and a Taylor expansion of the gravitational tensor components of the barycenter of the satellites, called *gradiometry approach* afterward, are two outcomes of the two concepts combination.

Global gravity field determination in terms of spherical harmonic coefficients, $\bar{c}_{nm}$ & $\bar{s}_{nm}$, can be preformed using the *LOS* acceleration differences directly. However, full implementation of the other observable is neither possible nor required. On the other hand, being satisfied just with the applicable form of the observable corresponding to linear combination of the components of the tensor, causes linearization error. Unfortunately, contribution of this systematic error to the estimated coefficients is considerable. Therefore, the observable should be either modified or expanded at least up to third order to lower the effect of the neglected terms. Herein, the modified form of the observable will be employed due to complexity of cubic term expansion for full gravitational potential expansion.

One possible modification is replacing the gravitational potential and all corresponding quantities with the incremental ones. Low-degree ($n \leq 30$) coefficients can be perfectly estimated by just using an incremental quantity corresponding to an ellipsoidal reference field. Due to simplicity of the cubic term of the expansion for an ellipsoidal reference field, a mixed linear-cubic approximation of the observable can be

applied for low-degree harmonic coefficients estimation as well. Both of them yield the same numerical results. However, a reasonable accuracy can not be achieved in the higher degree ($n > 30$) coefficients estimation with the aforementioned modification. An incremental potential correspond with a spheroidal reference field of the degree l ($l > 2$) can be utilized instead. Redefinition of the reference field leads to an acceptable accuracy in the higher degree estimated coefficients. Another alternative is using a mixed equation in which equations of the types $\Delta\Gamma^{LOS}$ and $\mathbf{e}^T\mathbf{G}\mathbf{e}$ are considered for low-degree ($n \leq l$) and higher degree ($n > l$) harmonics respectively. It's equivalent to removing the contribution of a spheroidal reference field of the degree l to the observations as a deterministic trend of the measurements. Implementation of these modifications results much the same accuracy as the other approach yields.

For better understanding of the *commission error* behavior, the simulated observations are contaminated with a simulated Gaussian random noise sequence. Its contribution to the estimated coefficients with respect to other errors are analyzed. Besides, *aliasing/ omission* error, the dominant degradation factor and its contribution to the estimated coefficients are studied. The numerical analysis indicates that overestimating the coefficients and weeding out the higher degree harmonics as the affected terms seems to be one of the possible strategies for minimizing the aliasing.

The Gradiometry approach takes more CPU time as compared to the LOS acceleration differences. It is due to the second order derivatives of the potential calculation besides the first order derivatives which is common to both approaches. In contrast, the observable in gradiometry approach is a one-point function while the other observable is a two-point function. Therefore, in space-wise approach and local gravity field determination (i.e. local geoid), the gradiometry approach would be preferable to the other. In addition, the tensor elements indicate curvature of the gravitational potential which directly corresponds to geometry of the field.

Acknowledgements

First and foremost, I would like to thank God for life itself. All that I have is due to his grace and I would glorify him for all his blessings.

I would like to express my sincere gratitude to the Ministry of Science, Research and Technology of Iran for providing me the financial support to further my education to this level without whose assistance, this opportunity would not have been realized.

My sincere appreciation is conveyed to my distinguished supervisor **Prof. Dr. sc. techn. Wolfgang Keller** for his continuous guidance, discussions and helpful advice throughout my studies. His patience and constant availability played a key role in reaching the goals of this research.

I would also like to thank the head of Geodetic Institute, **Prof. Dr.-Ing.habil. Dr.tech.h.c.mult Dr.-Ing.E.h.mult Erik W. Grafarend** for his thoughtful suggestions and advice throughout the course of my program.

I thank my wife, Parvin Bolouri, M.D., and my daughter, Yeganeh, for their endless support and encouragement. I could not have done it without them.

I wish to thank M.j. Bolouri for his amazing patience and time dedicated in correcting my grammar and stylistic errors. I owe a great deal to him.

Last, but not least, I would like to emphasize that many other people helped me with this research directly and indirectly. Unfortunately, I cannot thank everyone explicitly here. Nevertheless, I hereby would like to extend my sincere gratitude to all of them.

Declaration

The material contained within this thesis has not previously been submitted for a degree at the University of Stuttgart or any other university. The research reported within this thesis has been conducted by the author unless indicated otherwise.

Copyright Notice

Contents

List of Tables

List of Figures

Chapter 1

Introduction

The classical definition of Geodesy according to one of the *fathers of geodesy* is:

the science of the measurement and mapping of the Earth's surfaces

[Helmert 1880].

Accordingly, geodesists' preliminary task has been measuring and portraying the Earth's surface. In order to preform the turned over duty, local horizontal and vertical networks of different orders have been established. Location of the points in the networks have been determined using terrestrial geodetic measurements horizontal angles, distances, zenith angles, and levelled height differences. Besides, astronomical observations and gravimetry measurements have been essential for either realization of both horizontal and vertical datum or correction and reduction of the observed quantities on the datum surfaces. Therefore, the definition has inherently included determination of the Earth'gravity field behavior near to its surface as well as the surface of the ocean as an equipotential surface and height datum. Hence, we understand the scope of geodesy to be somewhat wider. It is captured by the following definition [Vaníček & Krakiwsky 1986]:

Geodesy is the discipline that deals with the measurement and representation of the Earth, including its gravity field, in a three-dimensional time varying space.

Therefore, understanding the geometry of the Earth, geometrical geodesy and the behavior of the gravity field in outer space ($r \geq R_{Earth}$) physical geodesy are two

sub-disciplines in geodesy.

In this respect, unification of geodetic networks established in mainlands with those of the islands and set up of worldwide geodetic networks have been the challenges emerged in geometrical geodesy from about mid-twenties on. On the other hand, having a global coverage of gravimetry data has been a dire necessity for determining the long wavelengths of the gravity field. Since the launch of the first artificial satellite, *SPUTNIK-1*, on October 1957, satellites have served invaluable information both on the geometry and the physics of the Earth. Although, the moon as the natural satellite of the Earth and as a sensor in its gravity field, and natural celestial bodies, particularly fixed stars as known points have been utilized very earlier but due to some distinguished advantages of artificial satellites over the natural bodies, the challenges have been seriously propounded. Though most of the satellites which have been used and still are being used in geodesy were not dedicated to the solution of geodetic problems, geodesists have exploited them as either *fixed control points* or *gravity sensors*. As a consequence, applications of artificial satellites to geodesy have been categorized in two following classes [Seeber 2003]:

- They can be considered as high orbiting targets which are visible over large distances. They may be regarded as *fixed* control points of a three dimensional geodetic network with a global coverage. Locations of the satellites are determined as functions of time using the observations directly measured from ground control stations. In this respect, gravity field of the Earth as the main governing force of the motion is of no interest and the problem is solved from kinematic point of view. The related methods are considered as ***geometrical methods*** of satellite geodesy.

- Artificial satellites as moving objects in a $3D$ space can be assumed as sensors in the gravity field of the Earth. The orbital motion and the variation of the parameters describing the orbit are observed in order to understand the acting forces on the satellites, especially the Earth's gravitational force as the dominant one. In other words, the problem is analyzed from dynamical point of view. So the related methods are classified as ***dynamical methods*** of satellite geodesy.

Nearly homogenous and global coverage is the main advantage of the satellite-based methods either from geometrical or from dynamical point of view. Hence, since the satellites were lunched, more details about the geometry and the physics of the Earth have been emerged. For instance, by the year 1964, many basic geodetic problems (i.e. a reasonably accurate value of the Earth's flattening and the pear-shape of the Earth) had been successfully tackled [Seeber 2003].

In dynamical applications, Earth to space methods have been used for many years due to infeasibility of the others. However, most of the ideas which have been or are going to be implemented in other types of dynamical methods have been introduced very earlier. For instance,the idea of *direct measurements of the Earth's gravitational potential using a satellite pair* as a space to space method introduced by *M. Wolff* in 1969 [Wolff 1969], has been recently applied in **G**ravity **R**ecovery **A**nd **C**limate **E**xperiment (***GRACE***) mission. By the way, applicability of most of the introduced ideas were merely dreams for many years. They have been coming true since a few years ago. So, space to space or ***S**atellite to **S**atellite **T**racking* (***SST***) methods have been superseding Earth to space methods. Based on the configuration of the utilized satellites, two concepts can be introduced:

- High-low satellite to satellite tracking (***HL-SST***)

  Tracking a **L**ow **E**arth **O**rbiting **(LEO)** satellite as the gravity sensor by a group/groups of high orbiting satellites as the fixed orbiting control points. *See Fig. (1.1)*

- Low-low satellite to satellite tracking (***LL-SST***)

  Tracking two identical LEO satellites placed in the same low orbit, several hundred kilometers apart and with inter-satellite cross-link observing the inter-satellite range and range rate, as the gravity sensors by a group/groups of high orbiting satellites as the fixed orbiting control points. *See Fig. (1.1)*

Both the *HL-SST* and *LL-SST* concepts have been realized during the first years of the new century in the Earth gravity field dedicated satellites **CHA**llenging **M**ini-Satellite **P**ayload (***CHAMP***) and *GRACE* respectively. Therefore, this period is dubbed the *Decade of Geopotential Research* [Seeber 2003]. Although *HL-SST* has been typically

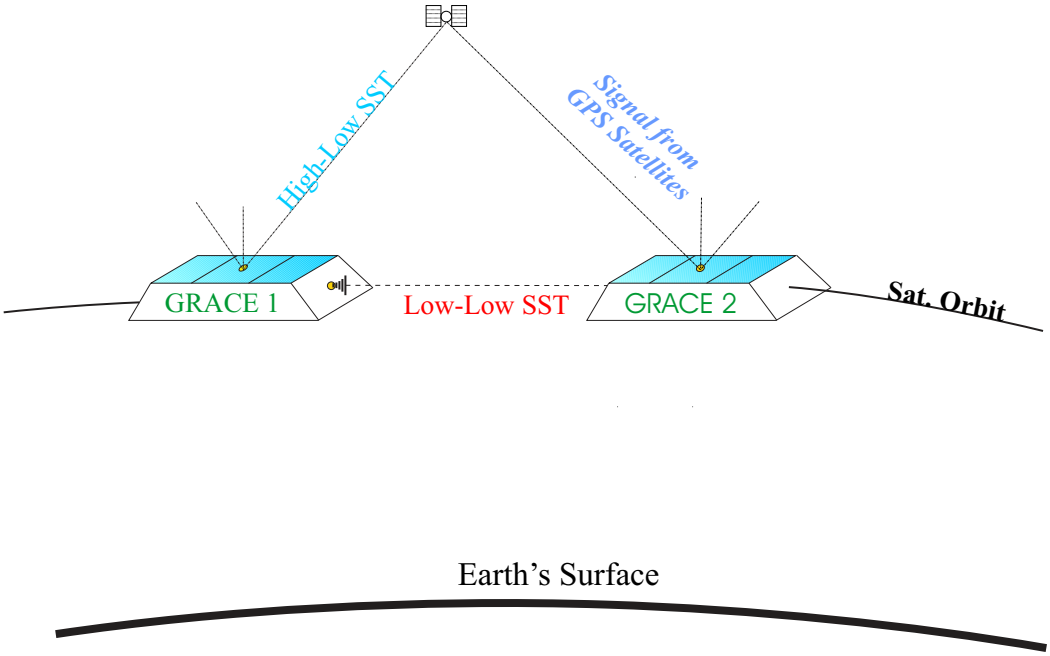

Figure 1.1: High-Low and Low-Low SST configurations

implemented in *CHAMP*, it can be combined with inter-satellite range and range-rate observations provided by *LL-SST* configuration of *GRACE* mission to achieve a much higher sensitivity. Herein, two possible forms of derived observable are discussed:

- the line of sight *(LOS)* acceleration differences between the twin satellites and
- a Taylor expansion of the gravitational tensor components around the barycenter of the satellites

The first part of chapter 2 is dedicated to mathematical formulation of the line of sight *(LOS)* acceleration differences between the twin satellites whereas the expansion of the gravitational tensor components of the barycenter of the satellites is derived as an alternative observable subsequently. Due to impossibility of full implementation of the expansion, some conceivable modifications are theoretically and numerically studied in the third part of this chapter. Some complicated expressions of this chapter are summarized in two Appendices.

In chapter 3, for a comparative study, different lengths of *GRACE* arc orbit are synthesized. Using the derived data sets, both the line of sight *(LOS)* acceleration differences and the modified forms of the expansion observable are calculated. The utilized signals

of the gravitational field are analyzed using both $\Delta\Gamma^{LOS}$ and modified expansion approaches. The *commission* and *omission* errors are investigated in each case. Finally, the numerically applicable method is proposed.

Conclusions and recommendations are summarized in chapter 4 and also, some ideas for the future studies are proposed.

Chapter 2

Mathematical Formulation

As already mentioned, the Gravity Recovery And Climate Experiment (GRACE) mission will be able to map the earth's gravity field by making accurate measurements of the position of the two satellites, inter-satellite range and range rate using GPS and a microwave ranging system respectively. Depending on the way of low-low SST data analysis, different approaches can be applied for mapping the field. The acceleration differences between the two satellites along the orbit can be computed by combining the inter-satellite range, range rate, position, velocity and acceleration. Writing the Earth's gravitational acceleration gradient as a functional of the potential differences, $1D$ *gradiometry*, is the alternative approach which seems to simplify the problem. Here, we formulate the approach and compare the achieving results numerically.

2.1 Gravitational Acceleration Differences

The following relationship is valid for each evaluation point:

$$\langle \Delta\ddot{\mathbf{r}} \ , \ \mathbf{e} \rangle = \ddot{\rho} + \frac{\dot{\rho}^2}{\rho} - \frac{\|\Delta\dot{\mathbf{r}}\|^2}{\rho} \tag{2.1}$$

where, $\Delta\mathbf{r}$, $\Delta\dot{\mathbf{r}}$ and $\Delta\ddot{\mathbf{r}}$ are the inter-satellite vector and its first and second time derivatives respectively. ρ and $\dot{\rho}$, the inter-satellite range and range-rate, are the ranging system output with which $\ddot{\rho}$ is derived computationally. $\mathbf{e}$ is the unit vector along the line of sight (LOS) between the two satellites. Writing $\Delta\ddot{\mathbf{r}}$ as the gravitational

acceleration differences between two satellites yields:

$$\Delta\ddot{\mathbf{r}} = \ddot{\mathbf{r}}_2 - \ddot{\mathbf{r}}_1 = \nabla V_2 - \nabla V_1 = \nabla(V_2 - V_1) = \begin{bmatrix} \frac{\partial V}{\partial x} \\ \frac{\partial V}{\partial y} \\ \frac{\partial V}{\partial z} \end{bmatrix}_2 - \begin{bmatrix} \frac{\partial V}{\partial x} \\ \frac{\partial V}{\partial y} \\ \frac{\partial V}{\partial z} \end{bmatrix}_1 = \Gamma_2 - \Gamma_1 \quad (2.2)$$

We use spherical harmonic expansion of the gravitational potential and derive the partial derivatives of the expansion with respect to x, y and z. It is possible to derive the derivatives in two ways:

- Deriving the derivatives directly by using Cartesian representation of the potential

- Deriving the partial derivatives with respect to curvilinear coordinates and transforming the components to the Cartesian ones

For direct derivation of the partial derivatives, we use the following representation of the gravitational potential [Schäfer 2000]:

$$\begin{gathered} V(x,y,z) = GM \sum_{n=0}^{\infty} R^n \sum_{m=0}^{n} \bar{n}_{n,m} \sum_{k=0}^{[\frac{n-m}{2}]} b_{n,m,k} z^{n-m-2k} r^{2k-2n-1} \\ \cdot[\bar{c}_{n,m} \sum_{i=0}^{[\frac{m}{2}]} (-1)^i \binom{m}{2i} x^{m-2i} y^{2i} + \bar{s}_{n,m} \sum_{i=0}^{[\frac{m-1}{2}]} (-1)^i \binom{m}{2i+1} x^{m-(2i+1)} y^{2i+1}] \end{gathered} \quad (2.3)$$

where, $[\frac{p}{2}]$ stands for the greatest integer $\leq \frac{p}{2}$; i.e. it is $\frac{p}{2}$ or $\frac{p-1}{2}$, whichever is an integer. Taking the derivatives, leads to the subsequent acceleration vector:

$$\Gamma(x,y,z) = \nabla V(x,y,z) = \begin{bmatrix} \frac{\partial V}{\partial x} \\ \frac{\partial V}{\partial y} \\ \frac{\partial V}{\partial z} \end{bmatrix} =$$

$$GM \sum_{n=0}^{\infty} R^n \sum_{m=0}^{n} \bar{n}_{n,m} \sum_{k=0}^{[\frac{n-m}{2}]} b_{n,m,k} z^{n-m-2k} r^{2k-2n-1}.$$

$$(\bar{c}_{n,m} \sum_{i=0}^{[\frac{m}{2}]} (-1)^i \binom{m}{2i} x^{m-2i} y^{2i} \begin{bmatrix} (2k-2n-1)xr^{-2} + (m-2i)x^{-1} \\ 2iy^{-1} + (2k-2n-1)yr^{-2} \\ (n-m-2k)z^{-1} + (2k-2n-1)zr^{-2} \end{bmatrix} +$$

$$\bar{s}_{n,m}\sum_{i=0}^{[\frac{m-1}{2}]}(-1)^i\binom{m}{2i+1}x^{m-(2i+1)}y^{2i+1}\begin{bmatrix}(2k-2n-1)xr^{-2}+(m-2i-1)x^{-1}\\(2i+1)+(2k-2n-1)yr^{-2}\\(n-m-2k)z^{-1}+(2k-2n-1)zr^{-2}\end{bmatrix}) \tag{2.4}$$

where, $\bar{n}_{n,m} = 2^{-n}\left[(2-\delta_{0,m})(2n+1)\frac{(n-m)!}{(n+m)!}\right]^{1/2}$ and $b_{n,m,k} = (-1)^k\frac{(2n-2k)!}{k!(n-k)!(n-m-2k)!}$. The above mentioned summation sequence is a very time-consuming process and for the higher degrees of the series expansion is much worse. Therefore, from numerical point of view, the other approach is preferred.

The gravitational potential for an arbitrary point (r,ϕ,λ) in the outer space $(r \geq R)$ in terms of fully normalized associated Legendre functions $\bar{P}_{nm}$ is:

$$V(\lambda,\phi,r) = \frac{GM}{r}\sum_{n=0}^{\infty}(\frac{R}{r})^n\sum_{m=0}^{n}(\bar{c}_{n,m}\cos m\lambda + \bar{s}_{n,m}\sin m\lambda)\bar{P}_{n,m}(\sin\phi) \tag{2.5}$$

which expresses the gravitational potential as a function of r,ϕ and λ. So, directly deriving the partial derivatives with respect to x,y and z are too complicated. Instead, we can easily define the requested partial derivatives in terms of $\frac{\partial}{\partial r}$, $\frac{\partial}{\partial\phi}$ and $\frac{\partial}{\partial\lambda}$ using the chain rule:

$$\frac{\partial V}{\partial x} = \frac{V(r,\phi,\lambda)}{\partial x} = \frac{\partial V}{\partial r}\cdot\frac{\partial r}{\partial x} + \frac{\partial V}{\partial\phi}\cdot\frac{\partial\phi}{\partial x} + \frac{\partial V}{\partial\lambda}\cdot\frac{\partial\lambda}{\partial x} \tag{2.6}$$

$$\frac{\partial V}{\partial y} = \frac{V(r,\phi,\lambda)}{\partial y} = \frac{\partial V}{\partial r}\cdot\frac{\partial r}{\partial y} + \frac{\partial V}{\partial\phi}\cdot\frac{\partial\phi}{\partial y} + \frac{\partial V}{\partial\lambda}\cdot\frac{\partial\lambda}{\partial y} \tag{2.7}$$

$$\frac{\partial V}{\partial z} = \frac{V(r,\phi,\lambda)}{\partial z} = \frac{\partial V}{\partial r}\cdot\frac{\partial r}{\partial z} + \frac{\partial V}{\partial\phi}\cdot\frac{\partial\phi}{\partial z} + \frac{\partial V}{\partial\lambda}\cdot\frac{\partial\lambda}{\partial z} \tag{2.8}$$

and in vector form:

$$\Gamma(x,y,z) = \nabla V(x,y,z) = \begin{bmatrix}\frac{\partial V}{\partial x}\\\frac{\partial V}{\partial y}\\\frac{\partial V}{\partial z}\end{bmatrix} = \begin{bmatrix}\frac{\partial r}{\partial x} & \frac{\partial\phi}{\partial x} & \frac{\partial\lambda}{\partial x}\\\frac{\partial r}{\partial y} & \frac{\partial\phi}{\partial y} & \frac{\partial\lambda}{\partial y}\\\frac{\partial r}{\partial z} & \frac{\partial\phi}{\partial z} & \frac{\partial\lambda}{\partial z}\end{bmatrix}\begin{bmatrix}\frac{\partial V}{\partial r}\\\frac{\partial V}{\partial\phi}\\\frac{\partial V}{\partial\lambda}\end{bmatrix} = \mathbf{J}^{(r,\phi,\lambda)}_{(x,y,z)}\cdot\begin{bmatrix}\frac{\partial V}{\partial r}\\\frac{\partial V}{\partial\phi}\\\frac{\partial V}{\partial\lambda}\end{bmatrix} \tag{2.9}$$

$\mathbf{J}^{(r,\phi,\lambda)}_{(x,y,z)}$ is the Jacobian of spherical coordinates with respect to Cartesian ones:

$$\mathbf{J}^{(r,\phi,\lambda)}_{(x,y,z)} = \begin{bmatrix} \frac{x}{r} & \frac{-xz}{r^2\sqrt{x^2+y^2}} & \frac{-y}{x^2+y^2} \\ \\ \frac{y}{r} & \frac{-yz}{r^2\sqrt{x^2+y^2}} & \frac{x}{x^2+y^2} \\ \\ \frac{z}{r} & \frac{\sqrt{x^2+y^2}}{r^2} & 0 \end{bmatrix} = \begin{bmatrix} \cos\phi\cos\lambda & \frac{-\sin\phi\cos\lambda}{r} & \frac{-\sin\lambda}{r\cos\phi} \\ \\ \cos\phi\sin\lambda & \frac{-\sin\phi\sin\lambda}{r} & \frac{\cos\lambda}{r\cos\phi} \\ \\ \sin\phi & \frac{\cos\phi}{r} & 0 \end{bmatrix} \tag{2.10}$$

One can easily derive Eq. (2.10) using the representation of (r, ϕ, λ) in terms of Cartesian coordinates:

$$\begin{bmatrix} x \\ y \\ z \end{bmatrix} = \begin{bmatrix} r\cos\phi\cos\lambda \\ r\cos\phi\sin\lambda \\ r\sin\phi \end{bmatrix} \Longleftrightarrow \begin{bmatrix} r \\ \phi \\ \lambda \end{bmatrix} = \begin{bmatrix} \sqrt{(x^2+y^2+z^2)} \\ \arcsin(\frac{z}{r}) \\ \arctan(\frac{y}{x}) \end{bmatrix} \tag{2.11}$$

Substituting Eq. (2.10) and expressing the partial derivatives appeared in Eq. (2.9) in terms of the harmonic series yields:

$$\Gamma(x,y,z) = \begin{bmatrix} \cos\phi\cos\lambda & \frac{-\sin\phi\cos\lambda}{r} & \frac{-\sin\lambda}{r\cos\phi} \\ \\ \cos\phi\sin\lambda & \frac{-\sin\phi\sin\lambda}{r} & \frac{\cos\lambda}{r\cos\phi} \\ \\ \sin\phi & \frac{\cos\phi}{r} & 0 \end{bmatrix}.$$

$$\frac{GM}{r}\sum_{n=0}^{\infty}(\frac{R}{r})^n \sum_{m=0}^{n} \begin{bmatrix} -\frac{n+1}{r}(\bar{c}_{n,m}\cos m\lambda + \bar{s}_{n,m}\sin m\lambda)\bar{P}_{n,m}(sin\phi) \\ (\bar{c}_{n,m}\cos m\lambda + \bar{s}_{n,m}\sin m\lambda)\bar{P}'_{n,m}(\sin\phi) \\ (-m\bar{c}_{n,m}\sin m\lambda + m\bar{s}_{n,m}\cos m\lambda)\bar{P}_{n,m}(\sin\phi) \end{bmatrix} \tag{2.12}$$

In Eq. (2.12), we have only two summations run over n and m, whereas, we have had five summations run over n, m, k, and i in Eq. (2.4). Having only two summations, proves our previous claim on higher numerical performance of spherical representation with respect to Cartesian one. We apply Eq. (2.12) for both satellites and substitute the subsequent equations in Eq. (2.1). The combined observation for each evaluation point, t, generates one linear observation equation in terms of $\bar{c}_{nm}$ and $\bar{s}_{nm}$, fully normalized harmonic coefficients of the series expansion.

$$\mathbf{a}(\mathbf{r}(t))\mathbf{x} = l(\rho(t), \dot{\rho}(t), \ddot{\rho}(t), \parallel \Delta\dot{\mathbf{r}} \parallel) \tag{2.13}$$

where, $\mathbf{a}$ is a vector correspond with coefficients of $\bar{c}_{nm}$ and $\bar{s}_{nm}$ in the design matrix. A sequence of observations with M evaluation points sets up a system of linear equations.

$$\mathbf{A}_{M\times u}\mathbf{x}_{u\times 1} = \mathbf{l}_{M\times 1} \tag{2.14}$$

In practice, the series expansion has to be truncated at an upper maximum degree N_{max}, i.e. the upper limit ∞ of the index n is replaced by a finite number N_{max}. Therefore, the total number of unknowns, u, is:

$$\text{u = zero degree coefficients + first degree coefficients + } N_{max}^{th} \text{ degree coefficients =}$$

$$= 1 + 3 + \ldots + 2(N_{max} + 1) - 1 = (N_{max} + 1)^2 \tag{2.15}$$

From the geometrical point of view, Eq. (2.14) is solvable if $M \geq u$. With fulfilment of this condition, only zonal harmonic coefficients are determined with an acceptable accuracy. This is due to heterogeneous distribution of GRACE data along the meridians and parallels. Thus, having an evenly spaced distribution of data along the meridians and parallels is an essential condition for fully unknown vector determination. The least square estimation of the vector of unknowns in the linear system of equation is:

$$\mathbf{x} = (\mathbf{A}^T {\mathbf{C}_\mathbf{l}}^{-1}\mathbf{A})\mathbf{A}^T {\mathbf{C}_\mathbf{l}}^{-1}\mathbf{l} \tag{2.16}$$

Further details are given in section 2.3. In addition, some numerical results are given in next section using simulated data.

2.2 Gravitational Acceleration Gradient

As previously mentioned, the GRACE mission consists of two identical satellites that follow each other in the same orbit at a distance of about 230 km. The relative distance between the two satellites and its temporal variations are continuously measured with a precision of $1mm$ and $1\mu m/sec$ respectively. Each of the two spacecrafts is equipped with a three dimensional precision accelerometer at its center of mass. Besides, time series of the GPS receivers and the ranging system observations provide an excellent

information about the relative position, velocity and acceleration vector of the geometrical configuration of the spacecrafts. Thus, the configuration can indeed be viewed as a huge one-component gradiometer with an arm length of $250km$. Like in the case of torsion balance, the precision of the GRACE gradiometer is determined by the arm length between the test masses [Rummel et al. 1993]. Hence, gradiometry with GRACE can be done with high level of precision. The principle is shown in Fig. (2.1).

This unique characteristic of GRACE motivates to switch from the first derivatives of the gravitational potential to the second derivatives of the field. In other words, we write the observation equation as a function of the gravitational acceleration gradient components instead of the gravitational potential gradient.

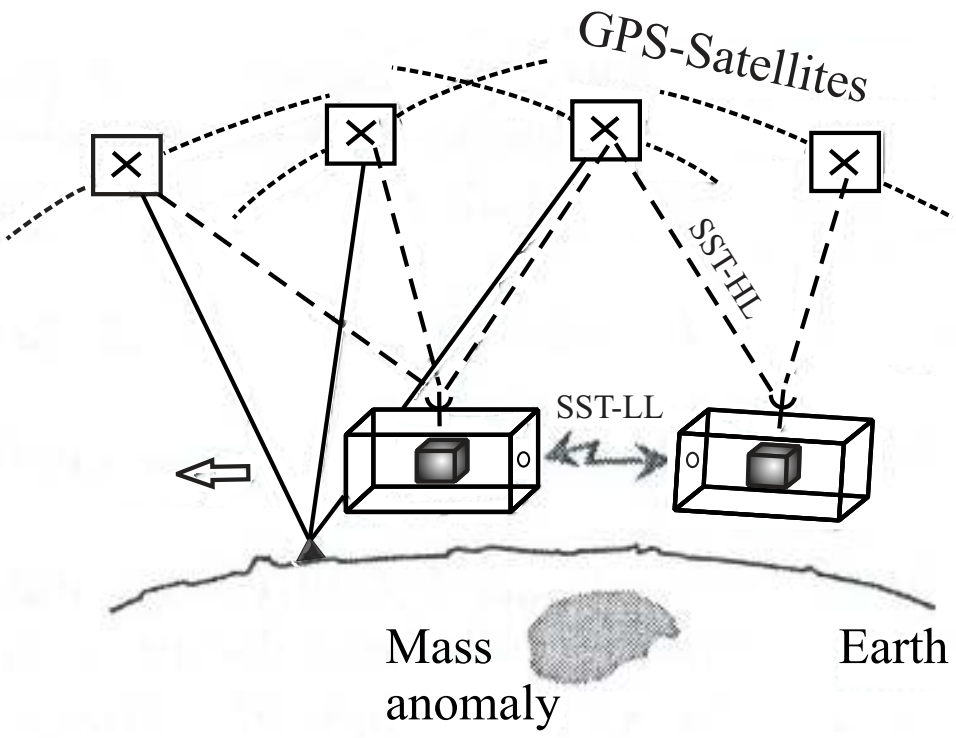

Figure 2.1: Gradiometry with GRACE (from Rummel et al. 2002)

At each evaluation point, the barycenter of the twin satellites is defined as:

$$\mathbf{r}(t) = \frac{\mathbf{r}_1(t) + \mathbf{r}_2(t)}{2} \tag{2.17}$$

and the satellites relative position vectors are:

$$\Delta\mathbf{r}_1(t) = \mathbf{r}_1(t) - \mathbf{r}(t) = -\tfrac{\Delta\mathbf{r}(t)}{2} \quad \Delta\mathbf{r}_2(t) = \mathbf{r}_2(t) - \mathbf{r}(t) = \tfrac{\Delta\mathbf{r}(t)}{2} \tag{2.18}$$

We can rewrite the gravitational acceleration differences using Taylor expansion of the gravitational potential around the barycenter as follows:

$$\Delta\Gamma = \nabla V(\mathbf{r}_2) - \nabla V(\mathbf{r}_1) = \nabla V(\mathbf{r} + \Delta\mathbf{r}_2(t)) - \nabla V(\mathbf{r} + \Delta\mathbf{r}_1(t)) = \sum_{j=1}^{\infty} \Delta\ddot{\mathbf{r}}^{(j)}(t) \tag{2.19}$$

where,

$$\Delta\ddot{\mathbf{r}}^{(j)}(t) = \begin{cases} \frac{2^{1-j}}{j!} \sum_{\nu=0}^{j} \binom{j}{\nu} \sum_{\mu=0}^{\nu} \binom{\nu}{\mu} \Delta x^{j-\nu} \Delta y^{\nu-\mu} \Delta z^{\mu} \frac{\partial^j \nabla V}{\partial x^{j-\nu} \partial y^{\nu-\mu} \partial z^{\mu}} & \text{odd } j \\ 0 & \text{even } j \end{cases} \tag{2.20}$$

where, the effect of even terms drops out and the resultant acceleration differences are only the odd term contributions. Mapping the acceleration differences for an arbitrary odd j along the LOS results:

$$\begin{gathered} \langle \Delta\ddot{\mathbf{r}}^{(j)}(t), \mathbf{e}(t) \rangle = \tfrac{2^{1-j}}{j!} \cdot \\ \sum_{\nu=0}^{j} \binom{j}{\nu} \sum_{\mu=0}^{\nu} \binom{\nu}{\mu} \Delta x^{j-\nu} \Delta y^{\nu-\mu} \Delta z^{\mu} \langle \tfrac{\partial^j \nabla V}{\partial x^{j-\nu} \partial y^{\nu-\mu} \partial z^{\mu}}, \mathbf{e}(t) \rangle \end{gathered} \tag{2.21}$$

Eq. (2.21) can be easily rewritten in terms of Kronecker product[1]:

$$\begin{gathered} \langle \Delta\ddot{\mathbf{r}}^{(j)}(t), \mathbf{e}(t) \rangle = \tfrac{2^{1-j}}{j!} \cdot \\ (\overbrace{\Delta\mathbf{r} \otimes \Delta\mathbf{r} \otimes \cdots \otimes \Delta\mathbf{r}}^{j \text{ times}} \otimes \mathbf{e})^T \cdot Vec(\overbrace{\nabla \otimes \nabla \cdots \otimes \nabla}^{j-1 \text{ times}} \otimes \mathbf{G}) \end{gathered} \tag{2.22}$$

in which, $\mathbf{G}$ is the gravitational acceleration gradient or Gravitational gradient tensor

[1]The Kronecker product of two matrices, $\mathbf{A}$ and $\mathbf{B}$, where $\mathbf{A}$ is $m \times n$ and $\mathbf{B}$ is $p \times q$, denoted by $\mathbf{A} \otimes \mathbf{B}$, is defined as [Graham 1981]

$$\mathbf{A} \otimes \mathbf{B} = \begin{bmatrix} a_{11}\mathbf{B} & a_{12}\mathbf{B} & \cdots & a_{1n}\mathbf{B} \\ a_{21}\mathbf{B} & a_{22}\mathbf{B} & \cdots & a_{2n}\mathbf{B} \\ \cdots & \cdots & \cdots & \cdots \\ a_{m1}\mathbf{B} & a_{m2}\mathbf{B} & \cdots & a_{mn}\mathbf{B} \end{bmatrix}$$

$\mathbf{A} \otimes \mathbf{B}$ is seen to be a matrix of order $(mp \times nq)$. It has mn blocks, the $(i,j)^{th}$ block is the matrix $a_{ij}\mathbf{B}$ of order $(p \times q)$.

in terms of Cartesian coordinates:

$$\mathbf{G} = \nabla^T \otimes \nabla V(\mathbf{r}) = \begin{bmatrix} \frac{\partial^2}{\partial x \partial x} & \frac{\partial^2}{\partial y \partial x} & \frac{\partial^2}{\partial z \partial x} \\ \frac{\partial^2}{\partial x \partial y} & \frac{\partial^2}{\partial y \partial y} & \frac{\partial^2}{\partial z \partial y} \\ \frac{\partial^2}{\partial x \partial z} & \frac{\partial^2}{\partial y \partial z} & \frac{\partial^2}{\partial z \partial z} \end{bmatrix} V(\mathbf{r}) \tag{2.23}$$

Substituting Eqs. (2.23) and (2.19) in Eq. (2.1) yields:

$$\begin{gathered} \langle \Delta\ddot{\mathbf{r}}\ ,\ \mathbf{e} \rangle = \sum_{j=1:2:\infty} \langle \Delta\ddot{\mathbf{r}}^{(j)}(t), \mathbf{e}(t) \rangle = \sum_{j=1:2:\infty} \frac{2^{1-j}}{j!} \cdot \\ (\ \overbrace{\Delta\mathbf{r} \otimes \Delta\mathbf{r} \otimes \cdots \otimes \Delta\mathbf{r}}^{j\ times} \otimes \mathbf{e}\ )^T \cdot Vec(\ \overbrace{\nabla \otimes \nabla \cdots \otimes \nabla}^{j-1\,times} \otimes \mathbf{G}) = \ddot{\rho} + \frac{\dot{\rho}^2}{\rho} - \frac{\|\Delta\dot{\mathbf{r}}\|^2}{\rho} \end{gathered} \tag{2.24}$$

As already mentioned, even terms have no contribution to the equation and j runs only over odd values. Eq. (2.24) can be considered as the general observation equation of GRACE as a gradiometer because each measurement is written as a function of the gravitational gradient tensor components in terms of Cartesian coordinates.

In practice, the series expansion appeared in Eq. (2.24) has to be truncated at an upper maximum degree j_{max}, i.e. the upper limit ∞ of the index j is replaced by a finite number j_{max} so the influence of the neglected terms as to be negligible. We start with *linear approximation* and gradually increase the upper maximum degree as long as we have achieved a reasonable level of accuracy. In this way, we will find both the simple and the accurate model. Let's start with $n_{max} = 1$.

2.2.1 Linear Approximation of the Two Satellites Acceleration Differences Around the Barycenter

Assuming $j = 1$ in Eq. (2.24) dismisses the summation out and makes the equation as simple as possible:

$$(\Delta\mathbf{r} \otimes \mathbf{e}\ )^T \cdot Vec(\mathbf{G}) \stackrel{?}{=} \ddot{\rho} + \frac{\dot{\rho}^2}{\rho} - \frac{\|\Delta\dot{\mathbf{r}}\|^2}{\rho} \tag{2.25}$$

which is equal to:

$$\Delta\mathbf{r}^T \cdot \mathbf{G} \cdot \mathbf{e} \stackrel{?}{=} \ddot{\rho} + \frac{\dot{\rho}^2}{\rho} - \frac{\|\Delta\dot{\mathbf{r}}\|^2}{\rho} \tag{2.26}$$

or:

$$\mathbf{e}^T \cdot \mathbf{G} \cdot \mathbf{e} \stackrel{?}{=} \frac{\ddot{\rho}}{\rho} + \frac{\dot{\rho}^2}{\rho^2} - \frac{\|\Delta\dot{\mathbf{r}}\|^2}{\rho^2} \tag{2.27}$$

Comparing Eqs. (2.27) and (2.1), provides us a useful equality which indicates whether the linear approximation is accurate enough:

$$\mathbf{e}^T \cdot \mathbf{G} \cdot \mathbf{e} \stackrel{?}{=} \frac{1}{\rho}\langle \Delta\mathbf{\Gamma} \ , \ \mathbf{e}\rangle \tag{2.28}$$

Like gravitational acceleration differences, we would like to expand second derivatives of the gravitational potential in terms of spherical harmonics. The aforementioned methods are applicable for deriving the second derivatives with respect to Cartesian coordinates. As done for the first derivatives, we obtain the second time derivatives simply by applying Eq. (2.23) to Eq. (2.3):

$$\nabla^T \otimes \nabla V(x,y,z) = GM \sum_{n=0}^{\infty} R^n \sum_{m=0}^{n} \bar{n}_{n,m} \sum_{k=0}^{[\frac{n-m}{2}]} b_{n,m,k} z^{n-m-2k} r^{2k-2n-1}.$$

$$\left(\bar{c}_{n,m} \sum_{i=0}^{[\frac{m}{2}]} (-1)^i \binom{m}{2i} x^{m-2i} y^{2i} \mathbf{C}_{3\times3} + \bar{s}_{n,m} \sum_{i=0}^{[\frac{m-1}{2}]} (-1)^i \binom{m}{2i+1} x^{m-(2i+1)} y^{2i+1} \mathbf{S}_{3\times3} \right) \tag{2.29}$$

where, $\mathbf{C}_{3\times3}$ and $\mathbf{S}_{3\times3}$ are two fully symmetric matrices defined in Appendix **A**. Similar to the Cartesian representation of the gravitational acceleration, the numerical computation of the tensor will be too time-consuming. Analogously, we use the spherical representation of the gravitational potential, Eq. (2.5), and calculate the second partial derivatives using the chain rule. First, let's split $\mathbf{G}$ and $\mathbf{J}^{r,\phi,\lambda}_{x,y,z}$ up into three column vectors $\mathbf{g}_1$, $\mathbf{g}_2$, $\mathbf{g}_3$ and three row vectors $\mathbf{J}_1$, $\mathbf{J}_2$, $\mathbf{J}_3$ respectively. Using the defined vectors, Eqs. (2.9) and (2.23), we can rewrite the tensor elements as:

$$\mathbf{g}_i = \nabla \otimes \mathbf{J}_i \cdot V_{r,\phi,\lambda} + \mathbf{J}\mathbf{G}^*\mathbf{J}_i^T \tag{2.30}$$

where, i runs over $\{1, 2, 3\}$ and

$$V_{r,\phi,\lambda} = \begin{bmatrix} V_r \\ V_\phi \\ V_\lambda \end{bmatrix} \tag{2.31}$$

$$\mathbf{G}^* = \begin{bmatrix} \frac{\partial^2 V}{\partial r \partial r} & \frac{\partial^2 V}{\partial r \partial \phi} & \frac{\partial^2 V}{\partial r \partial \lambda} \\ \frac{\partial^2 V}{\partial \phi \partial r} & \frac{\partial^2 V}{\partial \phi \partial \phi} & \frac{\partial^2 V}{\partial \phi \partial \lambda} \\ \frac{\partial^2 V}{\partial \lambda \partial r} & \frac{\partial^2 V}{\partial \lambda \partial \phi} & \frac{\partial^2 V}{\partial \lambda \partial \lambda} \end{bmatrix} = \begin{bmatrix} V_{rr} & V_{r\phi} & V_{r\lambda} \\ V_{\phi r} & V_{\phi\phi} & V_{\phi\lambda} \\ V_{\lambda r} & V_{\lambda\phi} & V_{\lambda\lambda} \end{bmatrix} \tag{2.32}$$

and $\nabla \otimes \mathbf{J}_i$ s are given in appendix **B** with more details.

Deriving the second order partial derivatives of V with respect to (r, ϕ, λ), is the next step:

$$\begin{aligned}
V_{rr} &= \tfrac{GM}{r} \textstyle\sum_{n=0}^{\infty} (\tfrac{R}{r})^n \sum_{m=0}^{n} \tfrac{(n+1)(n+2)}{r^2} (\bar{c}_{n,m} \cos m\lambda + \bar{s}_{n,m} \sin m\lambda) \bar{P}_{n,m}(sin\phi) \\
V_{r\phi} &= \tfrac{GM}{r} \textstyle\sum_{n=0}^{\infty} (\tfrac{R}{r})^n \sum_{m=0}^{n} \tfrac{-(n+1)}{r} (\bar{c}_{n,m} \cos m\lambda + \bar{s}_{n,m} \sin m\lambda) \bar{P}'_{n,m}(sin\phi) \\
V_{r\lambda} &= \tfrac{GM}{r} \textstyle\sum_{n=0}^{\infty} (\tfrac{R}{r})^n \sum_{m=0}^{n} \tfrac{-(n+1)}{r} (-m\bar{c}_{n,m} \sin m\lambda + m\bar{s}_{n,m} \cos m\lambda) \bar{P}_{n,m}(sin\phi) \\
V_{\phi\phi} &= \tfrac{GM}{r} \textstyle\sum_{n=0}^{\infty} (\tfrac{R}{r})^n \sum_{m=0}^{n} (\bar{c}_{n,m} \cos m\lambda + \bar{s}_{n,m} \sin m\lambda) \bar{P}''_{n,m}(sin\phi) \\
V_{\phi\lambda} &= \tfrac{GM}{r} \textstyle\sum_{n=0}^{\infty} (\tfrac{R}{r})^n \sum_{m=0}^{n} (-m\bar{c}_{n,m} \sin m\lambda + m\bar{s}_{n,m} \cos m\lambda) \bar{P}'_{n,m}(sin\phi) \\
V_{\lambda\lambda} &= -\tfrac{GM}{r} \textstyle\sum_{n=0}^{\infty} (\tfrac{R}{r})^n \sum_{m=0}^{n} m^2 (\bar{c}_{n,m} \cos m\lambda + \bar{s}_{n,m} \sin m\lambda) \bar{P}_{n,m}(sin\phi)
\end{aligned} \tag{2.33}$$

Computation of the fully normalized associated Legendre functions and their first and second derivatives with respect to the argument ϕ appearing in Eqs. (2.12) and (2.33), are based on the following recurrence relations ([Rummel et al. 1993] ; [Tsoulis 1999]):

- Diagonal recursion $n \geq 2$

$$\begin{aligned}
\bar{P}_{n,n} &= f_1 \cos\phi \bar{P}_{n-1,n-1} \\
\bar{P}'_{n,n} &= f_1 \left[\cos\phi \bar{P}'_{n-1,n-1} - \sin\phi \bar{P}_{n-1,n-1}\right] \\
\bar{P}''_{n,n} &= f_1 \left[\cos\phi \bar{P}''_{n-1,n-1} - 2\sin\phi \bar{P}'_{n-1,n-1} - \cos\phi \bar{P}_{n-1,n-1}\right]
\end{aligned} \tag{2.34}$$

- Horizontal recursion - first step $n \geq 1$

$$\begin{aligned}
\bar{P}_{n,n-1} &= f_2 \sin\phi \bar{P}_{n-1,n-1} \\
\bar{P}'_{n,n-1} &= f_2 \left[\cos\phi \bar{P}_{n-1,n-1} + \sin\phi \bar{P}'_{n-1,n-1}\right] \\
\bar{P}''_{n,n-1} &= f_2 \left[\sin\phi \bar{P}''_{n-1,n-1} + 2\cos\phi \bar{P}'_{n-1,n-1} - \sin\phi \bar{P}_{n-1,n-1}\right]
\end{aligned} \tag{2.35}$$

- Horizontal recursion - next step

$$\begin{aligned}
\bar{P}_{n,m} &= f_3 \left[f_4 \sin\phi \bar{P}_{n-1,m} - f_5 \bar{P}_{n-2,m}\right] \\
\bar{P}'_{n,m} &= f_3 \left[f_4 \sin\phi \bar{P}'_{n-1,m} + f_4 \cos\phi \bar{P}_{n-1,m} - f_5 \bar{P}'_{n-2,m}\right] \\
\bar{P}''_{n,m} &= f_3 \left[f_4 \sin\phi \bar{P}''_{n-1,m} + 2 f_4 \cos\phi \bar{P}'_{n-1,m} - f_4 \sin\phi \bar{P}_{n-1,n-1} - f_5 \bar{P}''_{n-2,m}\right]
\end{aligned} \tag{2.36}$$

where,

$$\begin{aligned}
f_1 &= \sqrt{\tfrac{2n+1}{2n}} \\
f_2 &= \sqrt{2n+1} \\
f_3 &= \sqrt{\tfrac{2n+1}{(n-m)(n+m)}} \\
f_4 &= \sqrt{2n-1} \\
f_5 &= \sqrt{\tfrac{(n+m-1)(n-m-1)}{2n-3}}
\end{aligned} \tag{2.37}$$

For initialization of Eqs. (2.34), (2.35) and (2.36), we use:

$$\begin{aligned}
\bar{P}_{0,0} &= 1 & \bar{P}'_{0,0} &= 0 & \bar{P}''_{0,0} &= 0 \\
\bar{P}_{1,1} &= \sqrt{3}\cos\phi & \bar{P}'_{1,1} &= -\sqrt{3}\sin\phi & \bar{P}''_{1,1} &= -\sqrt{3}\cos\phi
\end{aligned} \tag{2.38}$$

Now, we reach the point that we are able to set up the gradiometry linear system of

equations. Substituting Eq. (2.30) in Eq. (2.27) gives the linear gradiometry observation equation in terms of unknown coefficients correspondent with fully normalized associated Legendre functions:

$$\sum_{i=1}^{3} \mathbf{e}^T \left[\nabla \otimes \mathbf{J}_i \cdot V_{r,\phi,\lambda} + \mathbf{J}\mathbf{G}^* \mathbf{J}_i^T \right] e_i \stackrel{?}{=} \frac{\ddot{\rho}}{\rho} + \frac{\dot{\rho}^2}{\rho^2} - \frac{\|\Delta\dot{\mathbf{r}}\|^2}{\rho^2} \tag{2.39}$$

or in symbolic form of parametric equation:

$$\mathbf{a}(\mathbf{r}(t))\mathbf{x} = l(\rho(t), \dot{\rho}(t), \ddot{\rho}(t), \| \Delta\dot{\mathbf{r}} \|) \tag{2.40}$$

Finally, for a time series consisting of M observations, we set up the following linear system of equations:

$$\mathbf{A}_{M\times u}\mathbf{x}_{u\times 1} = \mathbf{l}_{M\times 1} \tag{2.41}$$

In practice, the series expansion has to be truncated at an upper maximum degree N_{max}, i.e. the upper limit ∞ of the index n is replaced by a finite number N_{max}. Therefore, the total number of unknowns, u, is:

$$\text{u} = \text{zero degree coefficients} + \text{first degree coefficients} + N_{max}^{th} \text{ degree coefficients} =$$

$$= 1 + 3 + \ldots + 2(N_{max} + 1) - 1 = (N_{max} + 1)^2 \tag{2.42}$$

From the geometrical point of view, Eq. (2.41) is solvable if $M \geq u$. With fulfilment of this condition, only zonal harmonic coefficients will be determined with an acceptable accuracy if the linear approximation is accurate enough. It is due to heterogeneous distribution of GRACE data along the meridians and parallels and also systematic error created by the higher order neglected terms in Taylor expansion of the acceleration differences. Apart from the systematic error, having an evenly spaced distribution of data along the meridians and parallels, is an essential condition for fully unknown vector determination. The least square estimation of the vector of unknowns in the linear system of equation is:

$$\mathbf{x} = (\mathbf{A}^T {\mathbf{C}_\mathbf{l}}^{-1} \mathbf{A}) \mathbf{A}^T {\mathbf{C}_\mathbf{l}}^{-1} \mathbf{l} \tag{2.43}$$

In the next subsection, we will show some numerical results based on linear approximation using the simulated data. Based on this numerical investigation, we will decide whether we need higher order approximation.

2.2.2 Cubic Approximation of the Two Satellites Acceleration Differences Around the Barycenter

Assuming $j = 3$ in Eq. (2.24), provides us a better approximation of the acceleration differences. One more term, called cubic term, will appear on the left-hand side of Eq. (2.25) as the resultant of adding the third order.

$$\begin{gathered}(\Delta\mathbf{r} \otimes \mathbf{e}\ )^T \cdot Vec(\mathbf{G}) + \\ \tfrac{1}{3!2^2}(\Delta\mathbf{r} \otimes \Delta\mathbf{r} \otimes \Delta\mathbf{r} \otimes \mathbf{e}\ )^T \cdot Vec(\nabla \otimes \nabla \otimes \mathbf{G}) \stackrel{?}{=} \ddot{\rho} + \tfrac{\dot{\rho}^2}{\rho} - \tfrac{\|\Delta\dot{\mathbf{r}}\|^2}{\rho}\end{gathered} \tag{2.44}$$

Alternatively, an equivalent form of Eq. (2.44) to the Eq. (2.27) is:

$$\mathbf{e}^T \cdot \mathbf{G} \cdot \mathbf{e} + \frac{1}{3!2^2}\mathbf{e}^T \otimes \Delta\mathbf{r}^T \otimes \Delta\mathbf{r}^T \cdot (\nabla \otimes \nabla \otimes \mathbf{G}) \cdot \mathbf{e} \stackrel{?}{=} \frac{\ddot{\rho}}{\rho} + \frac{\dot{\rho}^2}{\rho^2} - \frac{\|\Delta\dot{\mathbf{r}}\|^2}{\rho^2} \tag{2.45}$$

The second term of Eq. (2.45) is the improvement rate of linearization error. It is easily inferred from Eq. (2.45) that fourth partial derivatives of the gravitational potential should be calculated. Furthermore, due to better numerical performance, we prefer to carry out all computations in terms of spherical coordinates and transform the final results to Cartesian coordinates. So, we have to calculate much more complicated mathematical expressions with respect to the linear approximation. Before attempting to simplify the computation, we should answer a probable question which may occur to anyone's mind. *Is it really worth to pay such a price for the cubic term?* To answer this question, we need to know how much contribution the cubic term has to linearization error. Let us clarify the problem with few numerical examples.

Example 1: Earth as a spherical and homogeneous central body

Let us take only the zero term of the gravitational potential into account and synthesize *GRACE* spacecrafts orbits with Kepler elements given in Table (2.1), for 16

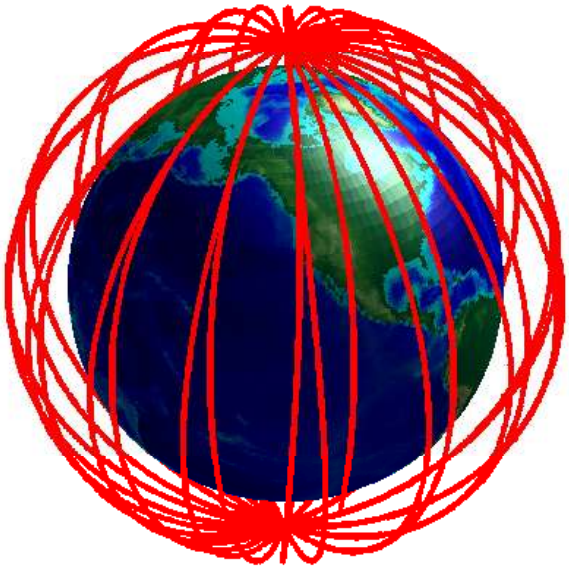

Figure 2.2: one-day revolutions of GRACE

revolutions which is shown in Fig. (2.2). For this simplest form of the field, we can

Table 2.1: GRACE satellites Kepler elements

Element	GRACE-1	GRACE-2
Semi-major axis (km)	6876.4816	6876.9926
Eccentricity	0.00040989	0.00049787
Inclination (Deg.)	89.025446	89.024592
RA Asc. Node (Deg.)	354.447149	354.442784
Arg. Perigee (Deg.)	302.414244	316.073923
Mean Anomaly (Deg.)	80.713591	67.044158

easily derive all required partial derivatives in terms of Cartesian coordinates. Briefly, the first and second partial derivatives are represented:

$$\begin{aligned} V(r) &= \tfrac{GM}{r} \\ \Gamma(x,y,z) &= -\tfrac{GM}{r^3}\mathbf{r} \\ \mathbf{G} &= 3\tfrac{GM}{r^5}\ \mathbf{r}^T \otimes \mathbf{r} - \tfrac{GM}{r^3}\ \mathbf{I}_{3\times 3} \end{aligned} \tag{2.46}$$

Left hand sides of Eqs. (2.25) and (2.44) are calculated. Differences between these values and the observed values are depicted in Figs. (2.3) and (2.4). For better understanding, the results of one revolution are shown.

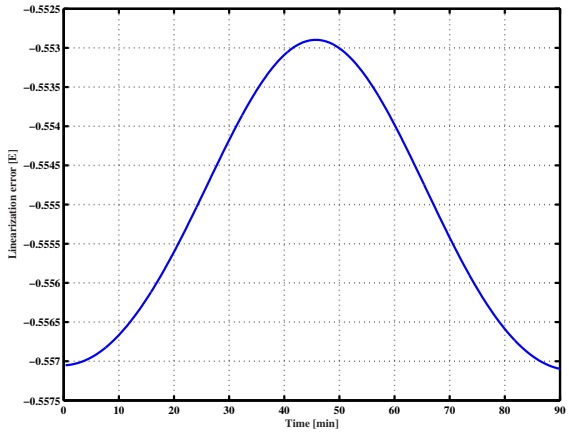

Figure 2.3: Gradiometry equation linearization error for the Earth as a spherical and homogeneous central body

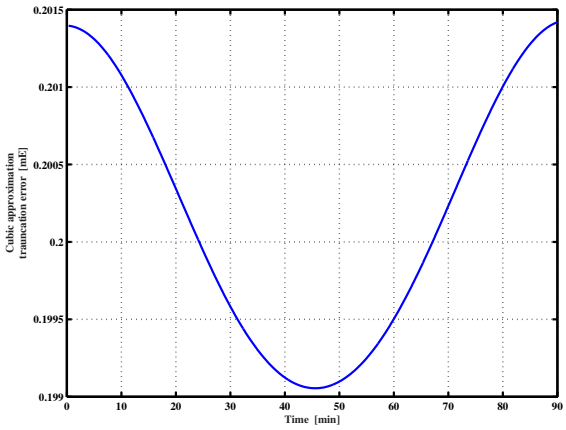

Figure 2.4: Truncation error of cubic approximation of Gradiometry equation for the Earth as a spherical and homogeneous central body

On the other hand, we need a rough estimation of the noise level of the observations to decide whether the contribution of the cubic term is considerable. Table (2.2) gives the simulated values for the GRACE observable and its simulated random error statistics. The simulated Gaussian random noise histograms are visualized in Fig. (2.5).

Table 2.2: Simulated observation statistics

QUANTITY	SIMULATED VALUES				SIMULATED RANDOM ERRORS			
	Min	*Max*	*Mean*	*Std*	*Min*	*Max*	*Mean*	*Std*
ρ	229832.817 m	230277.996 m	230002.083 m	114.243 m	-4.9 mm	4.02 mm	0.00000 mm	1.00 mm
$\dot{\rho}$	-0.35384 m/s	0.35637 m/s	-0.00398 m/s	0.19843 m/s	-10.72665 $\mu m/s$	9.83120 $\mu m/s$	0.00000 $\mu m/s$	2.524078 $\mu m/s$
$\ddot{\rho}$	-0.00075 m/s^2	0.00061 m/s^2	0.0000 m/s^2	0.00041 m/s^2	-139.72849 μGal	150.03429 μGal	0.00000 μGal	35.16657 μGal
$\left\|\Delta\dot{X}\right\|^2 m^2/s^2$	67544.36526	68208.05967	67812.37673	185.85339	-2.38880	1.86700	0.00000	0.498410
l	-1289.4529 E	-1276.0495 E	-1281.8767 E	4.12129 E	-42.07 mE	50.4 mE	0.00000 mE	9.6 mE
$l = \frac{\ddot{\rho}}{\rho} + \frac{\dot{\rho}}{\rho^2} - \frac{\left\|\Delta\dot{X}\right\|^2}{\rho^2}$								

The inter-satellite acceleration is computed using Hermite approximation algorithm. Considering $\sigma_\rho = \pm 1mm$ and $\sigma_{\dot{\rho}} = \pm 2.5\mu m/sec$, results in $\pm 35\mu Gal$ random error in $\ddot{\rho}$ (Keller & Sharifi 2003). The resultant accuracy of final observable is around $9.6mE$ ($1E = 1\,E\ddot{o}tv\ddot{o}s\,Unit = 10^{-9}s^{-2}$). Therefore, it seems that adding higher

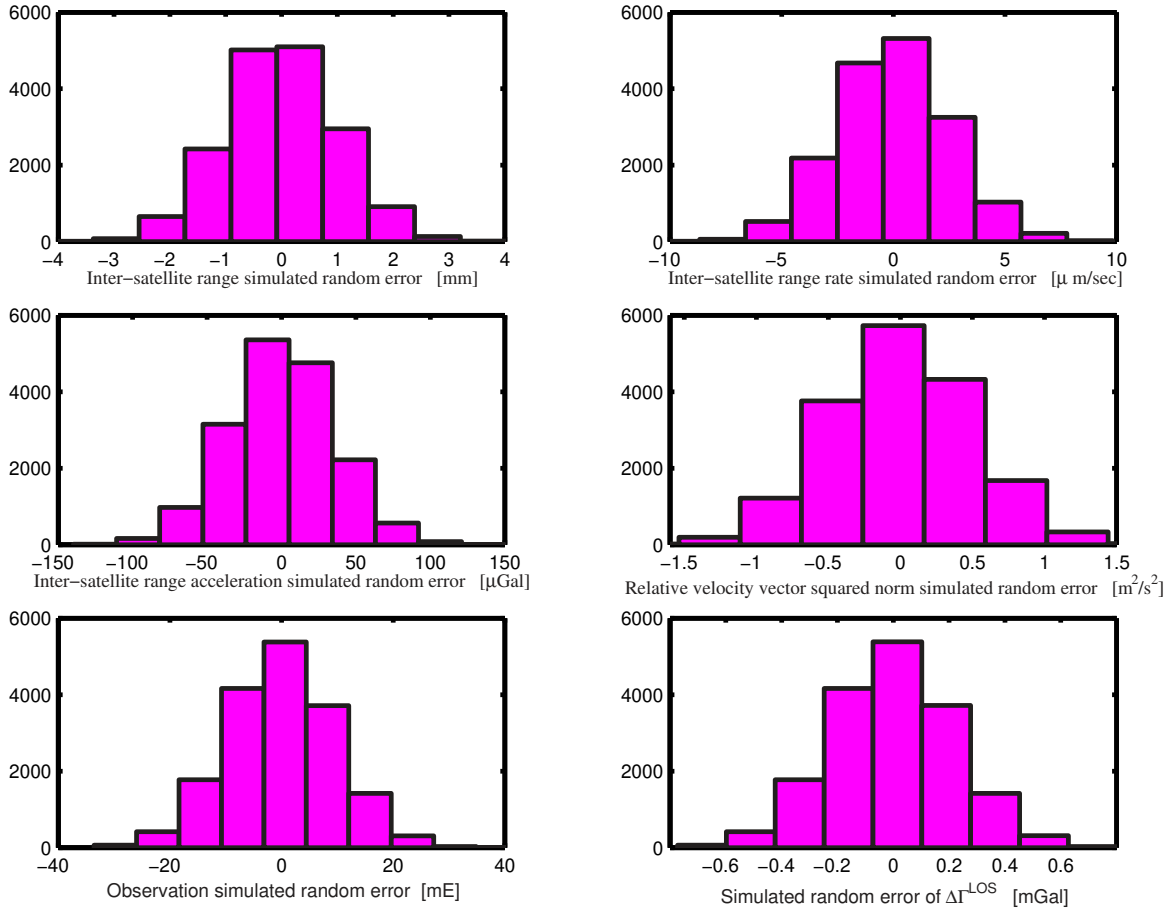

Figure 2.5: Simulated Gaussian random noise

terms of the expansion beyond the cubic term with its really complicated computations is not necessary, whereas having observation random error at the level few mE implies that replacement of gradiometry equation with the linear term of the expansion introduces a systematic error, linearization error, at the level of $-0.5550E \mp 2mE$. This is not acceptable even for zero term approximation of the potential unless we modify the algorithm such that the level of linearization error becomes much more smaller. There exist some modified linear approximation methods which we will describe later in this subsection.

Example 2: Earth as an ellipsoidal and homogeneous central body

To be a bit closer to the real potential, let's take the flattening of the Earth into account:

$$V(r,\phi) = \frac{GM}{r} + \frac{GM}{r}\frac{a^2}{r^2}\bar{C}_{20}\bar{P}_{20}(\sin\phi) \tag{2.47}$$

Writing r and $\bar{P}_{20}(\sin\phi)$ in terms of Cartesian coordinates yields an equivalent expression for the potential in terms of Cartesian coordinates:

$$\bar{P}_{20}(\sin\phi) = \frac{\sqrt{5}}{2}(3\sin^2\phi - 1) = \frac{\sqrt{5}}{2}(3\frac{z^2}{r^2} - 1) = \frac{\sqrt{5}}{2r^2}(2z^2 - x^2 - y^2) \tag{2.48}$$

$$V(x,y,z) = \frac{GM}{\sqrt{x^2+y^2+z^2}} + \frac{\alpha}{[x^2+y^2+z^2]^{\frac{5}{2}}}[2z^2 - x^2 - y^2] \tag{2.49}$$

Where, $\alpha := \frac{\sqrt{5}}{2}GMa^2\bar{C}_{20} \doteq -8.777e+024$ for $EGM96$. We derived the partial derivatives in *example one* directly in terms of Cartesian coordinates. Similarly, we derive the partial derivatives:

$$\Gamma(x,y,z) = -\frac{GM}{r^3}\mathbf{r} - \frac{5\alpha\, q}{r^7}\mathbf{r} - \frac{2\alpha}{r^5}\begin{bmatrix} x \\ y \\ -2z \end{bmatrix} \tag{2.50}$$

$$\begin{aligned}\mathbf{G}(x,y,z) = &\left[\tfrac{35\alpha\ q}{r^9} + \tfrac{20\alpha\, q}{r^7} + 3\tfrac{GM}{r^5}\right]\cdot\mathbf{r}^T\otimes\mathbf{r} - \left[\tfrac{5\alpha\, q}{r^7} + \tfrac{GM}{r^3}\right]\cdot\mathbf{I}_{3\times3} + \\ &\tfrac{20\alpha\, q}{r^7}\begin{bmatrix} 0 & 0 & \frac{-3}{2}xz \\ 0 & 0 & \frac{-3}{2}yz \\ \frac{-3}{2}zx & \frac{-3}{2}zy & z^2 \end{bmatrix} - \tfrac{2\alpha}{r^5}\begin{bmatrix} 1 & 0 & 0 \\ 0 & 1 & 0 \\ 0 & 0 & 2 \end{bmatrix}\end{aligned} \tag{2.51}$$

where, $q := [2z^2 - x^2 - y^2]$.

For the orbit, synthesized in *example one*, we generate a new set of data based on the governing gravitational potential expressed in Eq. (2.49). The comparative study preformed in *example 1* is considered for the Earth as an ellipsoidal and homogeneous central body and achieving results for the linear and cubic approximations are plotted in Figs. (2.6) and (2.7) respectively. As observed, the linearization error fluctuates between -0.564 and -0.547 E, whereas the cubic approximation truncation error ranges between 0.194 and 0.206 mE. These limits are nearly the same as the previous example.

The largest orbit perturbation for all satellite orbits is the so-called J_2-effect caused by the flattening of the Earth and the effect of the next three spherical harmonics in the expansion of the Earth's gravitational field is about two order of magnitude smaller than the perturbation from J_2, *See Fig. (2.8)*. Hence, the most dominant terms of gravitational potential have been taken into account in this analysis and the result is,

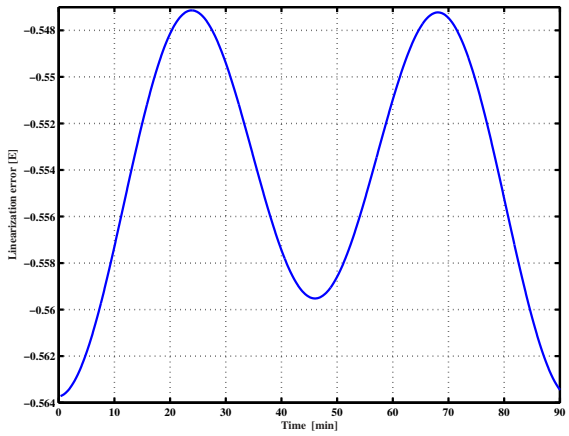

Figure 2.6: Gradiometry equation linearization error for the Earth as an ellipsoidal and homogeneous central body

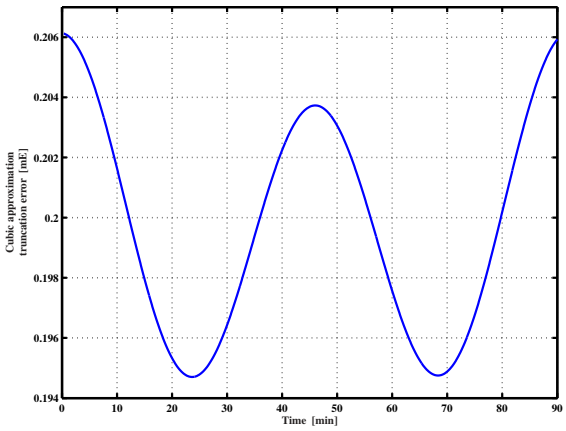

Figure 2.7: Truncation error of cubic approximation of Gradiometry equation for the Earth as an ellipsoidal and homogeneous central body

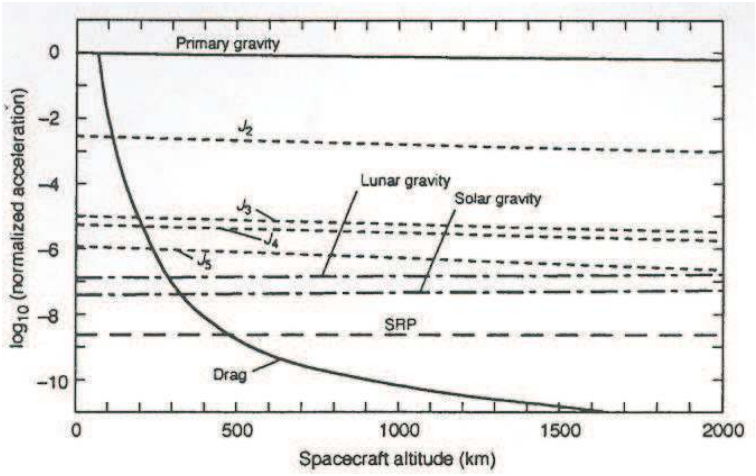

Figure 2.8: Relationship between the orbital height and the magnitude of the perturbing forces.

more or less, valid for the full expansion of the gravitational potential. Accordingly, we have to either use the cubic approximation or modify the linear approximation to achieve a better accuracy. Otherwise, we will degrade the measurements quality with a systematic error whose magnitude is about few hundreds order of measurement noise level. First let us try out the modified linear approximation.

2.2.3 Modified Linear Approximation of the Two Satellites Acceleration Differences Around the Barycenter

In this subsection, we develop mathematical formulations with higher accuracy than linear approximation and less difficulty than cubic approximation. We try to reduce the magnitude of truncation error in Taylor series expansion of the spacecrafts acceleration differences along the LOS. We put forward the following hypothesis for achieving the goal:

the truncation error will decrease if we are able to replace $\mathbf{G}$ *with some incremental quantity,* $\delta\mathbf{G}$*, of the type* $\mathbf{G}$

This approach has already been suggested earlier by Keller and Heß[keller & Heß1998]. Besides the approach implemented in the study, we will survey the idea from different points of view.

To show the truth of our claim, Let's begin with linear approximation. Splitting $\mathbf{G}$ in Eq. (2.27) gives:

$$\mathbf{e}^T \cdot [\mathbf{G}_0 + \delta\mathbf{G}] \cdot \mathbf{e} \stackrel{?}{=} \frac{\ddot{\rho}}{\rho} + \frac{\dot{\rho}^2}{\rho^2} - \frac{\|\Delta\dot{\mathbf{r}}\|^2}{\rho^2} \tag{2.52}$$

in which $\mathbf{G}_0$ is a reference gravitational gradient tensor corresponding to a reference gravitational field, U and $\delta\mathbf{G}$ is but the corresponding incremental gravitational gradient tensor governed by an incremental gravitational potential, δU.

$$\begin{aligned} V &= U + \delta U \\ \nabla^T \otimes \nabla V &= \nabla^T \otimes \nabla U + \nabla^T \otimes \nabla \delta U \end{aligned} \tag{2.53}$$

An equivalent expression to Eq. (2.52) results using Eq. (2.28):

$$\mathbf{e}^T \cdot \delta\mathbf{G} \cdot \mathbf{e} \stackrel{?}{=} \frac{1}{\rho}\langle \Delta\nabla\delta U \ , \ \mathbf{e}\rangle = \frac{\ddot{\rho}}{\rho} + \frac{\dot{\rho}^2}{\rho^2} - \frac{\|\Delta\dot{\mathbf{r}}\|^2}{\rho^2} - \frac{1}{\rho}\langle \Delta\nabla U \ , \ \mathbf{e}\rangle \tag{2.54}$$

Depending on the definition of the reference gravitational field, different solutions will come out. Among them, we will consider the two following categories:

- *second-order reference field*.

  This is the classical definition of either spherical or ellipsoidal gravitational reference field. Having the common terminology to classical physical geodesy, we

rewrite Eqs. (2.53) and (2.54) using classical notations:

$$V = U + T \tag{2.55}$$

$$\mathbf{e}^T \cdot \mathbf{G}_T \cdot \mathbf{e} \stackrel{?}{=} \frac{1}{\rho}\langle \Delta\delta\Gamma \ , \ \mathbf{e}\rangle = \frac{\ddot{\rho}}{\rho} + \frac{\dot{\rho}^2}{\rho^2} - \frac{\|\Delta\dot{\mathbf{r}}\|^2}{\rho^2} - \frac{1}{\rho}\langle \Delta\gamma \ , \ \mathbf{e}\rangle \tag{2.56}$$

where, T stands for gravitational disturbing potential.

- *higher-order reference field*.

  Instead of subtracting the effect of only first one or two zonal terms, we subtract the effect of an spheroidal gravitational reference field derived from other satellite missions. Like the notations used by many authors (e.g., [Vaníček & Krakiwsky 1986], [Vaníček & Sjöberg 1991] or [Martinek & Vaníček 1997]), it is denoted by V_l and corresponds to the first l degree terms of gravitational potential harmonic expansion. *EIGEN-2*, for instance, can be assumed as a reference spheroid which is derived from *CHAMP* mission. This actually splits the gravitational potential into the (a priori information) low-degree reference potential V_l and a (unknown) higher-degree gravitational potential V^l:

$$V = V_l + V^l \tag{2.57}$$

$$\Gamma = \Gamma_l + \Gamma^l \tag{2.58}$$

  and the preceding relation in the modified form is:

$$\mathbf{e}^T \cdot \mathbf{G}^l \cdot \mathbf{e} \stackrel{?}{=} \frac{1}{\rho}\langle \Delta\Gamma^l \ , \ \mathbf{e}\rangle = \frac{\ddot{\rho}}{\rho} + \frac{\dot{\rho}^2}{\rho^2} - \frac{\|\Delta\dot{\mathbf{r}}\|^2}{\rho^2} - \frac{1}{\rho}\langle \Delta\Gamma_l \ , \ \mathbf{e}\rangle \tag{2.59}$$

  where, $\mathbf{G}^l$ stands for higher-degree($\geq l$) gravitational gradient tensor.

Applying this strategy for dealing with linearization error leads to mapping the residual field, V^l, instead of V. Therefore, the estimated residual field is dependent on how we combine a priori information with the *GRACE* observable to remove the effect of the reference field. Two different approaches can be followed to perform data fusion:

- removing the effect of the reference field as a deterministic trend of *GRACE*

observations.

It is equivalent to assume a priori information as a vector of known values or a vector of observation with the following definition of weight matrix.

$$\Sigma_{ll}^{-1} \cong diag\{\ \infty \quad \infty \quad \cdots \quad \infty\ \} \tag{2.60}$$

- removing the effect of the reference field as a stochastic trend of *GRACE* measurements.

  This means considering the a priori information as a vector of observed values or a vector of observation with a given full variance-covariance matrix.

$$\Sigma_{ll}^{-1} = \Sigma_{o}^{-1} \tag{2.61}$$

  Where, Σ_o is the variance-covariance matrix of the data employed as a reference field. Using the accompanying error estimating data, at least we can define a diagonal matrix, instead.

Both cases play the same role in linearization error improvement. So, in first part of our analysis, we do not distinguish between them. Herein, we will just implement the first approach only for low-degree $n \leq 2$ and keep the other approach open for the future studies.
To clear up, let's recalculate *example 2* to see how much improvement can be obtained due to implementation of this modification.

Example 3: spherical reference field

Assuming the reference field generator as a homogenous spherical central body, decomposes the potential, acceleration and acceleration gradient in Eqs. (2.49) and (2.50) as follows:

$$U(x,y,z) = \frac{GM}{\sqrt{x^2+y^2+z^2}} \tag{2.62}$$

$$\gamma(x,y,z) = -\frac{GM}{\left[x^2+y^2+z^2\right]^{\frac{3}{2}}}\mathbf{r} \tag{2.63}$$

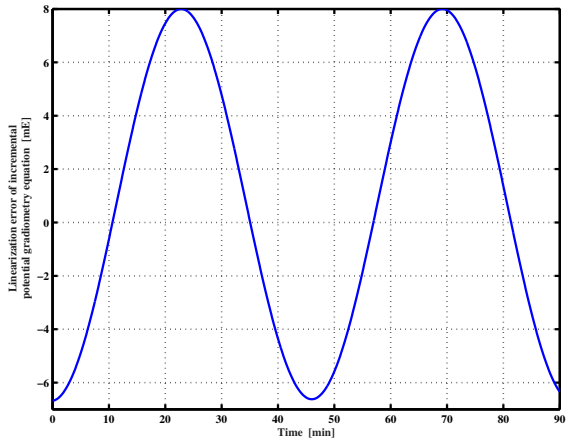

Figure 2.9: Linearization error of incremental potential

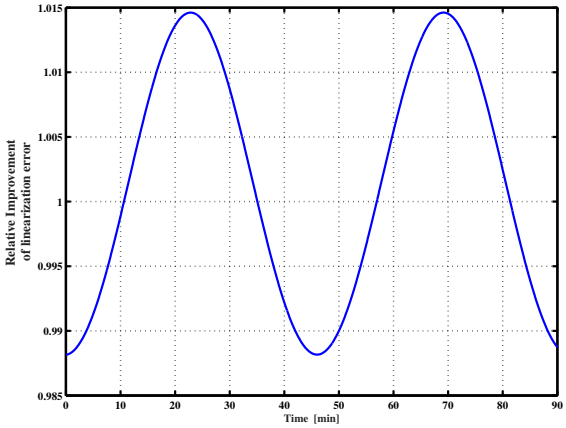

Figure 2.10: Relative improvement of linearization error

$$\mathbf{G}_U = 3\frac{GM}{r^5}\ \mathbf{r}^T \otimes \mathbf{r} - \frac{GM}{r^3}\ \mathbf{I}_{3\times 3} \tag{2.64}$$

$$T(x,y,z) = \frac{\alpha}{[x^2+y^2+z^2]^{\frac{5}{2}}}[2z^2 - x^2 - y^2] \tag{2.65}$$

$$\delta\Gamma(x,y,z) = -\frac{5\alpha\, q}{r^7}\mathbf{r} - \frac{2\alpha}{r^5}\begin{bmatrix} x \\ y \\ -2z \end{bmatrix} \tag{2.66}$$

$$\begin{aligned} \mathbf{G}_T = &\left[\tfrac{35\alpha\ q}{r^9} + \tfrac{20\alpha\ q}{r^7}\right]\cdot \mathbf{r}^T \otimes \mathbf{r} - \tfrac{5\alpha\, q}{r^7}\cdot \mathbf{I}_{3\times 3} + \\ &\tfrac{20\alpha\ q}{r^7}\begin{bmatrix} 0 & 0 & \frac{-3}{2}xz \\ 0 & 0 & \frac{-3}{2}yz \\ \frac{-3}{2}zx & \frac{-3}{2}zy & z^2 \end{bmatrix} - \tfrac{2\alpha}{r^5}\begin{bmatrix} 1 & 0 & 0 \\ 0 & 1 & 0 \\ 0 & 0 & 2 \end{bmatrix} \end{aligned} \tag{2.67}$$

Consequently, Fig. (2.6) will be changed into Fig. (2.9). Relative improvement of linearization error is depicted in Fig. (2.10). The linearization error has been improved significantly. However, it is at the same level as a minority of measurement noises are. Thus, we continue the investigation in order to find a better solution.

Example 4: Ellipsoidal reference field

As shown in Fig. (2.8), depart from zero and second order terms, J_3, J_4 and J_5 are the main dominant terms of gravitational perturbing forces. So, we consider the gravitational field generated by these higher zonal terms for evaluation of the effect

of removing contribution of an ellipsoidal reference field to the linearization error improvement.

$$V(r,\phi) = \frac{GM}{r}\left[1 + \sum_{n=2}^{5}(\frac{a}{r})^n \bar{C}_{n0}\bar{P}_{n0}(\sin\phi)\right] \tag{2.68}$$

And in terms of Cartesian coordinates:

$$V(x,y,z) = \frac{GM}{\sqrt{x^2+y^2+z^2}}\left[1 + \sum_{n=2}^{5}\alpha_n(x^2+y^2+z^2)^{-\frac{n}{2}}\bar{P}_{n0}(t)\right] \tag{2.69}$$

where, $t = \frac{z}{r}$ and $\alpha_n := a^n\bar{C}_{n0}$. Numerical values of these coefficients computed using $EGM96$ coefficients are given in Table (2.3):

Table 2.3: $\bar{C}_{n0}$ and α_n numerical values

n	$\bar{C}_{n0}$	α_n
2	-0.000484165371736	-3.088072732672375e+003
3	9.57254173792e-007	3.894169583506121e+007
4	5.39873863789e-007	1.400792121674252e+014
5	6.8532347563e-008	1.134150770225133e+020

$\bar{P}_{n0}(t)$ functions are derived using recurrence relations given in Eqs. (2.35) and (2.36):

$$\bar{P}_{20}(t) = \frac{\sqrt{5}}{2}\left[3t^2-1\right] \tag{2.70}$$

$$\bar{P}_{30}(t) = \frac{\sqrt{7}}{2}\left[5t^3-3t\right] \tag{2.71}$$

$$\bar{P}_{40}(t) = \frac{3}{8}\left[35t^4-30t^2+3\right] \tag{2.72}$$

$$\bar{P}_{50}(t) = \frac{\sqrt{11}}{8}\left[63t^5-70t^3+15t\right] \tag{2.73}$$

And corresponding acceleration vector is:

$$\Gamma(x,y,z) = -\frac{GM}{r^3}\mathbf{r} - \frac{GM}{r^3}\sum_{n=2}^{5}(n+1)\alpha_n r^{-n}\bar{P}_n(t)\mathbf{r} + \frac{GM}{r}\sum_{n=2}^{5}\alpha_n r^{-n}\frac{\partial\bar{P}_n(t)}{\partial t}\frac{\partial t}{\partial \mathbf{r}} \tag{2.74}$$

where,

$$\frac{\partial t}{\partial \mathbf{r}} = \frac{1}{r^3}\begin{bmatrix} -xz \\ -yz \\ x^2+y^2 \end{bmatrix} \tag{2.75}$$

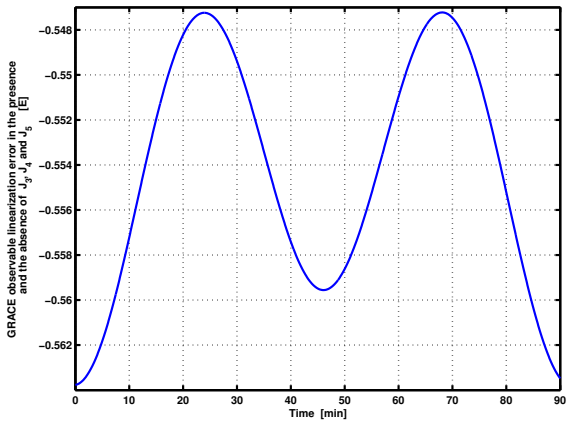

Figure 2.11: Linearization error in the presence of J_3, J_4 and J_5

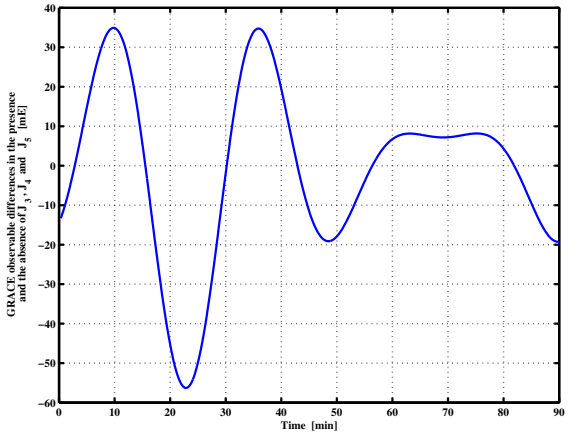

Figure 2.12: Observable differences in the presence and the absence of J_3, J_4 and J_5

For computing the partial derivatives of $\bar{P}_n(t)$ appeared in Eq. (2.74), Eq. (2.36) is modified slightly for ease of implementation:

$$\begin{aligned} \frac{\partial \bar{P}_n}{\partial t} &= f_3[f_4(\bar{P}_{n-1} + t\frac{\partial \bar{P}_{n-1}}{\partial t}) - f_5\frac{\partial \bar{P}_{n-2}}{\partial t}] \\ \frac{\partial^2 \bar{P}_n}{\partial t^2} &= f_3[f_4(2\frac{\partial \bar{P}_{n-1}}{\partial t} + t\frac{\partial^2 \bar{P}_{n-1}}{\partial t^2}) - f_5\frac{\partial^2 \bar{P}_{n-2}}{\partial t^2}] \end{aligned} \tag{2.76}$$

For initialization, we use:

$$\begin{aligned} \bar{P}_0 = 1 \qquad & \frac{\partial \bar{P}_0}{\partial t} = 0; \qquad \frac{\partial^2 \bar{P}_0}{\partial t^2} = 0 \\ \bar{P}_1 = \sqrt{3}t \qquad & \frac{\partial \bar{P}_1}{\partial t} = \sqrt{3} \qquad \frac{\partial^2 \bar{P}_1}{\partial t^2} = 0 \end{aligned} \tag{2.77}$$

Accordingly, the second order partial derivatives of the potential are computed using the recurrence formula given in Eq. (2.76). Herein, the derivatives are not presented to put it shortly.

The synthesized orbit in the preceding examples is determined based on the gravitational model given in Eq. (2.69). The observable linearization error and its differences in the presence and the absence of higher order terms of gravitational potential, J_3, J_4 and J_5, are visualized in Figs. (2.11) and (2.12). Comparing these two figures with Fig. (2.6) shows that departing from zero term, J_2 is the most dominant term of the gravitational potential.

To examine the efficiency of proposed idea, the effect of an ellipsoidal gravitational reference field is subtracted from the measurements and the analysis is done for the

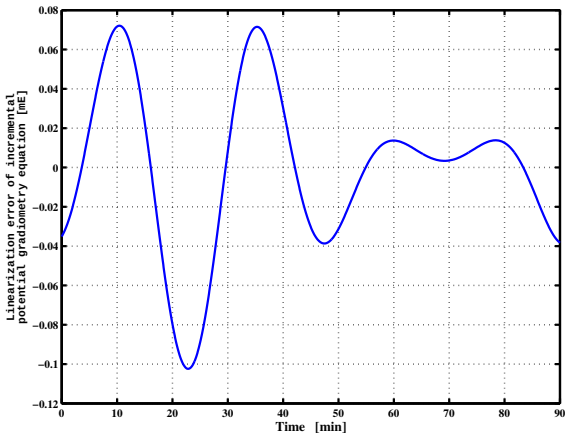

Figure 2.13: Linearization error of incremental potential after removing ellipsoidal reference field

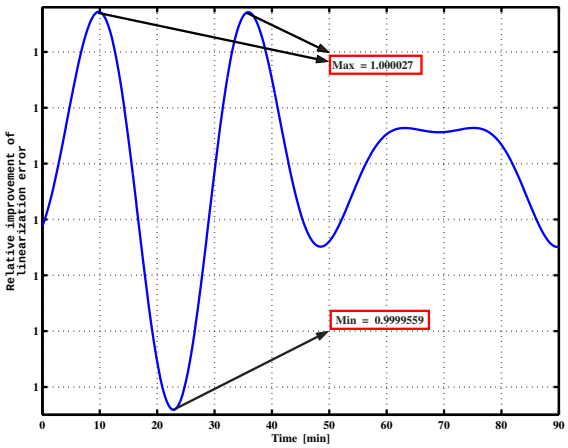

Figure 2.14: Relative improvement of linearization error after removing ellipsoidal reference field

remaining part of the field. As seen in Fig. (2.13), the linearization error level is much more lower than observation noise level. Fig. (2.14) shows nearly 100% improvement for all the points as well. In other words, it is an evidence for acceptability of our hypothesis.

Example 5: Spheroidal reference field

As already mentioned, *EIGEN-2* is an example of satellite-based Earth Gravitational Model which is derived from altogether six months of *CHAMP* data. It is a *CHAMP-only* gravity field model obtained from *CHAMP GPS* satellite-to-satellite and accelerometer data out of the period 2000, July to December, and 2001, September to December. The *EIGEN-2* solution contains fully normalized spherical harmonic coefficients complete to degree/order 120. Degree variances are computed for both *EIGEN-2* and *EGM96* using Eq. (2.78) which relates degree variances to fully normalized harmonic coefficients $\bar{c}_{nm}$ and $\bar{s}_{nm}$ [Heiskanen & Moritz 1967].

$$c_n = \sum_{m=0}^{n} \bar{c}_{nm}^2 + \bar{s}_{nm}^2 \tag{2.78}$$

Fig. (2.15) shows the concluding results. As it is clear, the two model discrepancies become visible for spherical harmonic degree higher than 50.

One-day *GRACE* gravitational potential and *LOS* acceleration differences are com-

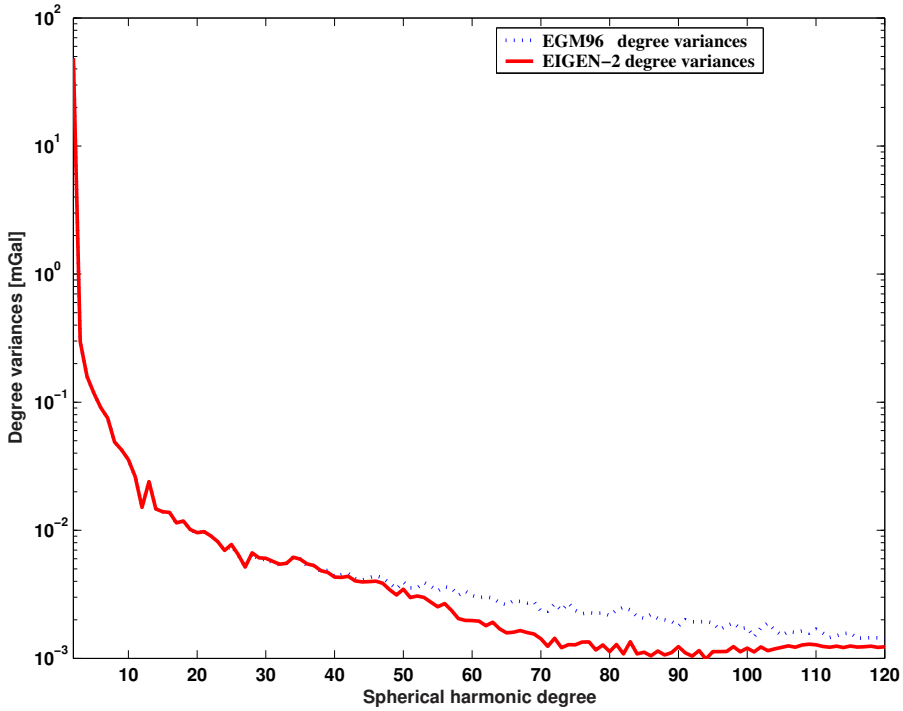

Figure 2.15: Degree variances

puted using both *EIGEN-2* and *EGM96*, and the differences are depicted in Figs. (2.16) and (2.17). The potential differences are at the level of $0.0218 \pm 0.5342\ m^2/s^2$ whereas, LOS acceleration differences differ from the other at the level of -0.0046 ± 11.4736 mE. The spherical harmonic coefficients differences lead to such variations in $GRACE$ observable. Let us assume LOS acceleration differences generated by $EGM96$ as the observation vector and the other as the contribution of the spheroidal reference field to the observable. *What would be the differences interpretation then?* It means that the differences at the reduce observable, $GRACE$ observable in which the contribution of reference field has been removed, might be meaningful. In other words, the differences standard deviation is about few order of observation noise level magnitude even though the mean value tends to be zero. *see Figs. (2.20) and (2.21).* The effect of mentioned error on the linearized gradiometry equation is depicted in Fig. (2.22), whereas, Fig. (2.23) shows its spectral density function. The pattern appeared in acceleration differences *psd function* has been appeared in linearized gradiometry equation as well. Therefore, we should be careful not to contaminate the observations in reduction process with a random noise sequences whose power spectrum is much more

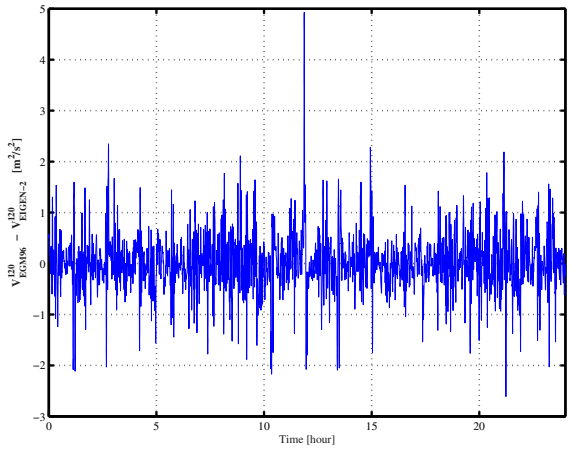

Figure 2.16: *GRACE* potential differences

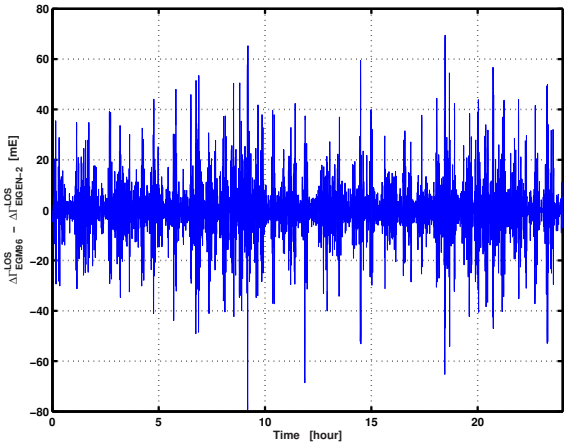

Figure 2.17: *GRACE* LOS acceleration differences

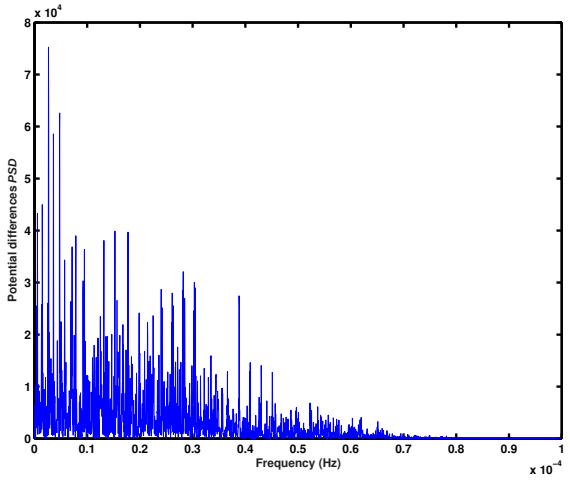

Figure 2.18: *GRACE* potential differences power spectral density function

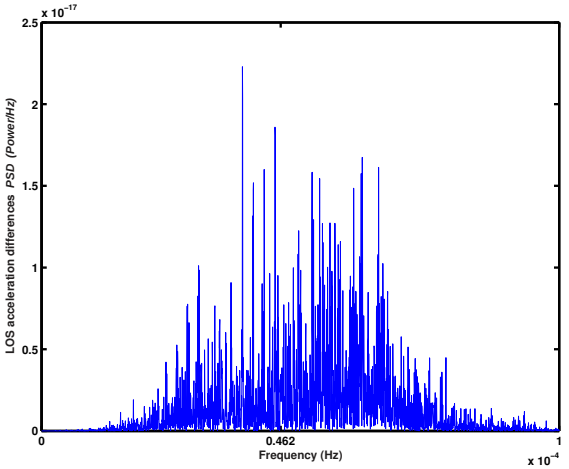

Figure 2.19: *GRACE* LOS acceleration differences power spectral density function

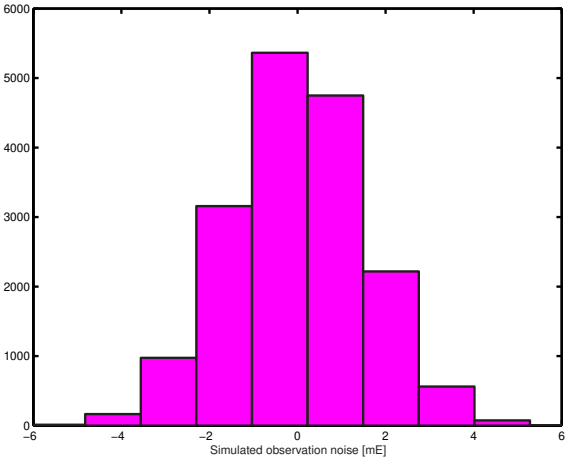

Figure 2.20: *GRACE* observable simulated random error

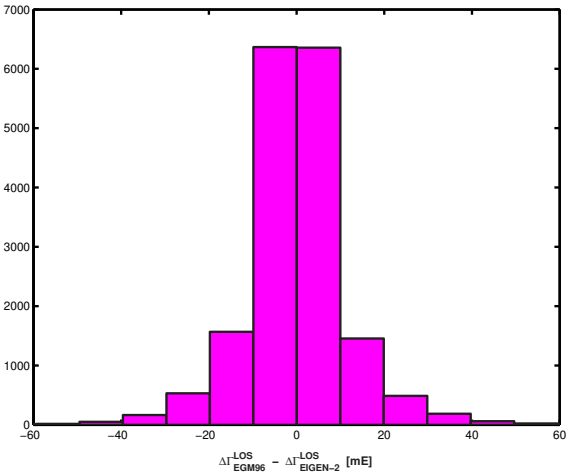

Figure 2.21: *GRACE* LOS acceleration differences histogram

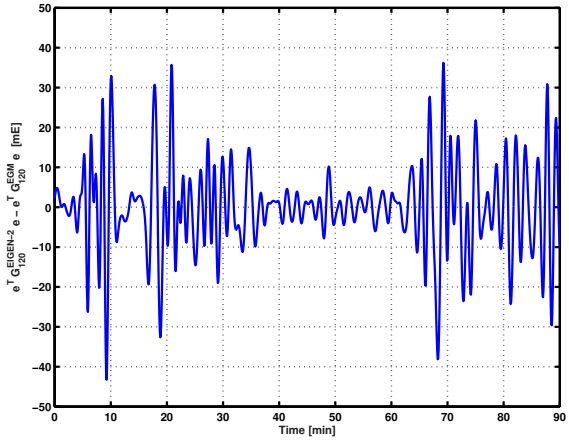

Figure 2.22: Linearized gradiometry equation differences

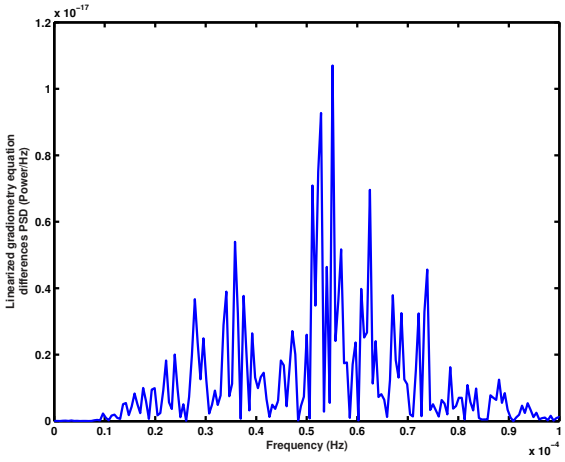

Figure 2.23: Linearized gradiometry equation differences PSD function

wider than the observations'. Merging the reference field functionals as a vector of quasi-observations with the measurements, would be the best way to minimize any interference of the errors of the mentioned type.

Apart from differences in different realizations of the gravitational field, let's compute the linearization error of the reduced observable. As visualized in Fig. (2.25), the linearization error is in the range of -7.13 to 7.715 mE whereas using $EGM96$ model upto an equivalent degree, 120, will squeeze the error to ± 0.80 mE. Therefore, the linearization error as a systematic type of error can be ignored due to its negligible magnitude with respect to the higher level of resultant random errors of the observable.

2.2.4 Cubic-Linear Approximation of the Two Satellites Acceleration Differences Around the Barycenter

In this subsection, we develop a new mathematical model for the acceleration differences approximation in which $GRACE$ appears as a standalone space-born gradiometer with an acceptable accuracy without any other gravity dedicated satellite mission contribution. We use cubic approximation for low-degree (≤ 2) gravitational potential whereas we retain the linear approximation for the higher degree terms. There is two reasons for applying this mixed approximation:

- J_0 and J_2 are dominant, so any attempt for a better approximation of the cor-

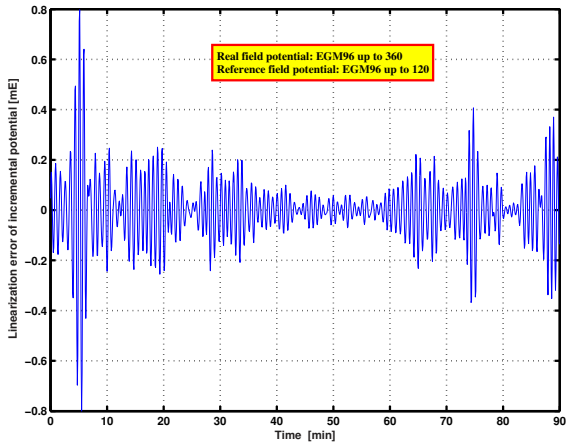

Figure 2.24: Linearization error of incremental potential($EGM96$ upto degree 120 as the reference field)

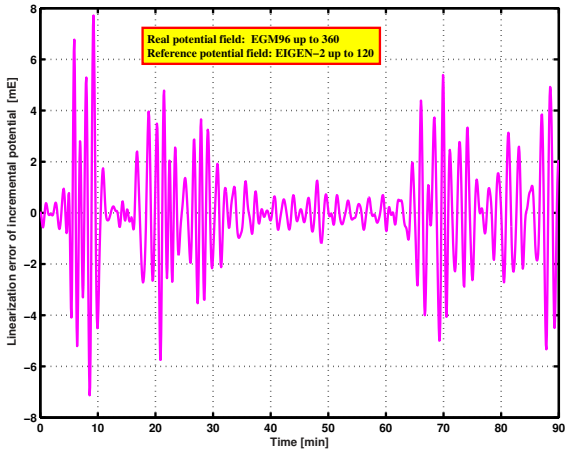

Figure 2.25: Linearization error of incremental potential ($EIGEN$-2 as the reference field)

responding quantities leads to better results.

- We are getting in difficulty in harmonic series expansion of sectorial and tesseral harmonic computations in terms of Cartesian coordinates. As seen, the zonal terms have much less difficulty. J_0 and J_2, as the first two terms of zonal harmonics, are perfectly straightforward.

Let us thus split the gravitational potential V into the low-degree ($l \leq 2$) potential, V_2 and a higher degree gravitational potential, V^2:

$$V = V_2 + V^2 \tag{2.79}$$

$$\Gamma = \Gamma_2 + \Gamma^2 \tag{2.80}$$

$$\mathbf{G} = \mathbf{G}_2 + \mathbf{G}^2 \tag{2.81}$$

Accordingly, the cubic term, the second term in right hand side of Eq. (2.45) is split up into two terms:

$$\begin{aligned} &\mathbf{e}^T \cdot \mathbf{G} \cdot \mathbf{e} + \tfrac{1}{3!2^2}\mathbf{e}^T \otimes \Delta\mathbf{r}^T \otimes \Delta\mathbf{r}^T \cdot (\nabla \otimes \nabla \otimes \mathbf{G}_2) \cdot \mathbf{e} \\ &+\tfrac{1}{3!2^2}\mathbf{e}^T \otimes \Delta\mathbf{r}^T \otimes \Delta\mathbf{r}^T \cdot (\nabla \otimes \nabla \otimes \mathbf{G}^2) \cdot \mathbf{e} \stackrel{?}{=} \tfrac{\ddot{\rho}}{\rho} + \tfrac{\dot{\rho}^2}{\rho^2} - \tfrac{\|\Delta\dot{\mathbf{r}}\|^2}{\rho^2} \end{aligned} \tag{2.82}$$

Instead of neglecting the cubic term totally, we only ignore the third term in left hand side of Eq. (2.82) and set up a new gradiometry observation equation:

$$\mathbf{e}^T \cdot \mathbf{G} \cdot \mathbf{e} + \tfrac{1}{3!2^2}\mathbf{e}^T \otimes \Delta\mathbf{r}^T \otimes \Delta\mathbf{r}^T \cdot (\nabla \otimes \nabla \otimes \mathbf{G}_2) \cdot \mathbf{e} \stackrel{?}{=} \tfrac{\ddot{\rho}}{\rho} + \tfrac{\dot{\rho}^2}{\rho^2} - \tfrac{\|\Delta\dot{\mathbf{r}}\|^2}{\rho^2} \qquad (2.83)$$

The additional term contains contribution of J_0 and J_2 into the cubic term in the Taylor expansion of the acceleration differences which is the major introduced contribution among the others. Hence, it shall improve the truncation error significantly. Figs. (2.4) and (2.7) bear witness to high performance of the proposed idea. To be confident about using the derived equation as an alternative form of gradiometry observation equation, let us first see the numerical behavior of the proposed technique in truncation error improvement. Later on, we will set up the linear system of equations to estimate any set of requested harmonic coefficients.

Example 6: Cubic-Linear approximation

Let us consider the gravitational potential given in *example 4*. We preform all the computation which is done in the example unless we do not subtract the effect of ellipsoidal reference field. Instead, we will add just the contribution of J_0 and J_2 to the cubic term in left hand side of equations[2]. In order to obtain the added term, we apply $\nabla \otimes \nabla\otimes$ on Eq. (2.51). The result is a 27×3 matrix for each evaluation point in the orbit which is substituted into the Eq. (2.83) set up for the point. Improvement rate of truncation error can be figured out by comparing the two sides of the following equality, which corresponds to the equality given in Eq. (2.28) for the preceding form of linear approximation:

$$\mathbf{e}^T \cdot \mathbf{G} \cdot \mathbf{e} + \frac{1}{3!2^2}\mathbf{e}^T \otimes \Delta\mathbf{r}^T \otimes \Delta\mathbf{r}^T \cdot (\nabla \otimes \nabla \otimes \mathbf{G}_2) \cdot \mathbf{e} \stackrel{?}{=} \langle \Delta\Gamma \, , \, \frac{\mathbf{e}}{\rho} \rangle = \frac{1}{\rho}\Delta\Gamma^{LOS} \qquad (2.84)$$

The achieving results are plotted in Figs. (2.26) and (2.27). The truncation error is at level of 0.1995 $\pm$0.0416 mE whose *magnitude* is about one seventh of observation random error. Even though the mixed method of approximation has less efficiency with respect to the previously mentioned modification methods, it squeezes the systematic

[2]A geocentric coordinate system is considered as the Earth-fixed coordinate system

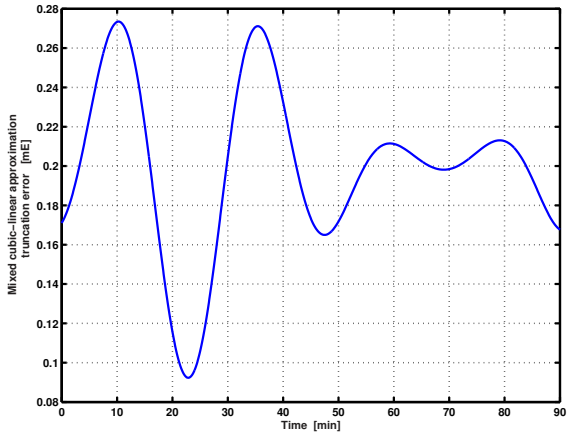

Figure 2.26: Mixed cubic-linear approximation truncation error in the presence of J_3, J_4 and J_5

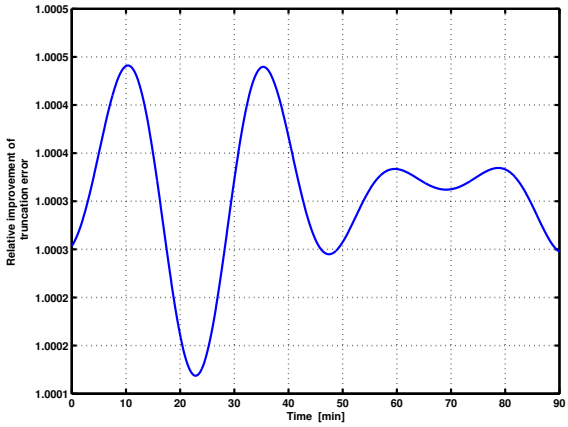

Figure 2.27: Mixed cubic-linear approximation relative improvement in the presence of J_3, J_4 and J_5

error into the random error level.

Fig. (2.28) shows mixed approximation of gradiometry equation of the real field ($EGM96$ upto degree 360). As it can be seen, the systematic error has decreased to the level of $\pm 14\ mE$ in its worst case. In Fig. (2.29), gradiometry equation mixed approximation error of the earth gravitational potential as an ellipsoidal field is compared with the real field. The error of higher degree ($l > 2$) harmonics as a high frequency signal is superimposed on the ellipsoidal field error. Hence, modelling the dominant part, significantly improves the linearization error.

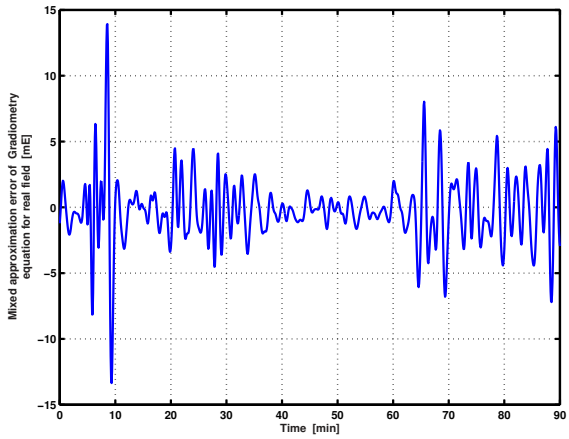

Figure 2.28: Mixed cubic-linear approximation truncation error of the real field

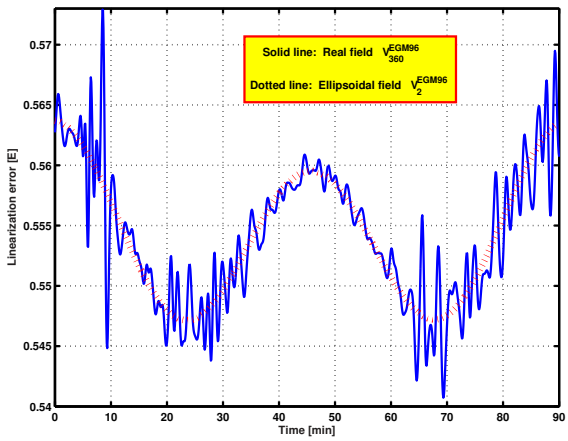

Figure 2.29: A comparison between linearization error of the earth gravitational potential as an ellipsoidal field and the real field

To put it in a nutshell, mixed cubic-linear innovation is a totally independent approximation method which assures us of omitting the major part of the linearization error with minimum possible complexity in comparison with the linear observation equation.

2.3 Set up of Linear System of Equations

In this section, we set up the linear system of equations corresponding to the different mathematical formulations of the problem. Independent of the type of mathematical formulations, vector of unknowns consists of $\bar{c}_{nm}$ & $\bar{s}_{nm}$, fully normalized harmonics coefficients of the gravitational potential expansion. However, each of them has its own particular design matrix. Herein, the design matrix description is in accordance with the mathematical model classification.

- along track acceleration differences as the observable
- gravitational acceleration gradient of the barycenter of the twin satellites as the observable (*linear approximation*)
- incremental acceleration gradient of the barycenter of the twin satellites as the observable
- gravitational acceleration gradient of the barycenter of the twin satellites as the observable (*mixed cubic-linear approximation*)

Each item is described with more details in the subsequent pages.

2.3.1 Along Track Acceleration Differences as the Observable

As already mentioned in section 2.1, each evaluation point, t, introduces an equation of the type of Eq. (2.13) in the linear system of equations. Instead of Eq. (2.5), representation of gravitational potential, let's use the compact form of the potential (e.g. [Heiskanen & Moritz 1967]) in order to simplify the representation of the observation equations:

$$V(\lambda,\phi,r) = \frac{GM}{r}\sum_{n=0}^{N_{max}}(\frac{R}{r})^n\sum_{m=0}^{n}\bar{c}_{nm}\bar{R}_{nm}(\phi,\lambda)+\bar{s}_{nm}\bar{S}_{nm}(\phi,\lambda) \qquad (2.85)$$

And its partial derivatives with respect to the spherical coordinates are:

$$V_{r,\phi,\lambda} = \frac{GM}{r}\sum_{n=0}^{N_{max}}(\frac{R}{r})^n\sum_{m=0}^{n}\begin{bmatrix} -\frac{n+1}{r}\bar{R}_{nm} \\ \bar{R}'_{nm} \\ -m\bar{S}_{nm} \end{bmatrix}\bar{c}_{nm} + \begin{bmatrix} -\frac{n+1}{r}\bar{S}_{nm} \\ \bar{S}'_{nm} \\ m\bar{R}_{nm} \end{bmatrix}\bar{s}_{nm} \tag{2.86}$$

where,

$$\bar{R}_{nm} = \bar{R}_{nm}(\phi,\lambda) = \cos m\lambda\,\bar{P}_{n,m}(\sin\phi) \tag{2.87}$$

$$\bar{S}_{nm} = \bar{S}_{nm}(\phi,\lambda) = \sin m\lambda\,\bar{P}_{n,m}(\sin\phi) \tag{2.88}$$

$$\bar{R}'_{nm} = \bar{R}'_{nm}(\phi,\lambda) = \cos m\lambda\,\bar{P}'_{n,m}(\sin\phi) \tag{2.89}$$

$$\bar{S}'_{nm} = \bar{S}'_{nm}(\phi,\lambda) = \sin m\lambda\,\bar{P}'_{n,m}(\sin\phi) \tag{2.90}$$

According to Eq. (2.9):

$$V_{x,y,z} = \frac{GM}{r}\sum_{n=0}^{N_{max}}(\frac{R}{r})^n\sum_{m=0}^{n}\mathbf{J}\begin{bmatrix} -\frac{n+1}{r}\bar{R}_{nm} \\ \bar{R}'_{nm} \\ -m\bar{S}_{nm} \end{bmatrix}\bar{c}_{nm} + \mathbf{J}\begin{bmatrix} -\frac{n+1}{r}\bar{S}_{nm} \\ \bar{S}'_{nm} \\ m\bar{R}_{nm} \end{bmatrix}\bar{s}_{nm} \tag{2.91}$$

Writing Eq. (2.91) for both satellites at each evaluation point and substituting in Eq. (2.2) leads to:

$$\begin{aligned}\Delta\ddot{\mathbf{r}} = \frac{GM}{R}\sum_{n=0}^{N_{max}}(\frac{R}{r_2})^{n+1}\sum_{m=0}^{n} \\ \left\{\mathbf{J}_2\begin{bmatrix} -\frac{n+1}{r_2}\bar{R}_{nm} \\ \bar{R}'_{nm} \\ -m\bar{S}_{nm} \end{bmatrix}_{\mathbf{2}} - (\frac{r_2}{r_1})^{n+1}\mathbf{J}_1\begin{bmatrix} -\frac{n+1}{r_1}\bar{R}_{nm} \\ \bar{R}'_{nm} \\ -m\bar{S}_{nm} \end{bmatrix}_{\mathbf{1}}\right\}\bar{c}_{nm} \\ \left\{\mathbf{J}_2\begin{bmatrix} -\frac{n+1}{r_2}\bar{S}_{nm} \\ \bar{S}'_{nm} \\ m\bar{R}_{nm} \end{bmatrix}_{\mathbf{2}} - (\frac{r_2}{r_1})^{n+1}\mathbf{J}_1\begin{bmatrix} -\frac{n+1}{r_1}\bar{S}_{nm} \\ \bar{S}'_{nm} \\ m\bar{R}_{nm} \end{bmatrix}_{\mathbf{1}}\right\}\bar{s}_{nm}\end{aligned} \tag{2.92}$$

Replacing Eq. (2.92) into Eq. (2.1) gives:

$$\Delta\Gamma^{LOS} = \langle \Delta\ddot{\mathbf{r}}\ ,\ \mathbf{e}\rangle = \mathbf{e}^T \cdot \Delta\ddot{\mathbf{r}} = \frac{GM}{R}\sum_{n=0}^{N_{max}}(\frac{R}{r_2})^{n+1}\sum_{m=0}^{n}$$

$$\mathbf{e}^T\left\{\mathbf{J}_2\begin{bmatrix} -\frac{n+1}{r_2}\bar{R}_{nm} \\ \bar{R}'_{nm} \\ -m\bar{S}_{nm}\end{bmatrix}_{\mathbf{2}} - (\frac{r_2}{r_1})^{n+1}\mathbf{J}_1\begin{bmatrix} -\frac{n+1}{r_1}\bar{R}_{nm} \\ \bar{R}'_{nm} \\ -m\bar{S}_{nm}\end{bmatrix}_{\mathbf{1}}\right\}\bar{c}_{nm}$$

$$\mathbf{e}^T\left\{\mathbf{J}_2\begin{bmatrix} -\frac{n+1}{r_2}\bar{S}_{nm} \\ \bar{S}'_{nm} \\ m\bar{R}_{nm}\end{bmatrix}_{\mathbf{2}} - (\frac{r_2}{r_1})^{n+1}\mathbf{J}_1\begin{bmatrix} -\frac{n+1}{r_1}\bar{S}_{nm} \\ \bar{S}'_{nm} \\ m\bar{R}_{nm}\end{bmatrix}_{\mathbf{1}}\right\}\bar{s}_{nm} \qquad (2.93)$$

The expressions given in the curly brackets are nothing else but the coefficients of $\bar{c}_{nm}$ & $\bar{s}_{nm}$ which are calculated at each evaluation point. As already mentioned, each evaluation point corresponds to a row in design matrix, $\mathbf{A}$. Hence, assuming N_{max} as the maximum resolvable degree of harmonic coefficients, results a row vector of the size $(N_{max}+1)^2$, number of unknown coefficients[1], whose entries are $\bar{c}_{nm}$ & $\bar{s}_{nm}$ coefficients. Having a sequence of observations with M evaluation points, sets up the design matrix of linear system of equation $\mathbf{A}_{M\times(N_{max}+1)^2}$.

2.3.2 Gravitational Acceleration Gradient of the Barycenter of the Twin Satellites as the Observable (*Linear Approximation*)

Linear system of gradiometry equations can be expressed similarly in term of design matrix and vector of unknowns. According to Eq. (2.39), in addition to first partial derivatives, we need second partial derivatives of the potential as well. So, let's express the compact form of the second order partial derivatives in terms of R_{nm} and S_{nm} and

[1]Of course the total number of unknowns is $(N_{max}+1)(N_{max}+2)$ but the zonal harmonic coefficients of the type $\bar{S}_{nm}$, $\bar{S}_{n0}$, are inestimable. Therefore, they should be either removed form the vector of unknowns or fixed using functional constraint adjustment approach, otherwise normal matrix of the linear system will be strongly singular. It should be noted that they have no contribution to gravitational functionals even if they are estimated.

their first and second derivatives:

$$\mathbf{G}^* = \frac{GM}{r}\sum_{n=0}^{N_{max}}(\frac{R}{r})^n\sum_{m=0}^{n}$$

$$\begin{bmatrix} \frac{(n+1)(n+2)}{r^2}\bar{R}_{nm} & -\frac{(n+1)}{r}\bar{R}'_{nm} & \frac{m(n+1)}{r}\bar{S}_{nm} \\ -\frac{(n+1)}{r}\bar{R}'_{nm} & \bar{R}''_{nm} & -m\bar{S}'_{nm} \\ \frac{m(n+1)}{r}\bar{S}_{nm} & -m\bar{S}'_{nm} & -m^2\bar{R}_{nm} \end{bmatrix}\bar{c}_{nm}+$$

$$\begin{bmatrix} \frac{(n+1)(n+2)}{r^2}\bar{S}_{nm} & -\frac{(n+1)}{r}\bar{S}'_{nm} & -\frac{m(n+1)}{r}\bar{R}_{nm} \\ -\frac{(n+1)}{r}\bar{S}'_{nm} & \bar{S}''_{nm} & m\bar{R}'_{nm} \\ -\frac{m(n+1)}{r}\bar{R}_{nm} & m\bar{R}'_{nm} & -m^2\bar{S}_{nm} \end{bmatrix}\bar{s}_{nm} \tag{2.94}$$

where,

$$\bar{R}''_{nm} = \bar{R}''_{nm}(\phi,\lambda) = \cos m\lambda\, \bar{P}''_{n,m}(\sin\phi) \tag{2.95}$$

$$\bar{S}''_{nm} = \bar{S}''_{nm}(\phi,\lambda) = \sin m\lambda\, \bar{P}''_{n,m}(\sin\phi) \tag{2.96}$$

$P'_{n,m}(\sin\phi)$ & $P''_{n,m}(\sin\phi)$ are computed using Eqs. (2.34), (2.35) and (2.36). Substituting Eqs. (2.86) and (2.94) into Eq. (2.30) yields:

$$\mathbf{g}_i = \frac{GM}{r}\sum_{n=0}^{N_{max}}(\frac{R}{r})^n\sum_{m=0}^{n}$$

$$\left\{\nabla\otimes\mathbf{J}_i\cdot\begin{bmatrix} -\frac{n+1}{r}\bar{R}_{nm} \\ \bar{R}'_{nm} \\ -m\bar{S}_{nm} \end{bmatrix} + \mathbf{J}\begin{bmatrix} \frac{(n+1)(n+2)}{r^2}\bar{R}_{nm} & -\frac{(n+1)}{r}\bar{R}'_{nm} & \frac{m(n+1)}{r}\bar{S}_{nm} \\ -\frac{(n+1)}{r}\bar{R}'_{nm} & \bar{R}''_{nm} & -m\bar{S}'_{nm} \\ \frac{m(n+1)}{r}\bar{S}_{nm} & -m\bar{S}'_{nm} & -m^2\bar{R}_{nm} \end{bmatrix}\mathbf{J}_i^T\right\}\bar{c}_{nm}+$$

$$\left\{\nabla\otimes\mathbf{J}_i\cdot\begin{bmatrix} -\frac{n+1}{r}\bar{S}_{nm} \\ \bar{S}'_{nm} \\ m\bar{R}_{nm} \end{bmatrix} + \mathbf{J}\begin{bmatrix} \frac{(n+1)(n+2)}{r^2}\bar{S}_{nm} & -\frac{(n+1)}{r}\bar{S}'_{nm} & -\frac{m(n+1)}{r}\bar{R}_{nm} \\ -\frac{(n+1)}{r}\bar{S}'_{nm} & \bar{S}''_{nm} & m\bar{R}'_{nm} \\ -\frac{m(n+1)}{r}\bar{R}_{nm} & m\bar{R}'_{nm} & -m^2\bar{S}_{nm} \end{bmatrix}\mathbf{J}_i^T\right\}\bar{s}_{nm} \tag{2.97}$$

Substituting Eq.(2.97), in Eq. (2.39) results the following expressions which correspond to coefficients of $\bar{c}_{nm}$ & $\bar{s}_{nm}$ in design matrix:

$$\textit{coefficient of } \bar{c}_{nm} = \frac{GM}{R}\left(\frac{R}{r}\right)^{(n+1)} \sum_{i=0}^{3}$$

$$\mathbf{e}^T \left\{ \nabla \otimes \mathbf{J}_i \cdot \begin{bmatrix} -\frac{n+1}{r}\bar{R}_{nm} \\ \bar{R}'_{nm} \\ -m\bar{S}_{nm} \end{bmatrix} + \mathbf{J} \begin{bmatrix} \frac{(n+1)(n+2)}{r^2}\bar{R}_{nm} & -\frac{(n+1)}{r}\bar{R}'_{nm} & \frac{m(n+1)}{r}\bar{S}_{nm} \\ -\frac{(n+1)}{r}\bar{R}'_{nm} & \bar{R}''_{nm} & -m\bar{S}'_{nm} \\ \frac{m(n+1)}{r}\bar{S}_{nm} & -m\bar{S}'_{nm} & -m^2\bar{R}_{nm} \end{bmatrix} \mathbf{J}_i^T \right\} e_i \tag{2.98}$$

$$\underline{\textit{coefficient of}}\ \bar{s}_{nm} = \frac{GM}{R}\left(\frac{R}{r}\right)^{(n+1)} \sum_{i=0}^{3}$$

$$\mathbf{e}^T \left\{ \nabla \otimes \mathbf{J}_i \cdot \begin{bmatrix} -\frac{n+1}{r}\bar{S}_{nm} \\ \bar{S}'_{nm} \\ m\bar{R}_{nm} \end{bmatrix} + \mathbf{J} \begin{bmatrix} \frac{(n+1)(n+2)}{r^2}\bar{S}_{nm} & -\frac{(n+1)}{r}\bar{S}'_{nm} & -\frac{m(n+1)}{r}\bar{R}_{nm} \\ -\frac{(n+1)}{r}\bar{S}'_{nm} & \bar{S}''_{nm} & m\bar{R}'_{nm} \\ -\frac{m(n+1)}{r}\bar{R}_{nm} & m\bar{R}'_{nm} & -m^2\bar{S}_{nm} \end{bmatrix} \mathbf{J}_i^T \right\} e_i \tag{2.99}$$

Like previous case, each evaluation point generates an observation equation which is written at the barycenter of the two satellites. As seen, the resultant equation is a linear equation in terms of the potential unknown coefficients. Hence, similar to gravitational acceleration differences, each observation is corresponds to one row in design matrix. Having a sequence of observations with M evaluation points, sets up the design matrix of linear system of equation $\mathbf{A}_{M\times(N_{max}+1)^2}$.

2.3.3 Incremental Acceleration Gradient of the Barycenter of the Twin Satellites as the Observable

Removing the effect of the reference field of any degree and order, will remold the original design matrix structure. In general terms, let's consider a reference field of the type V_l, where $l \geq 2$. Accordingly, vector of unknowns will be split up into two independent sub-vectors, $\mathbf{x}_l$ and $\mathbf{x}^l$, each of which contains:

$$\begin{aligned} \mathbf{x}_l &= \begin{bmatrix} \bar{c}_{nm} \\ \bar{s}_{nm} \end{bmatrix} \qquad n, m \leq l \\ \mathbf{x}^l &= \begin{bmatrix} \bar{c}_{nm} \\ \bar{s}_{nm} \end{bmatrix} \quad l < n, m \leq N_{max} \end{aligned} \tag{2.100}$$

Consequently, the design matrix can be fragmented into $\mathbf{A}_l$ and $\mathbf{A}^l$ of the size $M\times(l+1)^2$ and $M\times(N_{max}+l+2)(N_{max}-l)$ respectively. Let's start with Eq. (2.59) to detail these two sub-matrices:

$$\frac{1}{\rho}\Delta\Gamma_l^{LOS}+\mathbf{e}^T\mathbf{G}^l\mathbf{e}\stackrel{?}{=}\frac{\ddot{\rho}}{\rho}+\frac{\dot{\rho}^2}{\rho^2}-\frac{\|\Delta\dot{\mathbf{r}}\|^2}{\rho^2} \tag{2.101}$$

where, first term in left hand side can be replaced with modified form of the expression given in Eq. (2.93). Meanwhile, an equivalent expression derived from Eq. (2.97) takes the place of the second term:

$$\frac{1}{\rho}\Delta\Gamma_l^{LOS}=\frac{GM}{\rho R}\sum_{n=0}^{l}(\frac{R}{r_2})^{n+1}\sum_{m=0}^{n}$$

$$\mathbf{e}^T\left\{\mathbf{J}_2\begin{bmatrix}-\frac{n+1}{r_2}\bar{R}_{nm}\\ \bar{R}'_{nm}\\ -m\bar{S}_{nm}\end{bmatrix}_{\mathbf{2}}-(\frac{r_2}{r_1})^{n+1}\mathbf{J}_1\begin{bmatrix}-\frac{n+1}{r_1}\bar{R}_{nm}\\ \bar{R}'_{nm}\\ -m\bar{S}_{nm}\end{bmatrix}_{\mathbf{1}}\right\}\bar{c}_{nm}$$

$$\mathbf{e}^T\left\{\mathbf{J}_2\begin{bmatrix}-\frac{n+1}{r_2}\bar{S}_{nm}\\ \bar{S}'_{nm}\\ m\bar{R}_{nm}\end{bmatrix}_{\mathbf{2}}-(\frac{r_2}{r_1})^{n+1}\mathbf{J}_1\begin{bmatrix}-\frac{n+1}{r_1}\bar{S}_{nm}\\ \bar{S}'_{nm}\\ m\bar{R}_{nm}\end{bmatrix}_{\mathbf{1}}\right\}\bar{s}_{nm} \tag{2.102}$$

and

$$\mathbf{e}^T\mathbf{G}^l\mathbf{e}=\mathbf{e}^T\begin{bmatrix}\mathbf{g}_1^l & \mathbf{g}_2^l & \mathbf{g}_3^l\end{bmatrix}\mathbf{e} \tag{2.103}$$

where,

$$\mathbf{g}_i^l=\frac{GM}{r}\sum_{n=l+1}^{N_{max}}(\frac{R}{r})^n\sum_{m=0}^{n}$$

$$\left\{\nabla\otimes\mathbf{J}_i\cdot\begin{bmatrix}-\frac{n+1}{r}\bar{R}_{nm}\\ \bar{R}'_{nm}\\ -m\bar{S}_{nm}\end{bmatrix}+\mathbf{J}\begin{bmatrix}\frac{(n+1)(n+2)}{r^2}\bar{R}_{nm} & -\frac{(n+1)}{r}\bar{R}'_{nm} & \frac{m(n+1)}{r}\bar{S}_{nm}\\ -\frac{(n+1)}{r}\bar{R}'_{nm} & \bar{R}''_{nm} & -m\bar{S}'_{nm}\\ \frac{m(n+1)}{r}\bar{S}_{nm} & -m\bar{S}'_{nm} & -m^2\bar{R}_{nm}\end{bmatrix}\mathbf{J}_i^T\right\}\bar{c}_{nm}+$$

$$\left\{ \nabla \otimes \mathbf{J}_i \cdot \begin{bmatrix} -\frac{n+1}{r}\bar{S}_{nm} \\ \bar{S}'_{nm} \\ m\bar{R}_{nm} \end{bmatrix} + \mathbf{J} \begin{bmatrix} \frac{(n+1)(n+2)}{r^2}\bar{S}_{nm} & -\frac{(n+1)}{r}\bar{S}'_{nm} & -\frac{m(n+1)}{r}\bar{R}_{nm} \\ -\frac{(n+1)}{r}\bar{S}'_{nm} & \bar{S}''_{nm} & m\bar{R}'_{nm} \\ -\frac{m(n+1)}{r}\bar{R}_{nm} & m\bar{R}'_{nm} & -m^2\bar{S}_{nm} \end{bmatrix} \mathbf{J}_i^T \right\} \bar{s}_{nm} \tag{2.104}$$

Hence, $\mathbf{A}_l$ is filled with the expression of the type:

$$\textit{coefficient of } \bar{c}_{nm} = \tfrac{GM}{\rho R}(\tfrac{R}{r_2})^{n+1}$$

$$\mathbf{e}^T \left\{ \mathbf{J}_2 \begin{bmatrix} -\frac{n+1}{r_2}\bar{R}_{nm} \\ \bar{R}'_{nm} \\ -m\bar{S}_{nm} \end{bmatrix}_{\mathbf{2}} - (\frac{r_2}{r_1})^{n+1} \mathbf{J}_1 \begin{bmatrix} -\frac{n+1}{r_1}\bar{R}_{nm} \\ \bar{R}'_{nm} \\ -m\bar{S}_{nm} \end{bmatrix}_{\mathbf{1}} \right\} \tag{2.105}$$

$$\textit{coefficient of } \bar{s}_{nm} = \tfrac{GM}{\rho R}(\tfrac{R}{r_2})^{n+1}$$

$$\mathbf{e}^T \left\{ \mathbf{J}_2 \begin{bmatrix} -\frac{n+1}{r_2}\bar{S}_{nm} \\ \bar{S}'_{nm} \\ m\bar{R}_{nm} \end{bmatrix}_{\mathbf{2}} - (\frac{r_2}{r_1})^{n+1} \mathbf{J}_1 \begin{bmatrix} -\frac{n+1}{r_1}\bar{S}_{nm} \\ \bar{S}'_{nm} \\ m\bar{R}_{nm} \end{bmatrix}_{\mathbf{1}} \right\} \tag{2.106}$$

$$\underline{n, m \leq l}$$

where, $\mathbf{A}^l$ is filled with:

$$\textit{coefficient of } \bar{c}_{nm} = \tfrac{GM}{R}(\tfrac{R}{r})^{n+1}$$

$$\mathbf{e}^T \left\{ \sum_{i=1}^{3} \nabla \otimes \mathbf{J}_i \cdot \begin{bmatrix} -\frac{n+1}{r}\bar{R}_{nm} \\ \bar{R}'_{nm} \\ -m\bar{S}_{nm} \end{bmatrix} e_i + \right.$$

$$\left. \mathbf{J} \begin{bmatrix} \frac{(n+1)(n+2)}{r^2}\bar{R}_{nm} & -\frac{(n+1)}{r}\bar{R}'_{nm} & \frac{m(n+1)}{r}\bar{S}_{nm} \\ -\frac{(n+1)}{r}\bar{R}'_{nm} & \bar{R}''_{nm} & -m\bar{S}'_{nm} \\ \frac{m(n+1)}{r}\bar{S}_{nm} & -m\bar{S}'_{nm} & -m^2\bar{R}_{nm} \end{bmatrix} \sum_{i=1}^{3} \mathbf{J}_i^T e_i \right\} \tag{2.107}$$

$$coefficient\ of\ \bar{s}_{nm} = \frac{GM}{R}(\frac{R}{r})^{n+1}$$

$$\mathbf{e}^T \left\{ \sum_{i=1}^{3} \nabla \otimes \mathbf{J}_i \cdot \begin{bmatrix} -\frac{n+1}{r}\bar{S}_{nm} \\ \bar{S}'_{nm} \\ m\bar{R}_{nm} \end{bmatrix} e_i + \right.$$

$$\left. \mathbf{J} \begin{bmatrix} \frac{(n+1)(n+2)}{r^2}\bar{S}_{nm} & -\frac{(n+1)}{r}\bar{S}'_{nm} & -\frac{m(n+1)}{r}\bar{R}_{nm} \\ -\frac{(n+1)}{r}\bar{S}'_{nm} & \bar{S}''_{nm} & m\bar{R}'_{nm} \\ -\frac{m(n+1)}{r}\bar{R}_{nm} & m\bar{R}'_{nm} & -m^2\bar{S}_{nm} \end{bmatrix} \sum_{i=1}^{3} \mathbf{J}_i^T e_i \right\} \tag{2.108}$$

$$\underline{l < n, m \leq N_{max}}$$

Having design matrix, $\mathbf{A}$, partitioned into $\mathbf{A}_l$ and $\mathbf{A}^l$, results the following normal system of equations which is easily solved using matrix inversion by partitioning technique:

$$\begin{bmatrix} \mathbf{A}_l^T\mathbf{C}_\mathbf{l}^{-1}\mathbf{A}_l & \mathbf{A}_l^T\mathbf{C}_\mathbf{l}^{-1}\mathbf{A}^l \\ \mathbf{A}^{l^T}\mathbf{C}_\mathbf{l}^{-1}\mathbf{A}_l & \mathbf{A}^{l^T}\mathbf{C}_\mathbf{l}^{-1}\mathbf{A}^{l^T} \end{bmatrix} \begin{bmatrix} \mathbf{x}_l \\ \mathbf{x}^l \end{bmatrix} = \begin{bmatrix} \mathbf{A}_l^T\mathbf{C}_\mathbf{l}^{-1}\mathbf{l} \\ \mathbf{A}^{l^T}\mathbf{C}_\mathbf{l}^{-1}\mathbf{l} \end{bmatrix} \tag{2.109}$$

In which, $\mathbf{l}$ is the observation vector consisting of M measurements of the type, $\frac{\ddot{\rho}}{\rho} + \frac{\dot{\rho}^2}{\rho^2} - \frac{\|\Delta\dot{\mathbf{r}}\|^2}{\rho^2}$. The sought-after unknown coefficients, $\bar{c}_{nm}$ and $\bar{s}_{nm}$ are the solution of Eq. (2.109). Variance-covariance matrices corresponding to each component of the solution are by product of the normal equation solution.

2.3.4 Gravitational Acceleration Gradient of the Barycenter of the Twin Satellites as the Observable (*Mixed Cubic-Linear Approximation*)

Unless the entries of the design matrix correspond to $\bar{c}_{00}$ and $\bar{c}_{20}$, the rest of the design will be the same as the matrix in section 2.3.2. Therefore, the aforementioned entries should be modified according to the observation equation, Eq. (2.83), to achieve the corresponding normal matrix. The modification can be preformed using a new form

of the mathematical expression of $\mathbf{G}_2$ given in Eq. (2.51):

$$\mathbf{G}_2(x,y,z) = \left[3\tfrac{GM}{r^5}\mathbf{r}^T \otimes \mathbf{r} - \tfrac{GM}{r^3}\mathbf{I}_{3\times 3}\right]\bar{c}_{00} + \left\{\left[\tfrac{35\alpha q}{r^9} + \tfrac{20\alpha\, q}{r^7}\right]\mathbf{r}^T \otimes \mathbf{r} - \tfrac{5\alpha q}{r^7}\mathbf{I}_{3\times 3} + \tfrac{20\alpha q}{r^7}\begin{bmatrix} 0 & 0 & \frac{-3}{2}xz \\ 0 & 0 & \frac{-3}{2}yz \\ \frac{-3}{2}zx & \frac{-3}{2}zy & z^2 \end{bmatrix} - \tfrac{2\alpha}{r^5}\begin{bmatrix} 1 & 0 & 0 \\ 0 & 1 & 0 \\ 0 & 0 & 2 \end{bmatrix}\right\}\bar{c}_{20} \tag{2.110}$$

To get to the final point, we should apply $\otimes$ twice on $\mathbf{G}_2$. For ease of computation, one of the available softwares equipped with algebraic computations toolbox, e.g. *Matlab*, *Maple*, $\cdots$ can be employed.

Chapter 3

Numerical Analysis

In this chapter, we implement the aforementioned suggested ideas. Our numerical studies are based on a ten-day data subset of the IAG simulated data that can be downloaded from the following ftp-site:

```
ftp://geo@atlas.geod.unibonn.de/pub/SC7_SimulationScenarios
                    password reads: geo-ftp
```

In this directory, sub-directories contain the packed orbits of the new dedicated gravity field missions, *CHAMP, GRACE, GOCE* and error models as well as the gravity fields to be used. The simulated GRACE data set covers a time period of 30 days and includes the velocities and accelerations. The simulation scenario is simplified in so far as there is no noise on the data for the GPS-orbits and for GRACE data sets. The files of the GPS-satellites, of GRACE1/GRACE2 contain: *time*, x, y, z,$\dot{x}$, $\dot{y}$, $\dot{z}$,$\ddot{x}$, $\ddot{y}$, $\ddot{z}$ *time in Julian date - 2400000.0, position, velocity, acceleration.* The coordinates refer to a *quasi* inertial system with origin in the center of mass of the Earth and the axes directed to the principal axes of inertia, *these are the axes according to the spherical harmonics coefficients.* The relationship between this quasi-inertial system and the Earth fixed coordinate system is defined by the siderial time as specified on the following data sheet.

General Characteristics of the Simulated Data

```
PSEUDO-REAL-GRAVITY FIELD: EGM96 (COMPLETE UPTO DEGREE 300)
REFERENCE GRAVITY FIELD:  OSU91 (COMPLETE UPTO DEGREE 36) MISSION
```

```
PERIOD: 30 DAYS DATA SAMPLING RATE 0.2Hz, CORRESPONDING TO AN
INTEGRATION STEP SIZE OF 5 SEC RELATION BETWEEN INERTIAL SYSTEM
AND EARTH FIXED SYSTEM:
 siderial time[rad]=T[days]*86400.0D0*7.29211585531D-5[rad/sec]+5.133658456D0[rad]
      T[0,30days]
      T[days]:=TJU[Julian date]-2451740.5
      JULIAN DATE OF 15.07.2000, 0h: 2451740.5
```

For better understanding of the effect of observation random noise, the data sets are also contaminated with simulated Gaussian random noise.
As the final goal of the mission from geophysical point of view, some lower degree coefficients of the gravitational potential will be recovered.

3.1 LOS Acceleration Differences as the Observable

In this section, we consider *LOS* acceleration differences as the observable of the *GRACE* mission and try to analyze the consequent problems numerically.
The first data set is a one-day data of the mission which is taken form *IAG* data set. According to the given transformation relationship in data sheet, satellite positions are transformed from *quasi-inertial* to the *Earth-fixed* system. Fig. (3.1) shows the corresponding ground track in orthographic projection. Its distribution along the meridians and the parallels are depicted in Figs. (3.2) and (3.3), respectively. As it can be seen, we have nearly continuous distribution along the meridians while a sparse pattern of distribution of data is appeared along the parallels. Therefore, we expect *zonal harmonics* to be recovered with a higher accuracy than *sectorial and tesseral harmonics*, using the data set. Also, it seems that a higher zonal harmonics are detectable while the others are not.
Since position of the satellites and their first and second time derivatives are the only information given in *IAG* files, we should simulate the ranging system observations based on the given data as well. We simulate the inter-satellite range, velocity and

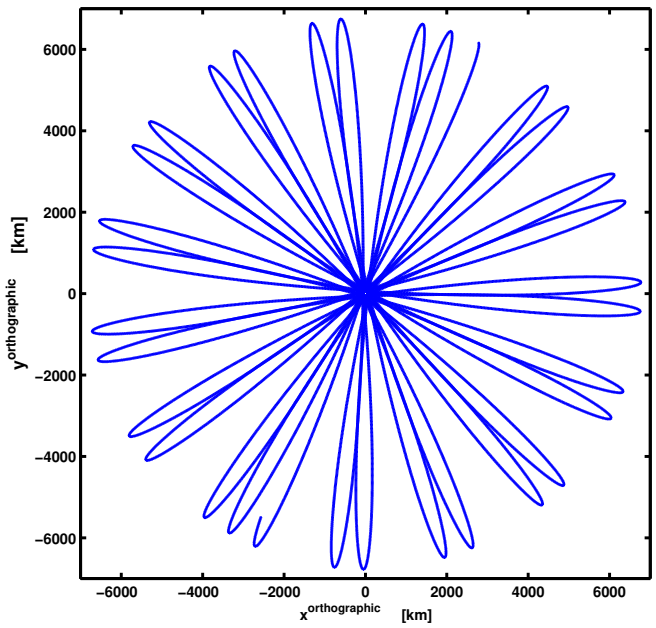

Figure 3.1: one-day ground track of *GRACE* in orthographic projection

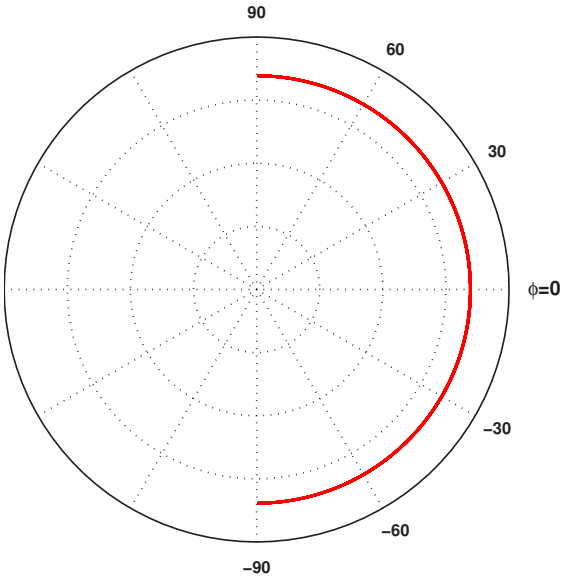

Figure 3.2: one-day *GRACE* distribution along the meridians $-89° \leq \phi \leq 89°$

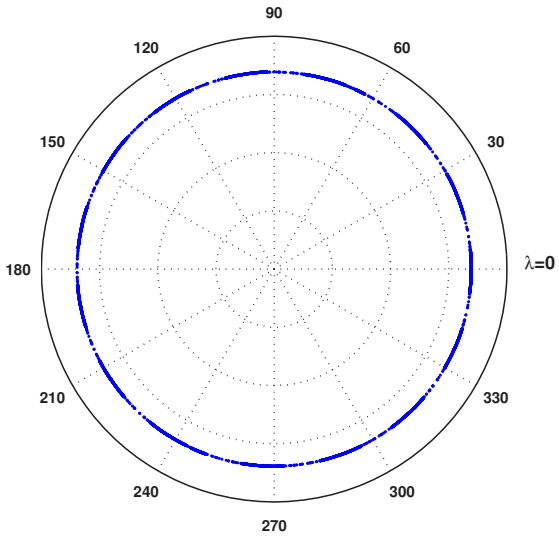

Figure 3.3: one-day *GRACE* distribution along the parallels $0° \leq \lambda \leq 360°$

acceleration denoting them as ρ, $\dot{\rho}$ and $\ddot{\rho}$ respectively.

$$\rho(t) = \sqrt{\langle \Delta\mathbf{r}(t)\,,\, \Delta\mathbf{r}(t)\rangle} \tag{3.1}$$

$$\dot{\rho}(t) = \frac{1}{\rho(t)} \langle \Delta\mathbf{r}(t)\,,\, \Delta\dot{\mathbf{r}}(t)\rangle \tag{3.2}$$

$$\ddot{\rho}(t) = \frac{1}{\rho(t)} \langle \Delta\mathbf{r}(t)\,,\, \Delta\ddot{\mathbf{r}}(t)\rangle + \frac{1}{\rho(t)} \Delta\dot{\mathbf{r}}^T(t) \left[\mathbf{I}_{3\times 3} - \frac{1}{\rho^2}\Delta\mathbf{r}^T(t) \otimes \Delta\mathbf{r}(t)\right] \Delta\dot{\mathbf{r}}(t) \tag{3.3}$$

ρ, $\dot{\rho}$, $\ddot{\rho}$ and LOS acceleration differences are depicted in Fig. (3.4). As shown, J_{20} has the most major contribution to the inter-satellite quantities as a linear functionals of the gravitational potential, so that the effect of the higher degree harmonics has not been clearly emerged.

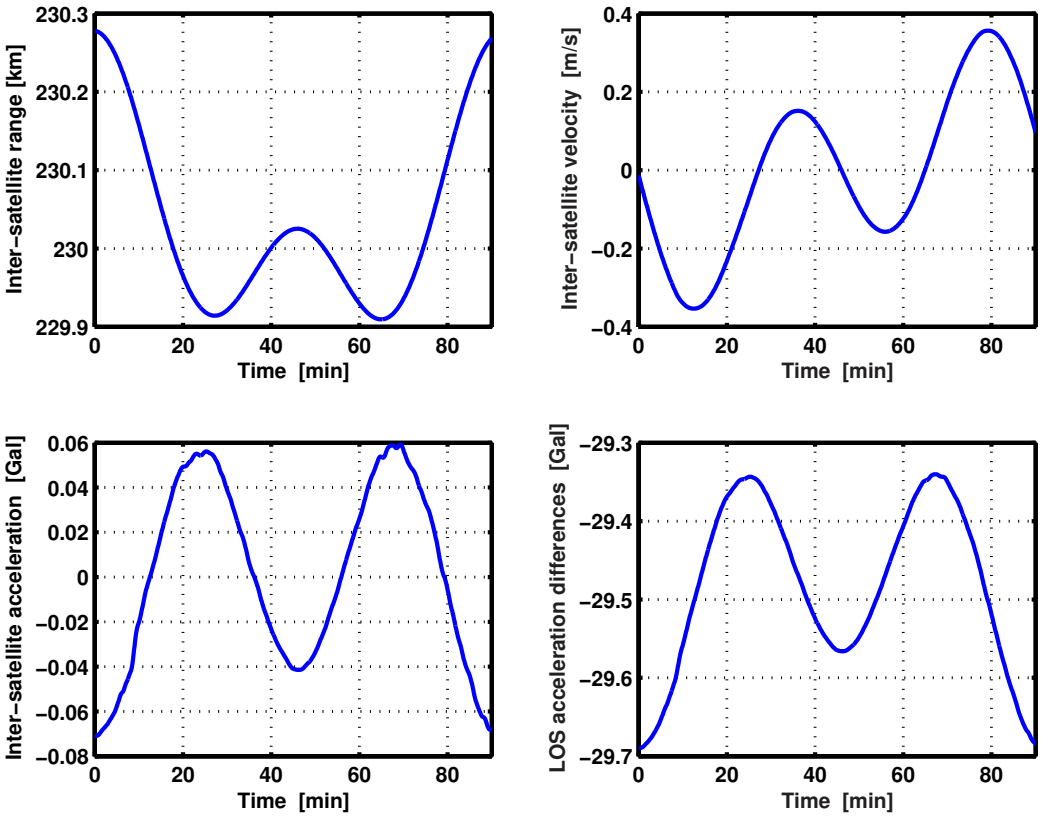

Figure 3.4: inter-satellite range, velocity, acceleration and LOS acceleration variations in one revolution of *GRACE*

In order to get a rough estimate of the maximum degree of resolvable spherical harmonics, a comparative study is carried out in which we calculate the LOS acceleration differences using different gravitational potential fields. For instance, $\Delta\Gamma^{LOS}$ differ-

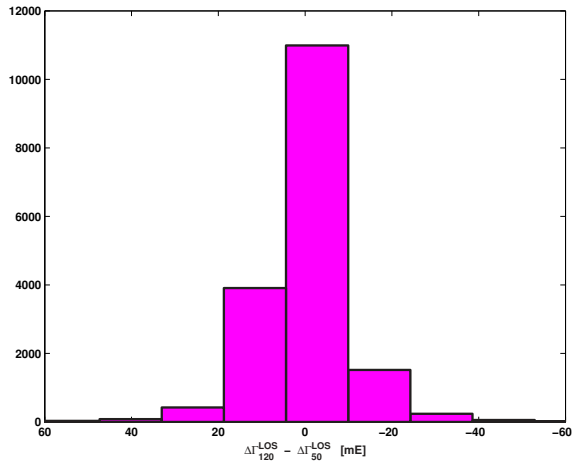

Figure 3.5: *LOS* acceleration differences for $n = 50$ and $n = 120$

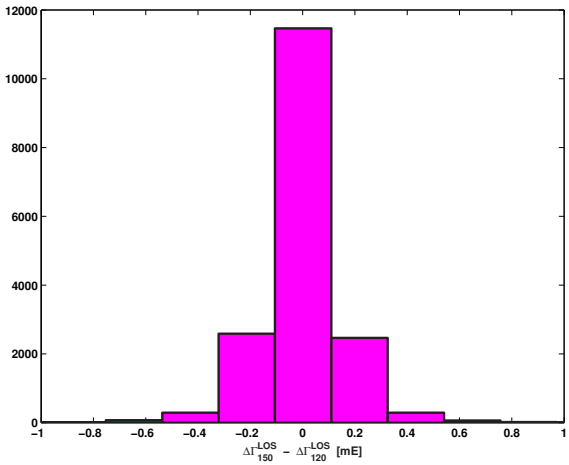

Figure 3.6: *LOS* acceleration differences for $n = 150$ and $n = 120$

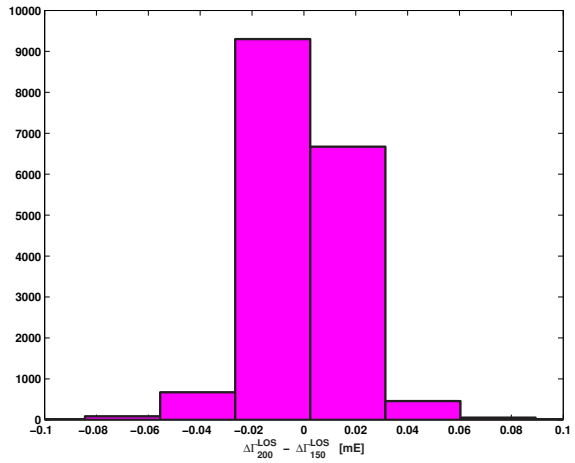

Figure 3.7: *LOS* acceleration differences for $n = 200$ and $n = 150$

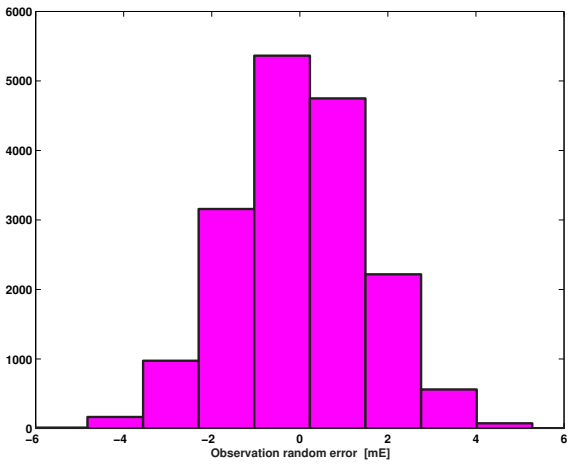

Figure 3.8: Observation random error

ences corresponding to $n = 50$, $n = 120$, $n = 150$ and $n = 200$ are depicted in Figs. (3.5), (3.6) and (3.7). As seen, only the differences for $n = 50$ and $n = 120$ are meaningful. Comparing Figs. (3.6) and (3.7) with Fig. (3.8), shows that the differences in the higher degree are about the order of the observable noise or even lower for $n > 150$. Therefore, in an optimistic situation, the spherical harmonic coefficients would be resolvable upto degree 120.

We establish a linear system of equations of the type Eq. (2.93) for the first data set. Considering $n = 10$, yields to 17281 equations with 121 unknowns. The solution vector contains $\bar{c}_{nm}$ and $\bar{s}_{nm}$ upto degree and order 10. The results in the form of degree variances are depicted in Fig. (3.9). Comparing the estimated values with $EGM96$'s shows nearly perfect estimation for lower harmonics. Increasing the maximum degree of estimable coefficients to 16, equal to the number of revolutions in the first data set, results nearly the same results for the lower degree $n \leq 10$, whereas the differences are considerable for the higher terms. Both the estimated and $EGM96$ degree variances are visualized in Fig. (3.10). As the degree of harmonics increases, the differences rise sharply and normal matrix stability gets worse. To make the stability behavior of the linear system of equations clear, we gradually increase the maximum degree of the estimated coefficients. The system will be singular for $n > 20$. *see Fig. (3.16).* The

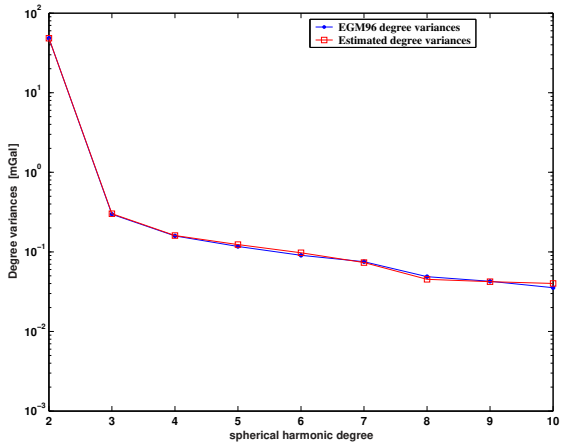

Figure 3.9: Estimated degree variances upto $n = 10$ using a one-day observations

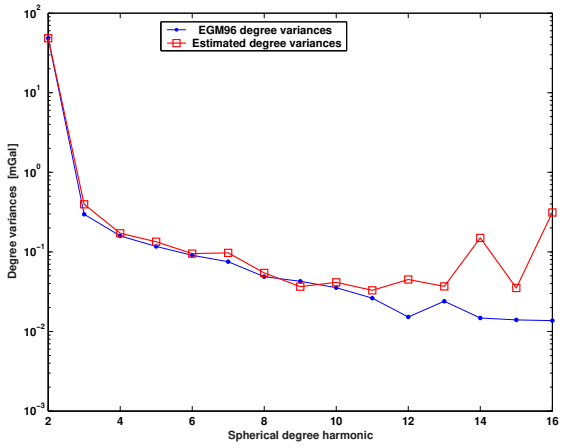

Figure 3.10: Estimated degree variances upto $n = 16$ using a one-day observations

two following errors causes the closure of degree variances:

- *commission errors*, arising from a formal error propagation and

- *omission/ aliasing error*, caused by neglecting signal corresponding to either missing or undetectable harmonics.

Like every parameter estimation process, random noise of the observation vector propagates through the mathematical model to the estimated parameters,$\bar{c}_{nm}$ & $\bar{s}_{nm}$ or equally to degree variances, whereas undersampling of the gravitational potential as a continuous function results aliasing error. In other words, the measurement (sampling) frequency must be at least twice the maximum frequency to be measured. This result is known as the *Sampling Theorem* and is due to *Claude Shannon* who first discovered it in 1949. Whenever Shannon's sampling theorem is not fulfilled, aliasing occurs. To avoid occurrence of aliasing error in simulated data we should either

- increase the sampling frequency to satisfy the theorem or
- decrease the maximum estimated harmonics after excluding the contribution of the frequency beyond the Nyquist limit to the observations.

There is no doubt that neither increasing the sampling frequency nor removing share of the missing terms is ever possible. Therefore, aliasing would be inevitable in the estimation process using real data. As a rough estimate, the degree variances are estimated after removing the commission and omission errors for $n = 16$ using a one-day data.

As seen, removing the estimated degree variances in the absence of observation noise are nearly the estimated values in the presence of the noise. Despite this, removing the effect of higher degree ($n > 16$) harmonics, aliasing generator has the major effect so that the estimated degree variances are the the same as *EGM96*'s. Afterward, we will consider aliasing as the dominant error of the estimated results due to its considerable effect with respect to commission error.

The second data set is a five-day observations of the mission which the orthographic projection of satellites ground track during the period of measurements is visualized in Fig. (3.12). In comparison with the first data set is much more denser, so we can expect to recover the unknowns with higher accuracy even in higher degrees. Similarly, we set up the linear system of equations using the new data set. We solve 86405 equations to estimate the coefficients upto degree and order 25 and draw the results in Fig. (3.13).

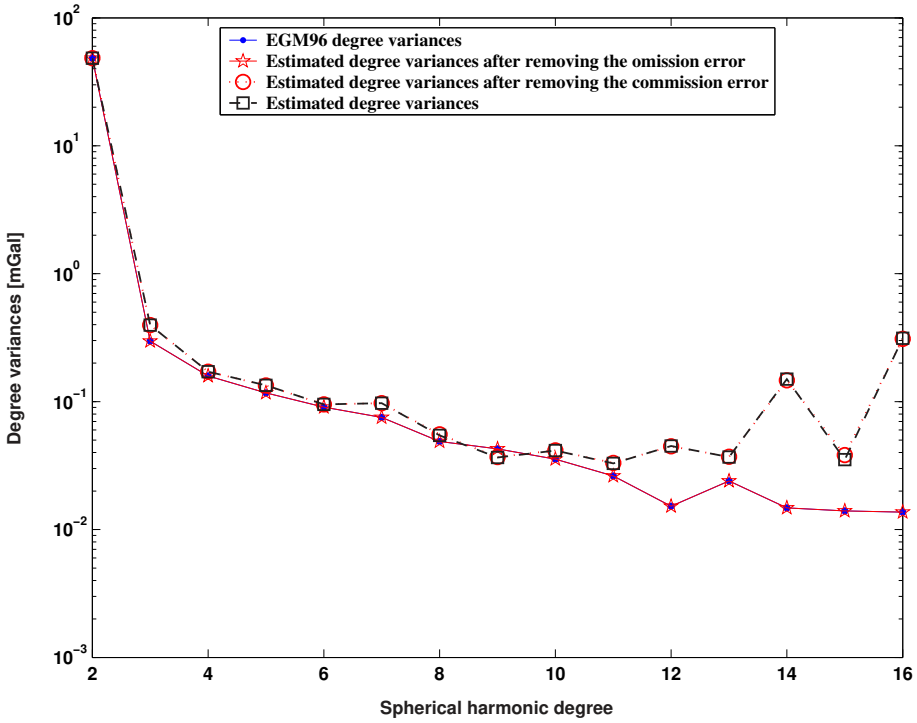

Figure 3.11: Different errors contribution to the closure of estimated degree variances upto $n = 16$ using a one-day measurements of the type $\Delta\Gamma_{16}^{LOS}$

Upto $n = 15$, the estimated degree variances are nearly the same as $EGM96$'s. Then, we replace $n = 50$ to see the stability of the system of equations. As seen in Fig. (3.14), the estimated and $EGM96$ degree variances are identical upto degree 25. Hence, the appeared differences in Fig. (3.13) is due to the aliasing effect which is shifted to the higher degree variances in the later solution ($n = 50$). In order to investigate the behavior of the system, we increase the maximum degree to 75. The results are shown in Fig. (3.15).

To compare the stability of five-day observations normal matrix with the one-day ones, the eigenvalues of the normal matrices are calculated and $\frac{\lambda_{max}}{\lambda_{min}}$ are depicted versus different values of maximum estimated degree of the spherical harmonic coefficients in Fig. (3.16). As seen, upto degree 10, the ratio is identical in both cases but it is completely different for higher terms. While passing $n = 20$, it exponentially rises in a one-day data set, whereas the ratio is still smooth in a five-day data set. Hence, using a longer arc of the orbit, solves the instability problem appeared in short-arc orbits. However, the coefficients can be estimated upto a reasonable degree using orbital arcs of different lengths. As a rule of thumb, we expect to resolve the spherical harmonic

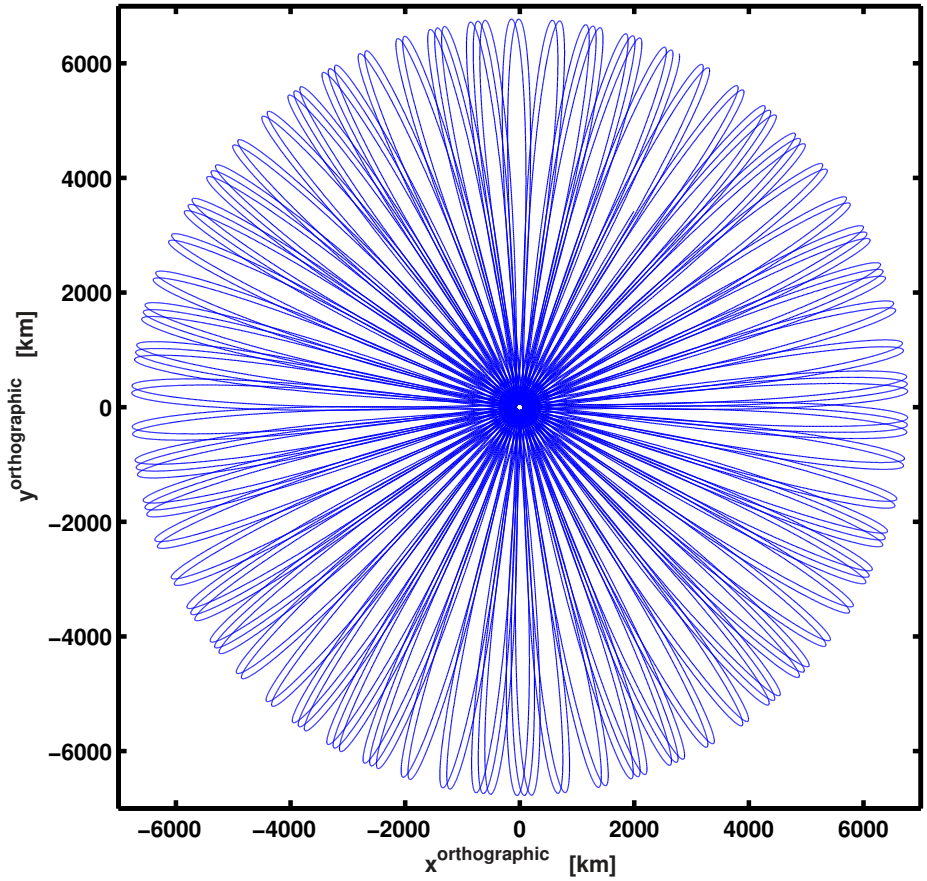

Figure 3.12: a five-day ground track of *GRACE* in orthographic projection

upto n_{max} which is defined as:

$$n_{max} = 8d \tag{3.4}$$

where, d [day] is the duration of observations. For instance, it is equal to 8 and 40 for one-day and five-day measurements respectively. Of course, the relationship is valid only for $n_{max} \leq N_{max}$ where, N_{max} is the maximum degree of resolvable spherical harmonics using the employed mission. As already mentioned, 120 is an optimistic estimate for *GRACE* mission.

As the harmonic degree increases, the discrepancies move along. So, overestimating the coefficients and weeding out higher-degree harmonics as the affected terms seem to be one of the possible strategies for minimizing the aliasing. For instance, we estimate the coefficients upto 75 and weed out the high 25 coefficients $(50 - 75)$. As it is seen, overestimating and weeding out the unnecessary coefficients, results in much more smaller differences. *Compare Figs. (3.14)* and *(3.17)*. Fig. (3.18) shows the estimated

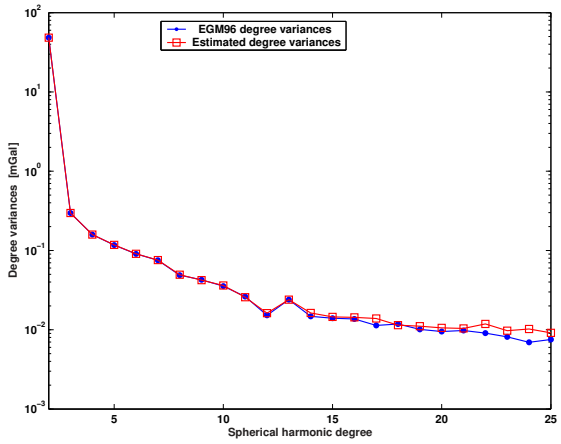

Figure 3.13: Estimated degree variances upto $n = 25$ using a five-day observations

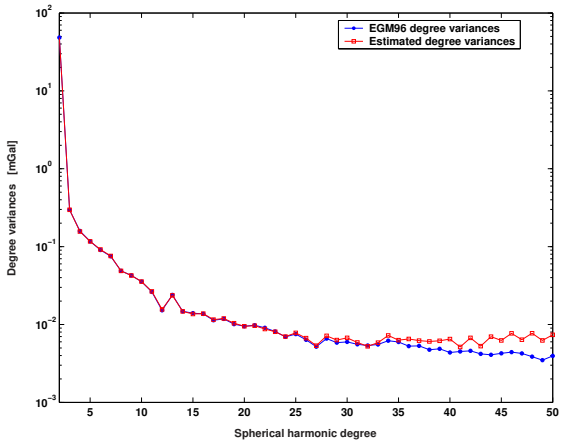

Figure 3.14: Estimated degree variances upto $n = 50$ using a five-day observations

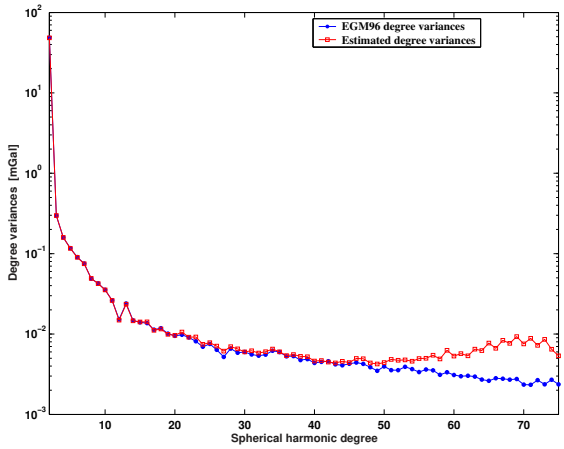

Figure 3.15: Estimated degree variances upto $n = 75$ using a five-day observations

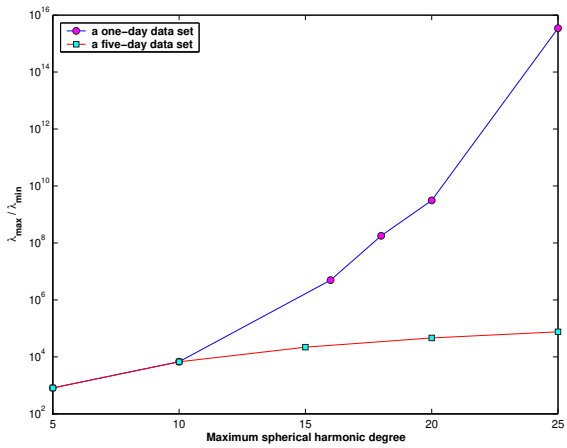

Figure 3.16: One-day and five-day observations normal matrix spectrum comparison

degree variances in the absence of aliasing which are equal to the *EGM96* values. Therefore, based on *LOS* acceleration differences, a reasonable set of the coefficients can be recovered using a fair length of orbit.

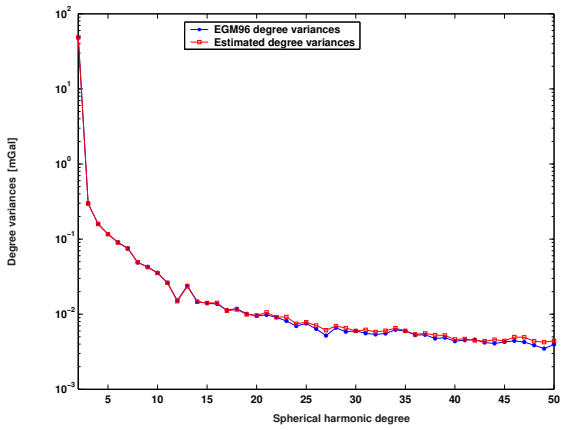

Figure 3.17: Overestimated degree variances upto $n = 50$ using a five-day observations

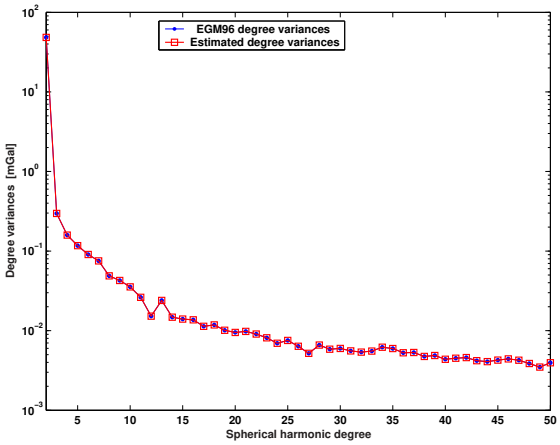

Figure 3.18: Estimated degree variances upto $n = 50$ using a five-day quasi-observations of the type $\Delta\Gamma^{LOS}_{50}$

3.2 Gravitational Acceleration Gradient as the Observable (*Linear Approximation*)

For a comparative analysis, we consider the two data sets used in previous section as the observations. We assume the gravitational acceleration gradient around the barycenter of the two satellites as the observable instead of *LOS* acceleration differences. Despite the $\Delta\Gamma^{LOS}$ as the observable, computation is done just for the barycenters. In other words, instead of two evaluation points involved in each observation equation of the type $\Delta\Gamma^{LOS}$, we have just one point in each equation of the gradiometry type. This can be considered as an advantage of this approach.

Let us consider the first data set. The corresponding linear system of equations coefficients given in Eqs. (2.98) and (2.99) are calculated for the data set. $\bar{c}_{nm}$ and $\bar{s}_{nm}$ upto degree and order 10 and 16 are the entries of the unknown vector which are visualized in Figs. (3.19) and (3.20) in the form of degree variances.

As it is seen, the differences are negligible upto degree 10 and the differences are clearly

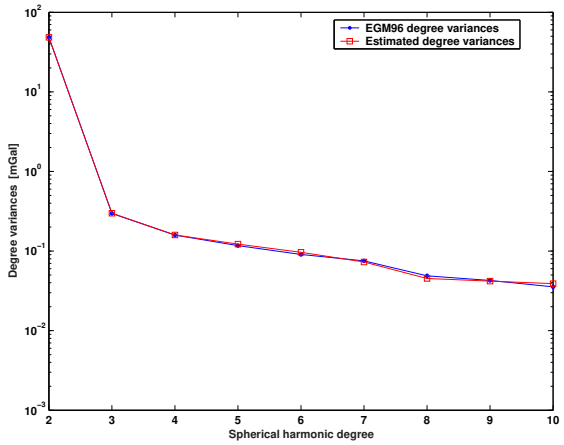

Figure 3.19: Estimated degree variances upto $n = 10$ using a one-day observations based on acceleration gradient

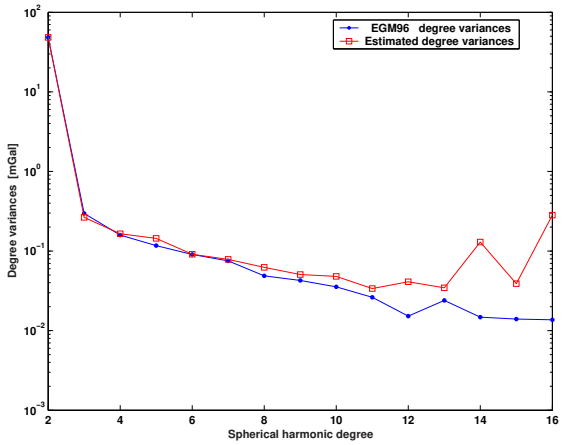

Figure 3.20: Estimated degree variances upto $n = 16$ using a one-day observations based on acceleration gradient

amplified for $n \geq 10$. There is no doubt that aliasing has the main rule and the linearization error is the second one which is caused by the neglected higher terms of the expansion in linear approximation of the gradiometry equation. The differences will be at the level of the corresponding discrepancies in the observable of the type $\Delta\Gamma_{LOS}$ if we implement one the proposed ideas for treatment of the linearization error. *see Fig. (3.25).*

A similar normal equations is set up for the second data set. Similar to the case of $\Delta\Gamma^{LOS}$ as the observable, a set of five-day observations with 0.2 Hz sampling frequency results in 86405 of observations equations, each of which is a function of $\bar{c}_{nm}$ and $\bar{s}_{nm}$. The achieved results, in the form of degree variances, are plotted for $n = 25$ and $n = 50$ in Figs. (3.21) and (3.22) respectively. The mentioned problem in a one-day data set occurred in a five-day data set even with a higher amplitude. Hence, we give up increasing the maximum degree of spherical harmonic and try to squeeze the error into an acceptable limit, first. Since aliasing and linearization cause the differences, each of them ia analyzed individually.

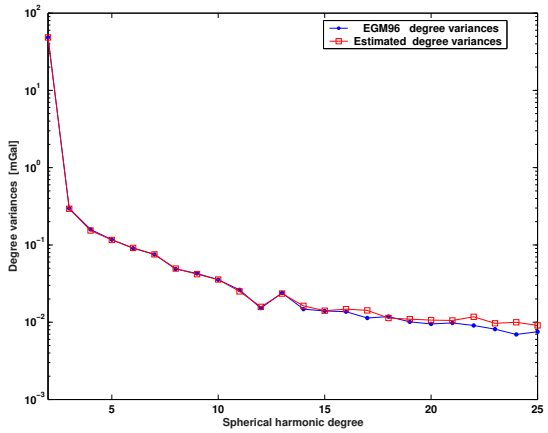

Figure 3.21: Estimated degree variances upto $n = 25$ using a five-day observations based on acceleration gradient

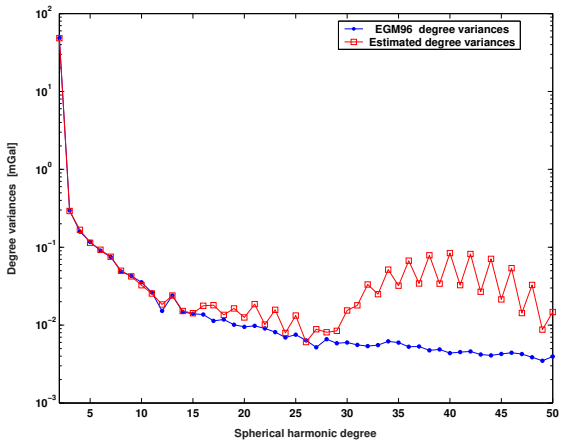

Figure 3.22: Estimated degree variances upto $n = 50$ using a five-day observations based on acceleration gradient

3.3 Incremental Acceleration Gradient as the Observable

As already mentioned in the preceding section, the linearization error discussed in subsection 2.2.2 has its own contribution to the estimated unknown vectors, $\bar{c}_{nm}$ & $\bar{s}_{nm}$. Therefore, for achieving a fair set of coefficients, implementation of either one of the modified linear approximation methods or the cubic-linear approach seems inevitable.

3.3.1 Removing the Effect of a Second-Order Reference Field

As mentioned earlier, removing the contribution of a second order reference field to the observable, is the simplest way to reduce the linearization error. On the other hand, estimation of the lower degree ($l \leq 2$) harmonic coefficients using such a limited data set is of no interest. Thus, we consider $\bar{c}_{00}$ & $\bar{c}_{20}$[1] as the constant values at the estimation process and rewrite Eq. (2.101) as:

$$\mathbf{e}^T\mathbf{G}^2\mathbf{e} \stackrel{?}{=} \frac{\ddot{\rho}}{\rho} + \frac{\dot{\rho}^2}{\rho^2} - \frac{\|\Delta\dot{\mathbf{r}}\|^2}{\rho^2} - \frac{1}{\rho}\Delta\Gamma_2^{LOS} \tag{3.5}$$

In order to figure out its numerical efficiency, we repeat the estimation process using

[1] A geocentric coordinate system is considered as the Earth-fixed coordinate system

both of the data sets. Estimated coefficients in the form of degree variances are plotted in Fig. (3.23). The estimated results in the absence of aliasing is depicted in Fig. (3.24) as well.

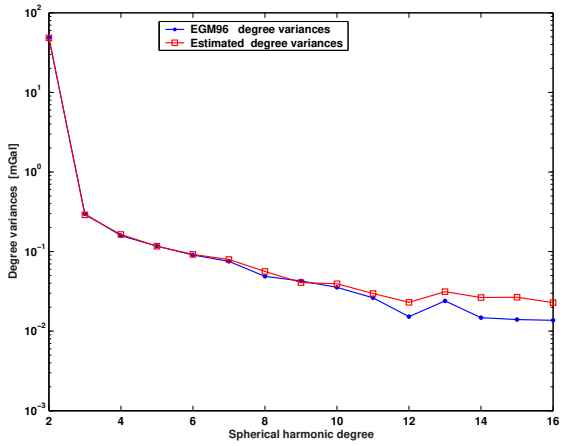

Figure 3.23: Estimated degree variances upto $n = 16$ using a one-day observations based on the modified linear approximation

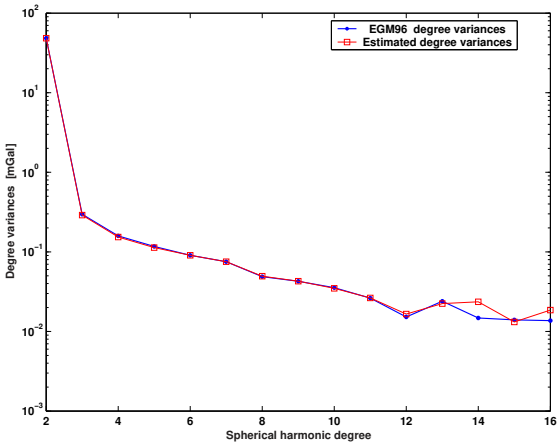

Figure 3.24: Estimated degree variances upto $n = 16$ using a one-day quasi-observations of the type $\mathbf{e}^T\mathbf{G}_2^{16}\mathbf{e}$

As it can be seen, a part of the appeared error in Fig. (3.20) has still re-emerged in Fig. (3.24). In order to compare the order of different errors contribution to the closure of estimation, all the estimated and $EGM96$ degree variances with the estimated degree variances after removing the mentioned errors are plotted all together.

As seen, aliasing correction does not noticeably improve the results individually while it makes a sensible improvement besides the linear error modification. The remaining error in Fig. (3.25) is nothing but either the effect of linearization error residual or aliasing effect on the higher degree coefficients because this simple modification just removes the dominant part of the error which corresponds to J_{00} and J_{20}. On the other hand, the sampling theorem seems not to be fulfilled even though we recover the coefficients perfectly in previous case using the same data set. One possible interpretation is that subtracting LOS of two satellites drops out the dominant part of the aliasing in the case of $\Delta\Gamma^{LOS}$ while in gradiometry approach just the barycenter of the two satellites at each evaluation point is involved. Anyway, It will be disappeared if a longer arc of the orbit (sampling with higher frequency) is used. Let us re-estimate the coefficients upto $n = 16$ using five-day observation. Fig. (3.26) shows the same degree

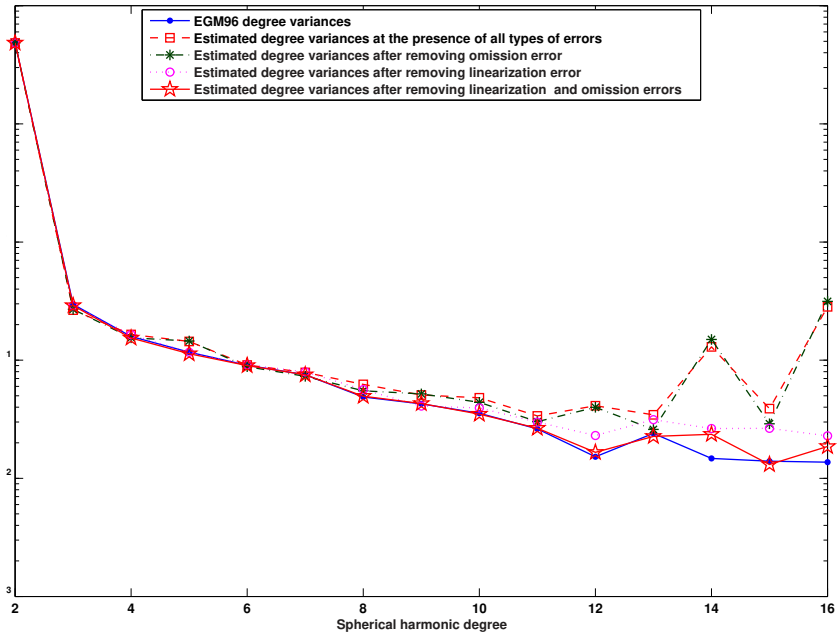

Figure 3.25: Different errors contribution to the closure of estimated degree variances upto $n = 16$ using a one-day measurements

variances estimated using the second. The remaining error is completely vanished.

As it can be seen, both the linearization error and the aliasing have much more smaller values without implementation of any correction. The estimated results are exactly the same as the original values after removing the contributions.

Figs. (3.27) and (3.28) show the estimated degree variances upto degree 25 and 50 in the absence of dominant part of linearization error. Amplified aliasing is visible in the case of $n = 50$.

Omission errors corresponding to degree 25 and 50 are removed from the data set to resolve the coefficients in the absence of aliasing. No linearization error correction has been implemented for $n = 25$ but the later case is obtained based on incremental potential equation. The achieving results are depicted in Figs. (3.29) and (3.30). For $n = 25$, reconstruction is nearly perfect but there is a visible sign of discrepancies for $n = 50$. We have encountered with the same problem that we have had in a one-day data for the coefficients estimation upto $n = 16$. So, Let us consider a ten-day observations and try to recover the coefficients upto $n = 50$. Longer arc of the orbit makes the solution converge to the original values upto degree $n = 30$. Even though the

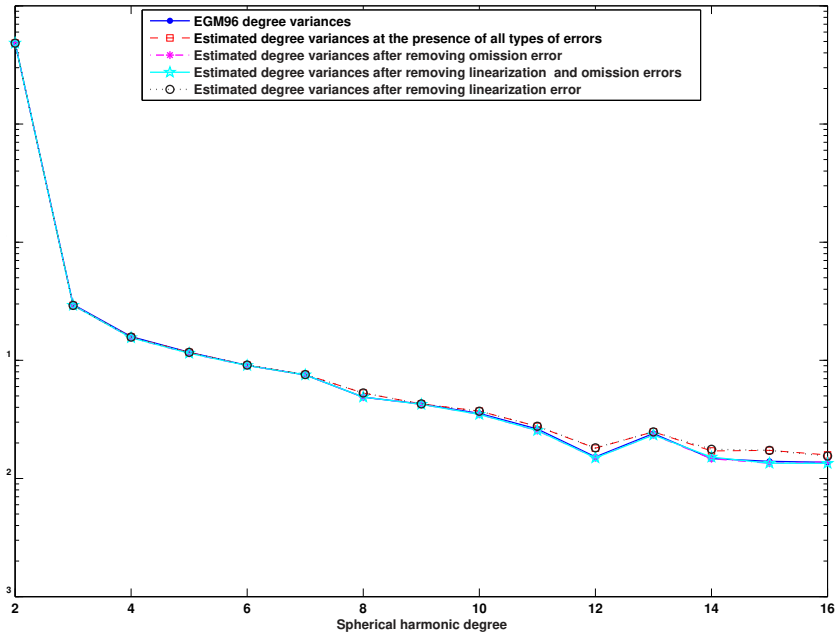

Figure 3.26: Different errors contribution to the closure of estimated degree variances upto $n = 16$ using a five-day measurements

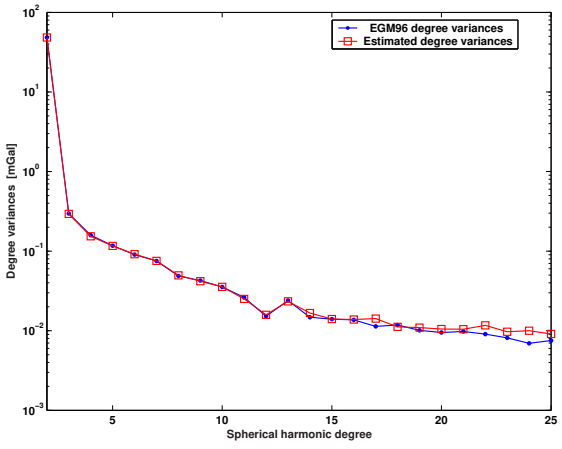

Figure 3.27: Estimated degree variances upto $n = 25$ using a five-day observations based on the modified linear approximation

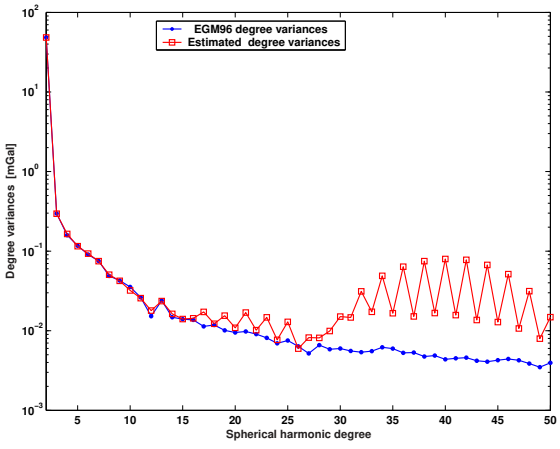

Figure 3.28: Estimated degree variances upto $n = 50$ using a five-day observations based on the modified linear approximation

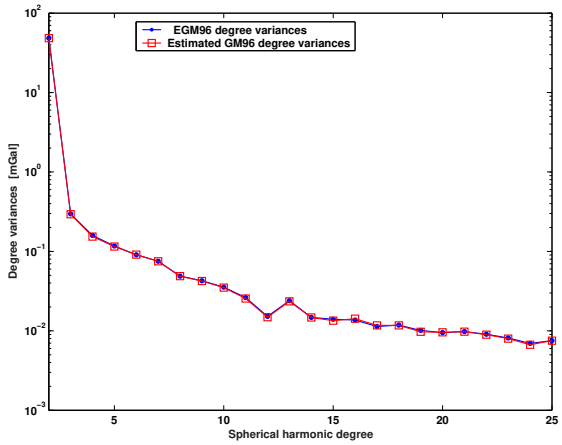

Figure 3.29: Estimated degree variances upto $n = 25$ using a five-day quasi-observations of the type $\mathbf{e}^T\mathbf{G}^{25}\mathbf{e}$

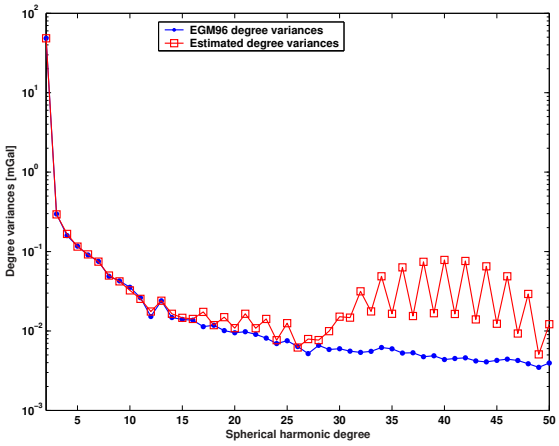

Figure 3.30: Estimated degree variances upto $n = 50$ using a five-day quasi-observations of the type $\mathbf{e}^T\mathbf{G}_2^{50}\mathbf{e}$

improvement is considerable, the differences are meaningful for higher degree $n \geq 30$. The only possibility is that the linearization error residual corresponding to higher degree ($n \geq 2$) has significant contribution to estimation of higher degree ($n \geq 30$) coefficients. Therefore, setting up the incremental potential linear system of equations based on a spheroidal reference field seems ineluctable. More details are given in next subsection.

Therefore, overestimating the coefficients using a long arc of the orbit and weeding out the affected higher degree coefficients seems to be the applicable strategy in this approach. For instance, we can weed out the harmonic with $n \geq 30$ in Fig. (3.31).

3.3.2 Incremental Potential Corresponding to a Spheroidal Reference Field

As already discussed, removing a homogeneous ellipsoidal Earth's gravity field contribution to the cubic term of the expansion is just valid for low-degree harmonics estimation and the linearization error residual effect can not be squeezed to an acceptable limit even by extending length of the employed arc of the orbit for higher degree. Hence, we should set up the linear system of equations of an incremental potential type corresponding to a spheroidal reference field (V_l). We can either remove the spheroidal references field contribution to the observations or utilize a combined linear system of

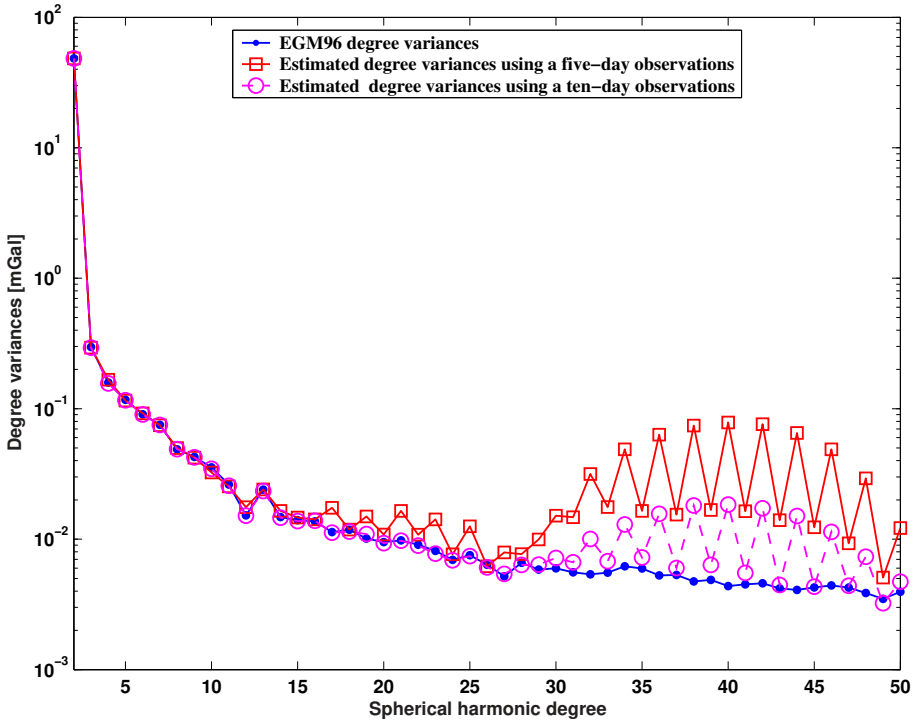

Figure 3.31: Estimated degree variances upto $n = 50$ using a five-day and a ten-day observations in the absence of aliasing and linearization error

equations of the type Eq. (2.101) in which observation equations of the types $\Delta\Gamma^{LOS}$ and $\mathbf{e}^T\mathbf{G}\mathbf{e}$ are considered for low-degree ($n \leq l$) and higher degree ($n > l$) harmonics respectively. We will just implement the second approach and keep the other for the future.

As a comparison, the coefficients are estimated upto degree 35 using a five-day observations based on incremental potential correspond with an ellipsoidal reference field. *See Fig. (3.32).* In spite of removing the dominant part of the linearization error and sampling with a reasonable frequency, degree variances differences are considerable. As already mentioned, the linearization error residual causes these differences. Let us estimate the coefficients using the same data set based on an incremental potential correspond with a spheroidal reference field of the degree 10 to figure out the residuals contribution to the estimated results. As it is seen in Fig. (3.33), corresponding degree variances differences are completely disappeared even with subtracting the contribution of the residuals correspond with $n = 10$.

In the next step, we estimate the coefficients upto $n = 50$ using both a five-day and ten-day measurements based on an incremental potential correspond with a spheroidal

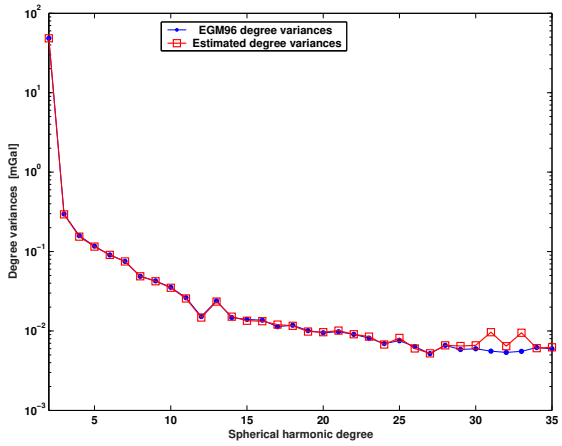

Figure 3.32: Estimated degree variances upto $n = 35$ using a five-day quasi-observations of the type $\mathbf{e}^T\mathbf{G}_2^{35}\mathbf{e}$

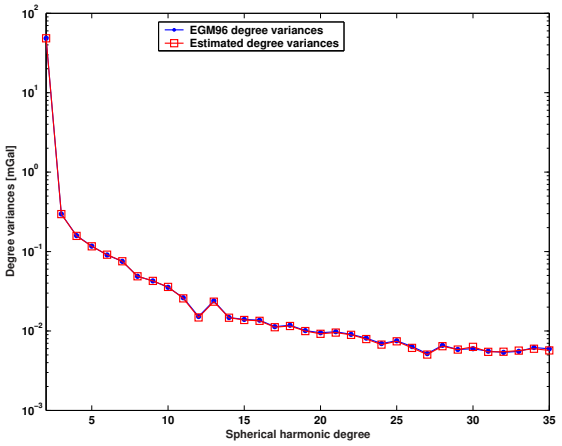

Figure 3.33: Estimated degree variances upto $n = 35$ using a five-day observations in the absence of aliasing and linearization+residual error

reference field of the degree 20 to make sure the algorithm is efficient even in higher degree of harmonics. Estimated coefficients are plotted in the form of degree variances in Figs. (3.35) and (3.34) corresponding to five and ten days of observations respectively.

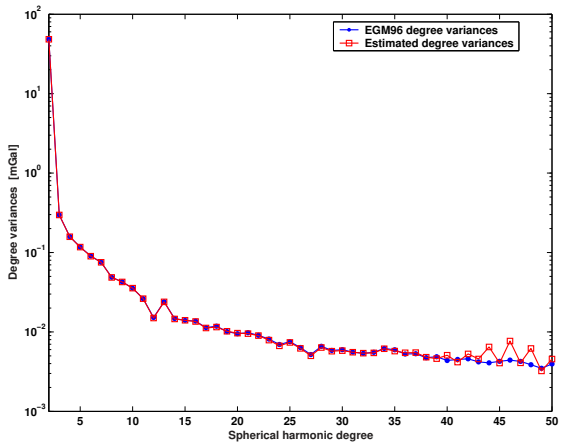

Figure 3.34: Estimated degree variances upto $n = 50$ using a five-day observations in the absence of omission and linearization+residual error

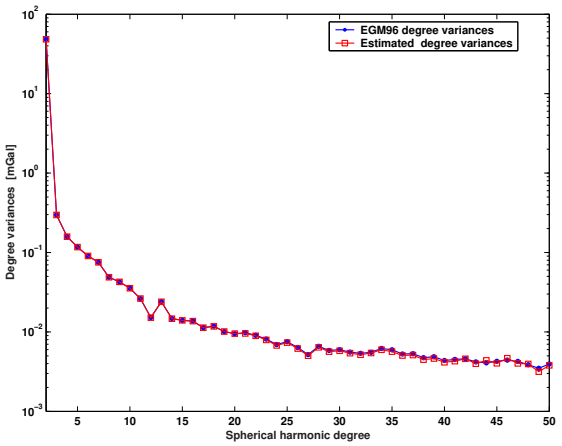

Figure 3.35: Estimated degree variances upto $n = 50$ using a ten-day observations in the absence of aliasing and linearization+residual error

As seen, using a spheroidal reference field lowers the discrepancies even in the estimated results using a five-day observations. $EGM96$ and estimated degree variances using a ten-day data set are identical in the absences of aliasing. Besides, Fig. (3.34) implies

that aliasing will emerge as soon as the spherical harmonic degree has exceeded n_{max}. Therefore, we can get rid of the linearization error residuals appeared in Fig. (3.31) by using a spheroidal reference field even in the presence of aliasing.
Hereby, we have presented two examples to show how much improvement can be achieved using a spheroidal reference field. A lot of questions still remain open concerning this approach. For instance:

- A right choice of spheroidal reference field degree l,
- suitable mathematical model for minimization of the residual error contribution using Earth gravitational models derived form other gravity field dedicated missions

are two examples of these questions that should be investigated profoundly.

Chapter 4

Conclusions and Recommendations

In this study, we have analyzed the feasibility of using *GRACE* mission as a one-dimensional gradiometer for global gravity field determination in terms of $\bar{c}_{nm}$ and $\bar{s}_{nm}$ as an alternative to the *LOS* acceleration differences approach. So, the achieving results are compared with the results of *LOS* acceleration differences as the most developed method.

All linear functionals of the gravitational potential utilized in this study have been derived both in Cartesian and in spherical coordinates. Transformation matrices(Jacobian) from spherical to Cartesian coordinates and their inverses have been derived both in Cartesian and curvilinear coordinates as well. Even though they are identical from the theoretical point of view, the expressions in terms of spherical coordinates are superior from the numerical point of view due to less computation CPU time. Hence, the functionals have been calculated in terms of spherical coordinates and transformed to the Cartesian ones eventually.

Computation of the fully normalized Legendre functions and their first and second derivatives with respect to the argument ϕ, have been calculated using a series of recurrence relationships. This part of the computation is the most time consuming part in both approaches even by using the mentioned relationships so that more than 90% of CPU time has been devoted to calculating the functions and their derivatives during the execution of the written codes. Speeding up the functions computation directly reduces running time of the whole process.

Gravitational acceleration gradient as the alternative observable has been derived in

the form of binomial series and its equivalent expression has been written in term of Kronecker product ($\otimes$) for ease of computation. As already mentioned, just the odd terms of the binomial series contribute to the observable and the even terms contribution drops out due to symmetry of the twin satellites configuration with respect to their barycenter at each evaluation point. Complexity of the higher order $j \geq 3$ terms even for representation in a closed form is the main obstacle to full implementation of the derived expression. So, only the observation equation corresponding to $j = 1$ has been represented.

As already discussed, both observables are of the type indirect measurements. In other words, both of them as linear functionals of the earth gravitational potential are directly immeasurable so they are calculated as functions of ρ, $\dot{\rho}$ and computationally derived $\ddot{\rho}$, the *LL-SST* observations, and $\dot{\mathbf{r}}$ as the *HL-SST* measurements. Assuming random errors of the observed values as white noise sequences with given standard deviations in Table (2.2) leads to $\sigma = \pm 1.5mE$ in gravitational acceleration gradient.

Linear approximation of the expansion is without no doubt an inaccurate approximation of the gravitational acceleration gradient equation even for a very low-degree $n \leq 2$ representation of the earth gravitational potential. For instance, neglecting the higher order terms of the expansion results in linearization error at the level of $-0.5550E \pm 2mE$ for the gravitational field produced only by a homogeneous spherical earth. Extending the expansion upto order $j = 3$ lowers this error to one-fifth mE. The same story is true for the gravitational potential generated by a homogeneous ellipsoidal earth. The linearization error fluctuates between -0.564 and -0.547 E whereas cubic approximation truncation error ranges between 0.194 & 0.206 mE. Comparing the achievable results by cubic approximation with the simulated random noise of the observations implies that the higher order $j \geq 5$ term of the expansion can be neglected without loss of accuracy. Although including cubic term will resolve the truncation problem, it makes even the representation of the equation very complicated. The modified linear or mixed cubic-linear approximations have been proposed instead, because their linearization errors are negligible. The proposed idea is based on the hypothesis that *replacing the gravitational potential with an incremental quantity lowers the truncation error.* As already seen, numerical analysis has certified its

validity.

Removing the contribution of an ellipsoidal reference field to the observable is the simplest modification which gives a reasonable result for low-degree $n \leq 30$ estimates of the harmonic coefficients. An equivalent accuracy has been achieved using the innovated mixed *cubic-linear* approximation of the equation. While these modified approaches are as simple as linear approximation, they are as accurate as the result of *LOS* acceleration differences approach.

A spheroidal reference field of the degree, l, should be superseded the reference field of the ellipsoidal type for higher degree ($n \geq 30$) coefficients estimating with an acceptable accuracy. Another alternative is using a mixed equation in which equations of the types $\Delta\Gamma^{LOS}$ and $\mathbf{e}^T\mathbf{G}\mathbf{e}$ are considered for low-degree ($n \leq l$) and higher degree ($n > l$) harmonics respectively. It is equivalent to removing the contribution of a spheroidal reference field of the degree, l, to the observations as a deterministic trend of the measurements. Of course, the combination can be done in other ways that may yield better results, however, discussing the all possible ways are really beyond the scope of this study. It is worth mentioning that the estimated coefficients using the second approach have been reasonably precise.

For better understanding of the *commission error* behavior, the simulated observations have been contaminated with a simulated Gaussian random noise sequences. Its contribution to the estimated coefficients with respect to other errors have been analyzed. Besides, *aliasing/ omission* error, the dominant degradation factor and its contribution to the estimated coefficients have been studied. The numerical analysis indicates that overestimating the coefficients and weeding out the higher degree harmonics as the affected terms seems to be one of the possible strategies for minimizing the aliasing.

Compared with *(LOS)* acceleration differences, gradiometry approach takes more CPU time. It is due to the second order derivatives of the potential calculation besides the first order derivatives which is common to both approaches. In contrast, the observable in gradiometry approach is a one-point function while the other observable is a two-point function. Therefore, in space-wise approach and local gravity field determination, (i.e, local geoid), the gradiometry approach would be preferable to the other.

Appendix A

C and **S** entries

$$\mathbf{C}(1,1) = (m-2i)(2k-2n-1)r^{-2} + (m-2i)(m-2i-1)x^{-2} + (2k-2n-1)(2k-2n-3)x^2r^{-4} + (m-2i+1)(2k-2n-1)r^{-2} \tag{A-1}$$

$$\mathbf{C}(1,2) = \mathbf{C}(2,1) = 2i(2k-2n-1)xy^{-1}r^{-2} + 2i(m-2i)x^{-1}y^{-1} + (2k-2n-1)(2k-2n-3)xyr^{-4} + (m-2i)(2k-2n-1)x^{-1}yr^{-2} \tag{A-2}$$

$$\mathbf{C}(1,3) = \mathbf{C}(3,1) = (n-m-2k)(2k-2n-1)xz^{-1}r^{-2} + (m-2i)(n-m-2k)x^{-1}z^{-1} + (2k-2n-1)(2k-2n-3)xzr^{-4} + (m-2i)(2k-2n-1)x^{-1}zr^{-2} \tag{A-3}$$

$$\mathbf{C}(2,2) = 2i(2k-2n-1)r^{-2} + 2i(2i-1)y^{-2} + (2k-2n-1)(2k-2n-3)y^2r^{-4} + (2i+1)(2k-2n-1)r^{-2} \tag{A-4}$$

$$\mathbf{C}(2,3) = \mathbf{C}(3,2) = (n-m-2k)(2k-2n-1)z^{-1}yr^{-2} + 2i(n-m-2k)y^{-1}z^{-1} + (2k-2n-1)(2k-2n-3)yzr^{-4} + 2i(2k-2n-1)y^{-1}zr^{-2} \tag{A-5}$$

$$\mathbf{C}(3,3) = (2k-2n-1)(n-m-2k)r^{-2} + (n-m-2k)(n-m-2k-1)z^{-2} + (2k-2n-1)(2k-2n-3)z^2r^{-4} + (n-m-2k+1)(2k-2n-1)r^{-2} \tag{A-6}$$

$$\mathbf{S}(1,1) =$$
$$(m-2i-1)(2k-2n-1)r^{-2} + (m-2i-1)(m-2i-2)x^{-2} +$$
$$(2k-2n-1)(2k-2n-3)x^2r^{-4} + (m-2i)(2k-2n-1)r^{-2} \tag{A-7}$$

$$\mathbf{S}(1,2) = \mathbf{S}(2,1) =$$
$$(1+2i)(2k-2n-1)xy^{-1}r^{-2} + (1+2i)(m-2i-1)x^{-1}y^{-1} +$$
$$(2k-2n-1)(2k-2n-3)xyr^{-4} + (m-2i-1)(2k-2n-1)x^{-1}yr^{-2} \tag{A-8}$$

$$\mathbf{S}(1,3) = \mathbf{S}(3,1) =$$
$$(n-m-2k)(2k-2n-1)xz^{-1}r^{-2} + (m-2i-1)(n-m-2k)x^{-1}z^{-1} +$$
$$(2k-2n-1)(2k-2n-3)xzr^{-4} + (m-2i-1)(2k-2n-1)x^{-1}zr^{-2} \tag{A-9}$$

$$\mathbf{S}(2,2) = (1+2i)(2k-2n-1)r^{-2} + (2i)(1+2i)y^{-2} +$$
$$(2k-2n-1)(2k-2n-3)y^2r^{-4} + (2+2i)(2k-2n-1)r^{-2} \tag{A-10}$$

$$\mathbf{S}(2,3) = \mathbf{S}(3,2) =$$
$$(n-m-2k)(2k-2n-1)yz^{-1}r^{-2} + (1+2i)(n-m-2k)y^{-1}z^{-1} +$$
$$(2k-2n-1)(2k-2n-1)yzr^{-4} + (1+2i)(2k-2n-1)y^{-1}zr^{-2} \tag{A-11}$$

$$\mathbf{S}(3,3) =$$
$$(2k-2n-1)(n-m-2k)r^{-2} + (n-m-2k)(n-m-2k-1)z^{-2} +$$
$$(2k-2n-1)(2k-2n-3)z^2r^{-4} + (n-m-2k+1)(2k-2n-1)r^{-2} \tag{A-12}$$

Appendix B

In this appendix, we calculate $\nabla \otimes \mathbf{J}_i$ both in terms of Cartesian and spherical coordinates. i runs over $\{1, 2, 3\}$.

$$\mathbf{j}_1 = \begin{bmatrix} \frac{x}{r} & \frac{-xz}{r^2\sqrt{x^2+y^2}} & \frac{-y}{x^2+y^2} \end{bmatrix} = \begin{bmatrix} \frac{x}{r} & \frac{-xz}{r^2 p} & \frac{-y}{p^2} \end{bmatrix} = \begin{bmatrix} \cos\phi\cos\lambda & -\frac{\sin\phi\cos\lambda}{r} & -\frac{\sin\lambda}{r\cos\phi} \end{bmatrix} \tag{B-1}$$

$$\mathbf{j}_2 = \begin{bmatrix} \frac{y}{r} & \frac{-yz}{r^2\sqrt{x^2+y^2}} & \frac{x}{x^2+y^2} \end{bmatrix} = \begin{bmatrix} \frac{y}{r} & \frac{-yz}{r^2 p} & \frac{x}{p^2} \end{bmatrix} = \begin{bmatrix} \cos\phi\sin\lambda & -\frac{\sin\phi\sin\lambda}{r} & \frac{\cos\lambda}{r\cos\phi} \end{bmatrix} \tag{B-2}$$

$$\mathbf{j}_3 = \begin{bmatrix} \frac{z}{r} & \frac{\sqrt{x^2+y^2}}{r^2} & 0 \end{bmatrix} = \begin{bmatrix} \frac{z}{r} & \frac{p}{r^2} & 0 \end{bmatrix} = \begin{bmatrix} \sin\phi & \frac{\cos\phi}{r} & 0 \end{bmatrix} \tag{B-3}$$

$$\nabla \otimes \mathbf{J}_1 = \begin{bmatrix} \frac{\partial}{\partial x} \\ \frac{\partial}{\partial y} \\ \frac{\partial}{\partial z} \end{bmatrix} \otimes \begin{bmatrix} \frac{x}{r} & \frac{-xz}{r^2 p} & \frac{-y}{p^2} \end{bmatrix} =$$

$$\begin{bmatrix} \frac{1}{r} - \frac{x^2}{r^3} & \frac{-z}{r^2 p} + \frac{2x^2 z}{r^4 p} + \frac{x^2 z}{r^2 p^3} & \frac{2xy}{p^4} \\ \frac{-xy}{r^3} & \frac{2xzy}{r^4 p} + \frac{xzy}{r^2 p^3} & \frac{-1}{p^2} + \frac{2y^2}{p^4} \\ \frac{-xz}{r^3} & \frac{2xz^2}{r^4 p} - \frac{x}{r^2 p} & 0 \end{bmatrix} =$$

$$= \begin{bmatrix} \frac{1}{r}[1-\cos^2\phi\cos^2\lambda] & \frac{\tan\phi}{r^2}[(2\cos^2\phi+1)\cos^2\lambda-1] & \frac{\sin 2\lambda}{r^2\cos^2\phi} \\ -\frac{\sin 2\lambda\cos^2\phi}{2r} & \frac{\sin 2\phi\sin 2\lambda}{4r^2}[3+\tan^2\phi] & -\frac{\cos 2\lambda}{r^2\cos^2\phi} \\ -\frac{\sin 2\phi\cos\lambda}{2r} & -\frac{\cos\lambda\cos 2\phi}{r^2} & 0 \end{bmatrix} \tag{B-4}$$

$$\nabla \otimes \mathbf{J}_2 = \begin{bmatrix} \frac{\partial}{\partial x} \\ \frac{\partial}{\partial y} \\ \frac{\partial}{\partial z} \end{bmatrix} \otimes \begin{bmatrix} \frac{y}{r} & \frac{-yz}{r^2p} & \frac{x}{p^2} \end{bmatrix} =$$

$$\begin{bmatrix} -\frac{xy}{r^3} & \frac{xyz}{r^2p^3}+\frac{2xyz}{r^4p} & \frac{1}{p^2}-\frac{2x^2}{p^4} \\ \frac{1}{r}-\frac{y^2}{r^3} & \frac{-z}{r^2p}+\frac{2y^2z}{r^4p}+\frac{y^2z}{r^2p^3} & \frac{-2xy}{p^4} \\ \frac{-yz}{r^3} & \frac{2yz^2}{r^4p}-\frac{y}{r^2p} & 0 \end{bmatrix} =$$

$$\begin{bmatrix} -\frac{\sin 2\lambda\cos^2\phi}{2r} & \frac{\sin 2\phi\sin 2\lambda}{4r^2}[3+\tan^2\phi] & -\frac{\cos 2\lambda}{r^2\cos^2\phi} \\ \frac{1}{r}[1-\cos^2\phi\sin^2\lambda] & \frac{\tan\phi}{r^2}[(2\cos^2\phi+1)\sin^2\lambda-1] & -\frac{\sin 2\lambda}{r^2\cos^2\phi} \\ -\frac{\sin 2\phi\sin\lambda}{2r} & -\frac{\sin\lambda\cos 2\phi}{r^2} & 0 \end{bmatrix} \tag{B-5}$$

$$\nabla \otimes \mathbf{J}_3 = \begin{bmatrix} \frac{\partial}{\partial x} \\ \frac{\partial}{\partial y} \\ \frac{\partial}{\partial z} \end{bmatrix} \otimes \begin{bmatrix} \frac{z}{r} & \frac{p}{r^2} & 0 \end{bmatrix} =$$

$$\begin{bmatrix} -\frac{xz}{r^3} & \frac{x}{r^2p}-\frac{2xp}{r^4} & 0 \\ -\frac{yz}{r^3} & \frac{y}{r^2p}-\frac{2yp}{r^4} & 0 \\ \frac{1}{r}-\frac{z^2}{r^3} & \frac{2pz}{r^4} & 0 \end{bmatrix} =$$

$$\begin{bmatrix} -\frac{\sin 2\phi\cos\lambda}{2r} & -\frac{\cos 2\phi\cos\lambda}{r^2} & 0 \\ -\frac{\sin 2\phi\sin\lambda}{2r} & -\frac{\cos 2\phi\sin\lambda}{r^2} & 0 \\ \frac{\cos^2\phi}{r} & \frac{\sin 2\phi}{r^2} & 0 \end{bmatrix} \tag{B-6}$$

where, $p = \sqrt{(x^2+y^2)}$.

Bibliography

[Graham 1981] Graham, A., 1981. *Kronecker Products and Matrix Calculus with Applications*, Ellis Horwood, Chichester, England.

[Heiskanen & Moritz 1967] Heiskanen, W.H. & Moritz, H., 1967. *Physical Geodesy*, Freeman, San Francisco, USA.

[Helmert 1880] Helmert, F.R. 1880. *Die mathematischen und physikalishen Theorien der hoheren Geodasie*. Vol. I, Minerva Gmbh. reprint, 1962.

[keller & Heß1998] Keller, W. and Heß, D. 1998. Gradiometrie mit GRACE, *Zfv*, **124**, 137-144.

[Keller & Sharifi 2004] Keller, W. Sharifi, M. A., 2004. *GRACE* intersatellite range and its time derivatives approximation based upon Hermite Interpolating polynomials, submitted to *J. Geod.*.

[Martinek & Vaníček 1997] Martinec Z., Vanicek, P. 1997. Formulation of the boundaryvalue problem for geoid determination with a higherdegree reference field, *Geophys J Int*, **126(3)**, 219-228.

[Rummel et al. 1993] Rummel, R., Gelderen, M. van, Koop, R., Schrama, E., Sanso, F., Brovelli, M., Migliaccio, F., Sacerdote, F. 1993. Spherical Harmonic Analysis of Satellite Gradiometry, Netherlands Geodetic Commission, New Series, 39, Delft.

[Schäfer 2000] Schäfer, Ch., 2000. Space Gravity Spectroscopy: The sensitivity analysis of GPS-tracked satellite missions (case study CHAMP), PhD. thesis, Geodetic Institute - Faculty of Aerospace Engineering and Geodesy, University of Stuttgart.

[Seeber 2003] Seeber, G., 1993. *Satellite Geodesy: Foundations, Methods & Applications*, Walter de Gruyter, Berlin.

[Tsoulis 1999] Tsoulis, D. 1999. Spherical harmonic computations with topographic/isostatic coefficients, Reports in the series IAPG / FESG (ISSN 1437-8280), Rep. No. 3 (ISBN 3-934205-02-X), Institute of Astronomical and Physical Geodesy, Technical University of Munich, 33 pp.

[Vaníček & Krakiwsky 1986] Vaníček, P., Krakiwsky E. J. 1986. *Geodesy: The Concepts*, Elsevier Health Sciences, Amsterdam - the Netherlands.

[Vaníček & Sjöberg 1991] Vanicek, P., Sjöberg, LE. 1991. Reformulation of Stokess theory for higher than second-degree reference field and modification of integration kernels, *J. Geophys Res*, **96(B4)**, 6529-6539.

[Wolff 1969] Wolff, M., 1969. Direct Measurements of the Earth's Gravitational Potential Using a Satellite Pair, *J. Geophys Res*, **74**, 5295-5300.